Rafael Freitas Pereira Costa

On electronic and magnetic properties of distorted kagome lattices

Uberlândia, Minas Gerais, Brasil
2025

Rafael Freitas Pereira Costa

On electronic and magnetic properties of distorted kagome lattices

Tese apresentada ao Programa de Pós-Graduação em Física da Universidade Federal de Uberlândia, como requisito parcial para obtenção do título de doutor em Física. Área de Concentração: Física da Matéria Condensada.

Universidade Federal de Uberlândia – UFU
Instituto de Física
Programa de Pós-Graduação

Supervisor: Prof. Dr. Edson Vernek

Uberlândia, Minas Gerais, Brasil
2025

Ficha Catalográfica Online do Sistema de Bibliotecas da UFU
com dados informados pelo(a) próprio(a) autor(a).

C837 Costa, Rafael Freitas Pereira, 1996-
2025 On electronic and magnetic properties of distorted kagome lattices [recurso eletrônico] / Rafael Freitas Pereira Costa. - 2025.

Orientador: Edson Vernek.
Tese (Doutorado) - Universidade Federal de Uberlândia, Pós-graduação em Física.
Modo de acesso: Internet.
DOI http://doi.org/10.14393/ufu.te.2025.569
Inclui bibliografia.

1. Física. I. Vernek, Edson,1973-, (Orient.). II. Universidade Federal de Uberlândia. Pós-graduação em Física. III. Título.

CDU: 53

Bibliotecários responsáveis pela estrutura de acordo com o AACR2:
Gizele Cristine Nunes do Couto - CRB6/2091
Nelson Marcos Ferreira - CRB6/3074

UNIVERSIDADE FEDERAL DE UBERLÂNDIA
Coordenação do Programa de Pós-Graduação em Física
Av. João Naves de Ávila, 2121, Bloco 1A, Sala 213 - Bairro Santa Mônica, Uberlândia-MG, CEP 38400-902
Telefone: (34) 3239-4309 - www.infis.ufu.br - cpgfisica@ufu.br

ATA DE DEFESA - PÓS-GRADUAÇÃO

Programa de Pós-Graduação em:	Física				
Defesa de:	Tese de Doutorado				
Data:	Quinze de agosto de 2025	Hora de início:	09:00	Hora de encerramento:	12:30
Matrícula do Discente:	12123FIS003				
Nome do Discente:	Rafael Freitas Pereira Costa				
Título do Trabalho:	On electronic and magnetic properties of distorted kagome lattices				
Área de concentração:	Física				
Linha de pesquisa:	Propriedades magnéticas e estrutura eletrônica e elétrica de materiais				
Projeto de Pesquisa de vinculação:	*N.A*				

Reuniu-se, por meio de videoconferencia, a Banca Examinadora, designada pelo Colegiado do Programa de Pós-graduação em Física , assim composta: Professores Doutores: George Balster Martins - INFIS/UFU, José Maria Villas Bôas - INFIS/UFU, Diego Rabelo da Costa - UFC, Sérgio Eduardo Ulloa - Universidade de Ohio/EUA e Edson Vernek - INFIS/UFU, orientador do discente.

Iniciando os trabalhos o presidente da mesa, Prof. Edson Vernek, apresentou a Comissão Examinadora e o candidato, agradeceu a presença do público, e concedeu ao discente a palavra para a exposição do seu trabalho. A duração da apresentação do discente e o tempo de arguição e resposta foram conforme as normas do Programa.

A seguir o senhor(a) presidente concedeu a palavra, pela ordem sucessivamente, aos(às) examinadores(as), que passaram a arguir o(a) candidato(a). Ultimada a arguição, que se desenvolveu dentro dos termos regimentais, a Banca, em sessão secreta, atribuiu o resultado final, considerando o(a) candidato(a):

Aprovado

Esta defesa faz parte dos requisitos necessários à obtenção do título de Doutor.

O competente diploma será expedido após cumprimento dos demais requisitos, conforme as normas do Programa, a legislação pertinente e a regulamentação interna da UFU.

Nada mais havendo a tratar foram encerrados os trabalhos. Foi lavrada a presente ata que após lida e achada conforme foi assinada pela Banca Examinadora.

Documento assinado eletronicamente por **Diego Rabelo da Costa**, **Usuário Externo**, em 18/08/2025, às 10:13, conforme horário oficial de Brasília, com fundamento no art. 6º, § 1º, do Decreto nº 8.539, de 8 de outubro de 2015.

Documento assinado eletronicamente por **José Maria Villas Boas**, **Professor(a) do Magistério Superior**, em 18/08/2025, às 10:39, conforme horário oficial de Brasília, com fundamento no art. 6º, § 1º, do Decreto nº 8.539, de 8 de outubro de 2015.

Documento assinado eletronicamente por **George Balster Martins**, **Professor(a) do Magistério Superior**, em 18/08/2025, às 12:43, conforme horário oficial de Brasília, com fundamento no art. 6º, § 1º, do Decreto nº 8.539, de 8 de outubro de 2015.

Documento assinado eletronicamente por **Edson Vernek**, **Membro de Comissão**, em 20/08/2025, às 07:52, conforme horário oficial de Brasília, com fundamento no art. 6º, § 1º, do Decreto nº 8.539, de 8 de outubro de 2015.

Documento assinado eletronicamente por **Sergio Eduardo Ulloa**, **Usuário Externo**, em 27/08/2025, às 23:33, conforme horário oficial de Brasília, com fundamento no art. 6º, § 1º, do Decreto nº 8.539, de 8 de outubro de 2015.

A autenticidade deste documento pode ser conferida no site https://www.sei.ufu.br/sei/controlador_externo.php?acao=documento_conferir&id_orgao_acesso_externo=0, informando o código verificador **6597534** e o código CRC **82B5FD51**.

Referência: Processo nº 23117.056441/2025-11 SEI nº 6597534

Acknowledgements

Quero prestar reconhecimento a todos meus ancestrais cuja linhagem ininterrupta permitiu o começo de minha jornada. Em especial, aos meus pais, Simone Freitas Pereira Costa e Valteir Costa de Sousa, por nunca terem feito menos que seu máximo em prol da minha formação enquanto ser-humano integral. Todo amor e carinho, toda elegância e prudência que me faltarem são única e exclusivamente responsabilidade deste que vos escreve.

À Evelyn Christiny Marques Prais, por seu companheirismo e suporte ao longo desses últimos 8 anos. Ela foi minha luz nos períodos mais escuros, mesmo quando eu não merecia.

Ao Prof. Dr. Edson Vernek pela paciência, insistência, sagacidade e sensibilidade que marcaram todo esse processo. Espero incorporar os aprendizados que fornecera à minha conduta, e que ainda trabalhemos em outros projetos empolgantes. É engraçado, porque nossos destinos se cruzaram algo que por acaso, mas a verdade é que eu não poderia ter sido orientado por alguém mais adequado.

Aos amigos e colegas desta jornada: a turma do gNano que aturou meus pitacos nos assuntos em que me autoconvidava, o pessoal do basquetinho e do vôlei, e todos que direta ou indiretamente deixaram sua marca na minha história. Vocês também acrescentaram peças fundamentais à minha formação.

Um amigo tardio que preciso enfatizar é o Prof. Dr. Gustavo Foresto Brito de Almeida. Muito obrigado por todas conversas e trocas de experiências.

Tenho muita gratidão pelos membros da banca que se disponibilizaram para apreciar e criticar meu trabalho. Espero reencontrá-los em convenções futuras! Particularmente, agradeço ao Prof. Dr. Sergio Ulloa, pela mentoria intelectual, os insights e todo acompanhamento do tronco principal que definiu nossos resultados centrais. Além de tudo, é um *gentleman* de primeira classe, como apropriadamente colocou Prof. Vernek.

Ao pessoal da MOAVI, especialmente Victor José Guerra e Lucas Rodrigues, que apostaram em mim, flexibilizando as condições para que eu concluísse o PhD. Com eles, aprendi muito mais do que apenas gerenciar escalas de trabalho no varejo integrado.

Agradeço a cada pagador de impostos, bem como às agências que fomentaram e viabilizaram minha formação. CNPq, CAPES, FAPEMIG, FAPESP pelas bolsas e auxílios nos mais diversos aspectos. Ao CENAPAD, em especial, pelo acesso a recursos computacionais indispensáveis.

A sorte sorriu para mim tantas vezes nesses anos, presenteando-me com pessoas e condições tão preciosas, que temo havê-la exaurido. Realmente espero ter demonstrado a todos, de coração, minha apreciação - por meios bem mais diretos que estes agradecimentos.

Por último, que será o primeiro, a Deus, cuja existência/essência insiste em zombar de minha inteligência e aquecer meu coração.

"Então Jó se levantou, rasgou seu manto, rapou sua cabeça, caiu por terra, inclinou-se no chão e disse: Iahweh o deu, Iahweh o tirou, bendito seja o nome de Iahweh."
Livro de Jó, 1:20-21.

Abstract

Many-body physics, frustrated magnetism and the knobs for tuning quantum materials intersect at a rich frontier of modern condensed matter physics. The kagome lattice, with its unique geometry and yet not completely understood phase diagram, has emerged as a key platform for exploring such phenomena. In this thesis, we investigate the effects of applied distortions on the magnetic properties of kagome lattices, focusing on the interplay between Geometric Frustration (GF) and correlations. We study a simple Hubbard model, and employ the Density Matrix Renormalization Group (DMRG) method to study the ground state properties of strained kagome systems. Two quantifiers for GF are proposed [1], and their predictive capabilities evidenced. Based on the literature review we conducted, one of said quantifiers features as the first local correlation-only way to "probe" GF. Our findings are thus a proof of concept in favor of not only that strain can significantly change "effective dimensionalities" and magnetic order, but also modify the "frustration content" and electronic structure of interacting kagome lattices, potentially leading to novel phases and emergent phenomena. This work paves the way for future studies on the interplay between strain, electronic correlations, frustration and elastic properties in interacting kagome lattices, with potential implications for the design of novel quantum materials and devices.

Keywords: Kagome lattice, straintronics, quantum materials, frustrated magnetism, Density Matrix Renormalization Group (DMRG), Hubbard model, Quantum Spin Liquids (QSL), anisotropic insulators, tensor networks.

Resumo

A física de muitos corpos, o magnetismo frustrado e os parâmetros de controle de materiais quânticos se encontram numa fronteira rica da física da matéria condensada moderna. A rede kagome, com sua geometria singular e um diagrama de fases ainda não completamente compreendido, tem emergido como uma plataforma central para a exploração desses fenômenos. Nesta tese, investigamos os efeitos de distorções aplicadas sobre as propriedades magnéticas de redes kagome, com foco na interação entre frustração geométrica e correlações. Estudamos um modelo de Hubbard simples e empregamos o método do grupo de renormalização da matriz densidade (DMRG) para analisar as propriedades do estado fundamental de sistemas kagome deformados. Dois quantificadores de frustração geométrica (FG) são propostos [1], e suas capacidades preditivas são evidenciadas. Com base na revisão bibliográfica que realizamos, um desses quantificadores configura-se como a primeira forma local de "sondar" a FG. Nossos resultados constituem, assim, uma prova de conceito de que deformações podem não apenas alterar significativamente as "dimensionalidades efetivas" e a ordem magnética, mas também modificar o "conteúdo de frustração" e a estrutura eletrônica de redes kagome interagentes, potencialmente levando a novas fases e fenômenos emergentes. Este trabalho abre caminho para estudos futuros sobre as relações entre deformações mecânicas, correlações eletrônicas, frustração e propriedades elásticas em redes kagome interagentes, com possíveis implicações para o desenho de novos materiais e dispositivos quânticos.

Palavras-chave: Rede de kagome, *straintronics*, materiais quânticos, magnetismo frustrado, grupo de renormalização da matriz densidade (DMRG), modelo de Hubbard, líquidos de spin quânticos (QSLs), isolantes anisotrópicos, redes tensoriais.

List of Figures

List of Acronyms

AF Antiferromagnetic. xiv, 11, 24, 25, 45, 47, 48

AI Artificial Intelligence. 1

AKLT Affleck-Kennedy-Lieb-Tasaki. 19

DMFT Dynamical Mean-Field Theory. 3, 12

DMRG Density Matrix Renormalization Group. ix, 3, 13, 14, 30, 39, 50

DQCP Deconfined Quantum Critical Points. 3

EE Entanglement Entropy. 18, 19, 22, 30, 50

FLT Fermi Liquid Theory. 8, 9, 12

FM Ferromagnetic. 11, 24

FQHE Fractional Quantum Hall Effect. 2

FRG Flat Ribbon Geometry. xiii, xiv, 38, 40–43

FSA Finite-System Algorithm. 15–17

GF Geometric Frustration. ix, xvii, 4, 5, 24, 27, 28, 30, 41–43, 45, 50–52

ISA Infinite-System Algorithm. 15–17

KAF Kagome Antiferromagnet. 2, 4, 5, 22, 24, 31, 32, 36, 40, 50

LCG Long Cylinder Geometry. xiii, xiv, 38, 40–43

LGS Local Geometrical Saturation. 45, 46, 51, 52

LLM Large Language Models. 1

LLT Luttinger Liquid Theory. 9, 12

MERA Multiscale Entanglement Renormalization Ansatz. 3, 30, 31

MG Majumdar-Ghosh. 19

MPS Matrix Product States. xiii, 17–22, 39, 40

NNSSC Nearest-Neighbor Spin-Spin Correlations. 39, 51, 52

NRG Numerical Renormalization Group. 3, 13–15

PEPS Projected Entangled Pair States. 3, 30, 31

PESS Projected Entangled Simplex States. 30, 31

QSL Quantum Spin Liquids. ix, 2, 4–6, 24, 28–32, 36, 40, 50–52

RG Renormalization Group. 3, 4, 12–14, 50

RVB Resonating Valence Bond. 2, 29

SG Spin Glass. 24

SVD Singular Value Decomposition. 16, 22

TN Tensor Network. xiii, 3, 6, 13, 17, 19–23, 30, 39, 50

VBS Valence Bond Solid. 19, 52

Contents

Chapter 1

Introduction

Humanity lives through fascinating, albeit troublesome times, indeed. The so-called "information age" and our supposedly current Fourth Industrial Revolution [2, 3] feature what are nothing short of modern-day miracles [4] which became as taken for granted as sunsets and sunrises. Its current pinnacle, Artificial Intelligence (AI for short), has led to, motivated and served as a playground for several deep advances in multidisciplinary fronts [5–9]. The Nobel prizes - plural, just in the last year - signal AI's range and power: from sentiment analysis and protein folding [5] to theoretical techniques applied in quantum chemistry and fundamental physics [8, 10]. The Large Language Models (LLM) [11], toddlers in human time scales, have continued the staggering improvement rate of Deep Neural Networks [12, 13], whose prominence became particularly notable in the last 10 to 15 years. A fan favorite movie, Her, depicts a reality that now seems just in reach - as eerie as it may sound.

Even though those consequences of AI are truly earth-shattering, this is not a thesis on the subject. It is much more aligned with something people believe to be an *even deeper and wider stressor over what we deem "normal life"*: the large scale production and usage of *quantum materials* and the applications of quantum computation [14, 15]. The latter, once a mere theoretical curiosity, now genuinely promises a reshaping of entire industries, from pharmaceuticals and cryptography to materials science and energy. We're glimpsing the ability to design entirely new structures atom-by-atom, effortlessly crack currently unbreakable encryptions, or simulate complex processes and solve other objectively impossible, as per today's methods, problems in many other economically essential fields, such as logistics. Once deemed mere fiction, such scenarios are now imminent possibilities. But the future is not our only concern, for just as Jacob's ladder, it is grasped one present step at a time. And there is plenty to grapple with right now. Reaching this "quantum-enabled" future requires overcoming formidable challenges. Some of them are deeply rooted in the intricacies of interacting quantum materials.

Quantum materials are a promising continuation - and major enhancement - of technological successes provided by quantum theory in the last century. There is no doubt about the impacts that transistors have made, and to the fact that band theory has semiconductor physics as one of its crowning achievements. But modern day discoveries, such as that of graphene and its two-dimensional "poor cousins" like borophene [16], have shed unprecedent light on the space of possibilities. Those materials showcase remarkable electronic, optical and mechanical properties, strengthening once again the links between fundamental physics and cutting-edge

technology. By the same token, topological insulators have not only beautifully expanded our understanding of matter configurations, bringing robust symmetry-protected effects and new roles for entanglement to the table [17], but also inspired outstanding practical applications - with spintronics, low-power electronics and metrological enhancements as important examples [18, 19].

The aforementioned examples highlight some of the successes achieved for quantum systems with weakly or essentially non-interacting particles, whose theoretical treatment was made quite manageable and precise by tools such as perturbative approaches, Landau's Fermi Liquid framework and Density Functional Theory [20–22]. Understanding and applying quantum matter is, however, a path littered with complexity. Drawing inspiration from Taleb's notion of antifragility [23], we must view such difficulties as "features, not bugs". That is especially true when addressing *strongly interacting* systems. These are characterized by particle-particle correlations so intense that standard simplifying assumptions become completely invalid [15]. Canonical theoretical approaches, like perturbation theory and (naïvely applied) quasiparticle descriptions, frequently fall short, and really break down spectacularly in systems like high-temperature superconductors [24], Mott insulators (e.g. NiO) [25, 26] and states exhibiting fractionalization such as the Fractional Quantum Hall Effect (FQHE) [27, 28]. The interplay between short and long-range scales can become so important that the "bare"[1] degrees of freedom might completely cease to resemble meaningful low-energy excitations [29, 30]. Instead, nontrivial collective modes emerge. Moreover, we insist, such "new" degrees of freedom are rarely - if ever - obvious from the microscopic theory at hand, thereby rendering helpless even the very powerful idea of *quasiparticles*, as it is customarily applied. Consequently, novel nonperturbative approaches become *crucial* for fundamentally new insights and novel quantum technologies.

Phenomena such as the Mott transition and quantum spin liquid physics stem precisely from this interplay between interactions and quantum fluctuations, whereby often unforeseen collective behaviors are crafted by nature. The pioneering work by Sir Nevill F. Mott helped with understanding the physics in, e.g. the canonical example of NiO, where Coulomb repulsion localizes electrons, whence its insulating properties, despite traditional band structure predictions of metallic behaviors [31, 32]. The failure of a system to settle into an unique lowest-energy configuration due to competing interactions defines frustration, which, along with strong correlations and quantum fluctuations, combines into yet another wealth of physical marvels, conceptualized by Anderson and his Resonating Valence Bond (RVB) theory [33]: the much sought-after Quantum Spin Liquids (QSLs) [34–36]. These exhibit no conventional long-range magnetic order, even at absolute zero temperature. Instead, they show massive entanglement, highly degenerate eigenstate manifolds, and might host fractionalized excitations such as spinons and visons [37, 38]. Unsurprisingly, given their topological nature, a satisfactory description of this physics seems to defy the highly successful Landau symmetry-breaking paradigm. At last, the acquisition of experimental data, a quite challenging endeavor in such realms, have been pursued in compounds like herbertsmithite ($ZnCu_3(OH)_6Cl_2$), a Kagome Antiferromagnet (KAF) believed to have a QSL ground state [39]. In a similar spirit, α-$RuCl_3$ has been extensively studied as a candidate for the *Kitaev Spin Liquid*, whose low-energy physics might behave as emergent

[1] To speak field theory lingo: the "microscopic Lagrangian".

Majorana fermions [40, 41].

From the collective behaviors brought by strongly correlated electron materials, a plethora of configurations - and *phases of matter* [42]- arise, well beyond these paradigmatic cases outlined above [43]. High-temperature superconductivity in copper-oxide (cuprate) materials figure as an archetypal example of emergent phenomena whose origins seem to fundamentally depend on electron correlations [24]. Heavy-fermion systems, $CeCu_2Si_2$ or $CeCoIn_5$ to name a few, have a characteristically extreme mass enhancement of their charge-carriers, due to localized f-electrons and conduction band electrons hybridization [44]. Apart from admitting unconventional superconductivity, heavy-fermion compounds might host other complex phenomena as well, such as Deconfined Quantum Critical Points (DQCP) [45]. Finally, iron-based superconductors, multiferroics and the celebrated colossal magnetoresistance materials exemplify the drastic implications that strong correlations might cause, often generating unexpected features that defy conventional frameworks and our mental models of nature [46].

How, then, may one study problems of this caliber? Aiding a theory for such phenomena requires treatments far beyond simple approximations, whence effective model constructions, some Dynamical Mean-Field Theory (DMFT) approaches [47, 48] or Tensor Network (TN) methods [49–51] like the well-established Density Matrix Renormalization Group (DMRG) [52, 53], the "2D-native" Projected Entangled Pair States (PEPS) [54] and the tailored-for-1D-criticality Multiscale Entanglement Renormalization Ansatz Ansatz (MERA) [55, 56] were devised. They have been bootstrapped into mandatory and respectable tools, serving as fundamental guides of rigour and benchmarks for new methods ever since their onset. DMFT, for instance, a quite imaginative approach that becomes (rigorously) exact in the limit of infinite dimensions, has been instrumental in capturing the essential features of systems such as those exhibiting Kondo physics [57–62], and is very well-suited for the so-called "single-impurity problems". DMRG, in retrospect a quite natural extension of Wilson's Numerical Renormalization Group (NRG) - the latter being developed to tackle the aforementioned Kondo problem, specifically - turns out to be a very deep gaze into nature's "economical approach" to encode information, a layer later on revealed by Tensor Network representations in general. Its remarkable success in tackling (quasi-)1D problems and delivering a precision well beyond what Quantum Monte Carlo or other "silver-bullet" methods can achieve continues to find fertile grounds for application and further insights. Carefully implemented, it is quite capable of optimizing 2D and 3D ground states as well. In fact, this is the method of choice for our problem, which will be introduced in due time.

But yet another dimension of the issue lies on "what *is* the problem to be solved, really?". One could start from first principles, and try his luck at dealing with Schrödinger's equation in its full glory. Realistically, though, solving even modest numbers of interacting particles is already intractable beyond comprehension. The truth about doing theoretical science, the author humbly believes, is that we should sometimes accept our deficiencies and ask nature - or God - indirect questions, whose answers allow some fathomable glimpses of reality, without us being blinded or crushed by her true weight. That such endeavors bear any fruit whatsoever is a miracle already well-awed by Wigner's famous statement about mathematics, which, it must be said, should be extended to what's revealed through e.g. Renormalization Group (RG) fixed-point analysis. So, we bow our heads and strive for "the second best things" in this enterprise.

But they allow for a paradise of their own. And theorists believe in heavens built upon models simple enough to be handled, yet rich in the right measure, thereby matching nature's complexity and beauty to the greatest extent any abstraction possibly can. The Hubbard model, originally introduced to describe strongly-repelled electrons, epitomizes this balance between minimalism and complexity.

Despite its deceptive simplicity - just hopping and onsite interaction terms in its minimal incarnation - the Hubbard model has profoundly impacted our understanding of strong correlations [63, 64]. It captures essential aspects of Mott insulators with success, gives room for antiferromagnetism at certain limits, and even seems to provide a conceptual foundation for cuprate superconductivity. Nevertheless, its analytical solution in general dimensions remain elusive, with exact solutions mainly restricted to one-dimensional integrable limits, famously addressed by the Bethe Ansatz. These cases yield remarkable phenomena such as solitons, spin-charge separation and non-Fermi liquid behavior. It is truly outstanding that so deep insights are achievable even from such simplified yet paradigmatic theoretical constructions. Tools like the RG fill us with the hopes that sometimes, rather curiously, such abstractions turn out closer to the truth than expected. For universal properties in critical systems, as an intriguing known example, one must simply build the "microscopic" model with certain right symmetries, in order to reach understanding of a whole class of systems. But by the same token, it is also remarkable that the physics held by those "simplified theoretical constructions" is so difficult to crack open. The message of thoughtfully crafted models is comforting, profound and challenging, all at once. But we must not digress any further. Let us be more concrete in what follows.

We turn back to the kagome lattices, since they occupy a special position in current affairs, and figure as one of our major concerns in this work. With their distinctive geometry of corner-sharing triangles, Geometric Frustration (GF) is inherent, which amounts to competing interactions that prevent conventional magnetic ordering, as we've previously alluded. Such frustration can lead to exotic states like the already mentioned QSL. Ground state searches in the quantum Heisenberg problem are still a particular controversy. Althought the scientific community seems to be now positive about its QSL character, the consensus still dwells mainly between Z_2 gapped and $U(1)$ gapless phases [38, 65–68]. It is not within our scope, however, to address the isotropic KAF within this manuscript, at least not with the level of detail it surely requires. Our context is bounded by exploring the anisotropic lattice through an innovative approach to manipulate quantum states that has emerged in the last 20 years or so: straintronics [69–71] - the application of mechanical deformations to systematically modify a material's properties.

Originating within the graphene community, straintronics has effectively tuned electronic structures, revealing new possibilities [69, 72, 73]. Extending this technique to strongly correlated materials could provide unprecedent control over frustration, localization and quantum phases in general. Inspired by these ideas, this thesis investigates two nanoribbon configurations in the quantum KAF problem. We employ a theoretical model based on the single band Hubbard Hamiltonian, approaching the strong coupling regime. The DMRG [52, 74, 75] is employed to find ground states, explore magnetic correlations, frustration and local magnetization patterns of the uniformly strained KAF. We also propose two simple ways with which

Geometric Frustration might be quantified, and discuss their general usefulness by contrasting with previously known frustration indicators. Our findings are evidence that, as one would intuitively expect, both the direction and strength of the applied deformations reshape magnetic structures. Moreover, by controlling the direction of strain at a large enough fixed strength, it is possible to effectively tune the KAF between 1D-like and 2D structures, with the former enabling a coexistence of antiferromagnetic lines and easily polarizable sites, whilst the latter hosts ferrimagnetic structures due to it essentially becoming a Lieb lattice.

This thesis is organized as follows: In Chapter 2, we provide essential background on quantum materials, the challenges of interacting problems and general frameworks for dealing with strong correlations effects. Theoretical tools are there presented, each in fitting detail, to overview state-of-the-art methods. We finish with an explanation of the chosen computational techniques. Chapter 3 presents Frustration, picturing the KAF as one *de facto* candidate for hosting QSL physics, thereby emphasizing our main concerns with frustration right away. Some classical results are outlined, and the KAF QSL controversy discussed. Finally, works on the anisotropic KAF are reviewed. Chapter 4 introduces *straintronics*, discusses some literature on the kagome lattice for non-interacting cases, related KAF results in either classical or quantum cases, and finishes by framing our problem as living in an intersection of the three major themes thus far exposed. Our main findings regarding applied strain are presented in Chapter 5, detailing the quantification and tuning of frustration, with the latter resulting from how strain affects magnetic properties in kagome nanoribbons. We contrast our findings with known literature, focusing on classical vs quantum behaviors, exotic anisotropic configurations, ferrimagnetism and mention alternative methods for inducing anisotropies already crafted. Finally, Chapter 6 holds our final reflections on the subject, summarizes the key contributions in this thesis, discusses their broader implications, and highlights promising future research directions.

Chapter 2

Quantum materials and strongly correlated systems

At the forefront of modern condensed matter physics, quantum materials stand promising transformative impacts on fundamental science and technology alike. These systems display behaviors explicitly dominated by quantum mechanical effects. In this chapter, we give a brief account on what has been and might be achieved through quantum materials exploration. Next, we introduce foundational concepts essential to their understanding, with a special emphasis on strong electronic correlations. Some difficulties on dealing with the latter are exemplified through the 1D Hubbard model, thereby motivating alternative theoretical approaches to these complex phenomena. Amounting to the bulk of this chapter, Tensor Network methods are briefly discussed in the last section, with the DMRG particularly emphasized in its traditional form.

2.1 Quantum materials: a brief overview

Quantum materials exhibit macroscopic properties governed by quantum mechanical effects, distinguishing them from classical systems. These effects—such as quantum confinement, coherence, entanglement, and topological characteristics—endow them with remarkable behaviors, driving advancements in fundamental science and technology. Graphene, a single-layer of carbon atoms in a honeycomb lattice, exemplifies this class with its Dirac-like electronic dispersion, exceptional mechanical strength, and optical transparency. Topological insulators, such as Bi_2Se_3, embody another subclass[1], featuring insulating bulks and robust, symmetry-protected conducting edge states.

Beyond these archetypes, quantum materials span a diverse range. Transition metal dichalcogenides (e.g., MoS_2) leverage quantum confinement in 2D layers, enabling tunable bandgaps for optoelectronics [76, 77]. Coherence underpins superconducting qubits in quantum computing, as seen in niobium-based circuits [78, 79]. Entanglement drives QSL, where spins form highly correlated, disordered states, a phenomenon central to our kagome lattice study [35, 38, 39]. Topological properties also manifest in Weyl semimetals (e.g., TaAs), hosting massless fermions

[1] Surely graphene can also host topological states, but the technical details of its mechanisms are different and we won't spend much lines on the subject. Interested readers can, for instance, refer to the excellent discussion by Castro Neto et. al. [70].

with potential for ultra-efficient electronics [80, 81].

Recent reviews highlight the interplay of these features in shaping material properties. For instance, symmetry and topology dictate robust edge states, while confinement and interactions amplify correlation effects in low dimensions [82, 83]. This synergy positions quantum materials as a frontier for both theoretical exploration and applications like quantum sensing [84, 85] and energy storage [86, 87], setting the stage for our investigation of strongly correlated kagome systems under strain.

2.2 Strongly correlated electron systems

Strong correlations are most easily spotted whenever a system's properties are affected by its constituents' interactions in non trivial manners. Contrary to widely used semiconductors such as silicon and germanium, whose behaviors mainly stem from electrons' delocalized nature, with a kinetic energy that overwhelmingly dictates the underlying physics, strongly correlated electron materials have their properties (magnetic, optical etc) fundamentally altered by e.g. electron-electron interactions. Emergent phenomena such as magnetic order, superconductivity and metal-insulator transitions arise from the interplay between interactions, lattice structures and quantum fluctuations. Strong correlation features are quite common in transition metals with d- or f- valence electrons, with their narrow bands and characteristically localized charge-carriers. Their nuances might be better understood through a "competition" lens, in either physical or mathematical terms.

It starts with what might be called the "root of all evil", regarding our difficulties in solving quantum mechanical problems - but it is also the root of much beauty: Hamiltonians $H = H_0 + V$ where we can solve either H_0 or V but $[H_0, V] \neq 0$. The cherry on top usually is that they either have different symmetries altogether, so simultaneous block-diagonalization is off the menu for starters, or the common set of conserved quantities does not partition the problem into manageable sectors - that is, treating the subproblems is essentially just as hard. Whence, mathematically speaking, different eigenbasis can give good quantum numbers for one term but not for the other. Physically, the distinctions are frequently noted through qualitative aspects, usually separated by one or more phase transitions. Not even an image compares to carefully crafted examples, so we proceed with one as follows.

2.2.1 Many ways of *not* solving the 1D Hubbard model

Consider the single band, half-filled, Hubbard problem for electrons (spin-$\frac{1}{2}$), since it is one of the main actors in this work anyways, but this time in 1D[2]:

$$H = \mu \sum_{i\sigma} n_{i\sigma} - t \sum_{<i,j>,\sigma} c^{\dagger}_{i\sigma} c_{j\sigma} + U \sum_{i} n_{i\uparrow} n_{i\downarrow}. \tag{2.1}$$

If $t \neq 0$ and $U = 0$ the low-energy physics is just that of a *perfect conductor*: Fermi Gas + lattice periodicity. For $U \neq 0$, and $t = 0$ however, the ground state favors singly-occupied

[2]Yes, the 1D Hubbard is very special, does have hidden symmetries, and is integrable through the so-called *nested coordinate Bethe Ansatz* indeed [88], but we won't delve into such level of detail in the main text, as it does no harm to the point at hand.

(doubly-occupied) lattice sites if $U > 0$ ($U < 0$). Notably, the $U > 0$ ground state is massively degenerate, due to spin multiplicity, and we have *perfectly insulating* behavior[3]. Mathematically, the conductor lives in a local-in-momentum basis, whilst the insulator at a local-in-position eigenspace. Such incompatibilites lie, as we've already mentioned, at the core of both "beauty and horror" that lurk in the way of those who attempt to solve even a *toy model*, if it is of any use.

At this point, one could try a few standard tricks. Say we are interested at $t \gg U > 0$ regimes. The natural instinct is having a go at naïve perturbation theory.

Perturbation theory divergence

Diagonalizing the kinetic term in momentum space with the hopes of finding perturbative corrections due to repulsion means that we should write Eq. (2.1) as

$$H = \sum_{k\sigma} \epsilon(k) c^\dagger_{k\sigma} c_{k\sigma} + U \sum_{k,k',q} c^\dagger_{k\uparrow} c_{k-q,\uparrow} c^\dagger_{k'\downarrow} c_{k'+q,\downarrow} \equiv H_0 + V, \tag{2.2}$$

where we've supposed that the lattice has periodic boundary conditions and N sites. The operators H_0 and V are implicitly defined as well. The ground state of H_0 is a completely filled fermi sea $|\mathrm{FS}\rangle = \prod_{k\leq k_F} c^\dagger_{k\downarrow} c^\dagger_{k\uparrow} |0\rangle$. Now, a true believer of the great Fermi Liquid Theory (FLT) would expect renormalized quasiparticles with effective masses, charges and whatnot. It is not hard to see that the first truly *peculiar* things start to appear at second order, whose energy correction is given by

$$E^{(2)} = \sum_{n \neq \mathrm{FS}} \frac{|\langle n|V|\mathrm{FS}\rangle|^2}{E_{\mathrm{FS}} - E_n}. \tag{2.3}$$

Now, please observe that the states $|n\rangle$ connected to $|\mathrm{FS}\rangle$ by V are *particle-hole-excited* ones: we take electrons from the Fermi Sea and put elsewhere. There are infinitely many such transitions, close and far away from the Fermi level. And in the many-particle limit ($N \gg 1$), H_0 becomes gapless whereby the integral we get out of Eq. (2.3) has a logarithmic divergence. This is a disaster people in the last century had to deal with. Let's pretend we don't know what they did, for now, and look for alternative approaches, before we attempt to understand why perturbation theory failed so badly.

Well, one of the only things we know to do whenever dealing with complicated problems have left us hanging. We are demoralized and hopeless, but never surrender. There is always mean-field to be tried.

Mean field failure

Looking at Eq. (2.1), one wonders whether electron occupations could be described as a mean value plus small fluctuations, such that the latter can be kept up to first order. This seems

[3] Of a different breed: it is a Mott, not band-insulator. We shall properly address it afterwards.

reasonable:

$$n_{i\sigma} \to \langle n_{i\sigma} \rangle + \delta n_{i\sigma} \tag{2.4}$$

$$n_{i\uparrow} n_{i\downarrow} \approx n_{i\uparrow} \langle n_{i\downarrow} \rangle + n_{i\downarrow} \langle n_{i\uparrow} \rangle - \langle n_{i\uparrow} \rangle \langle n_{i\downarrow} \rangle, \tag{2.5}$$

and since we're considering the half-filled lattice with spin-flip[4] ($\uparrow \leftrightarrow \downarrow$) symmetry, the mean-field Hamiltonian becomes (modulo an overall constant)

$$H_{MF} = \mu_{MF} \sum_{i\sigma} n_{i\sigma} - t \sum_{<i,j>,\sigma} c^{\dagger}_{i\sigma} c_{j\sigma}, \tag{2.6}$$

with $\mu_{MF} = \mu + U/2$. This is readily diagonalized in momentum space, provided the change $\epsilon(k) \to \epsilon(k) + U/2$ is made. Therefore, mean-field predicts metallic physics all around, should quadratic fluctuations be discarded. We fall into disgrace once more. But, fortunately, this is the miraculously specific situation where we contemplate an integrable problem.

The answer

In 1968, Professor Dr. Elliot H. Lieb, teamed with another giant of the exactly solvable models community, Professor Dr. Fa-Yueh Wu, to share their analytical solution of the one-dimensional Hubbard model. This was a great part of the reason behind choosing this problem as an example, since we rigorously know its solution, thereby enabling a reference for all approximations we might test it against. Indeed, for the 1D case, things are even more slippery[5], but those specificities leave the valuable messages untouched.

Perhaps the most important feature from the exact solution is that *no metal-insulator transition happens at finite U*. In other words, the Fermi Sea does not survive perturbatively in the face of Coulomb repulsion. Hence, expecting FLT to thrive is absolutely hopeless, in the sense that electrons cease to be the relevant low-energy degrees of freedom for any repulsion whatsoever. Landau's adiabaticity hypothesis does not fit. The perturbation theory we attempted was doomed from the start, for it only works if we're *close enough* to the answer.

2.2.2 A model for Hubbard and Mott

Quite differently from the other extremum of this deceptively simple Hamiltonian, we can get away with second order degenerate perturbation theory when computing the corrections for $U \to \infty$. Here we actually *are* close enough to the answer, only - again, but now trivially - not in the Fermi Liquid paradigm. The approximation is successful, provided we accept that an *effective model* will emerge to describe this phase. And it reveals an insulator of entirely distinct nature from band-theory's. Here, the absence of electrical conductivity is not due to, e.g., completely filled energy bands[6] that make available states reached by, say, an arbitrarily small electric field, only after the applied energy exceeds a finite treshold. In Mott insulators, charge mobility is prevented by large Coulomb repulsion, whereby the gap is of an entirely

[4] In fact, complete $SU(2)$ symmetry, as the model holds by construction.

[5] As they usually are, due to quantum fluctuations being much more important in lower dimensions [42, 89]. A prime example of such particularities is, of course, Luttinger Liquid Theory [90, 91].

[6] In fact, the whole concept of *bands* typically dies altogether.

distinct nature. Moreover, the charge carriers are now *correlated* in such a way that, for 1D in particular, *quasi long-range order* is attained. This will become very clear later on.

The following *hand-waving* argument, whose lack of rigor can be remedied by calculations shown in any good many-body physics book on condensed matter theory [92–94], captures the essential physical picture nonetheless. Reasoning with 2 sites is enough, as the fundamental aspects for nearest-neighbors do not depend on the lattice geometry. When $U \gg t > 0$, and we have L sites, the ground state is 2^L degenerate, since the only requirement is that of single occupancy[7], and each electron can have any of two spin projections $|\uparrow\rangle$ and $|\downarrow\rangle$- hereafter dubbed "up" and "down". For $L = 2$, then, the degeneracy is 4. Those states are

$$|\psi_1\rangle \equiv |\uparrow,\uparrow\rangle, \tag{2.7}$$
$$|\psi_2\rangle \equiv |\downarrow,\downarrow\rangle, \tag{2.8}$$
$$|\psi_3\rangle \equiv |\uparrow,\downarrow\rangle, \tag{2.9}$$
$$|\psi_4\rangle \equiv |\downarrow,\uparrow\rangle. \tag{2.10}$$

Now, it is quite easy to convince oneself that, as our perturbation is here

$$V = -t \sum_{\sigma\in\uparrow,\downarrow} \left(c^\dagger_{1\sigma} c_{2\sigma} + h.c. \right), \tag{2.11}$$

the first order corrections vanish identically: doubly-occupied states are accessed, and have no overlap with singly-occupied ones. The leading contributions are due to virtual processes whereby a configuration in our ground state is excited and returns to either itself or another ground state vector. This is allowed, since we are dealing with second-order degenerate perturbation theory. Also, please observe that the energy correction should be an operator indeed, for V does not lift the degeneracy completely. Our effectivel model should thus be calculated from

$$H^{(2)} = \sum_{n\neq \mathrm{GS}} \frac{|\langle n|V|\mathrm{GS}\rangle|^2}{E_{\mathrm{GS}} - E_n} = -\frac{t^2}{U} \sum_{n\neq \mathrm{GS}} \left| \langle n| \sum_{\sigma\in\uparrow,\downarrow} \left(c^\dagger_{1\sigma} c_{2\sigma} + h.c. \right) |\mathrm{GS}\rangle \right|^2 . \tag{2.12}$$

Bearing in mind that V moves an electron from its origin site to a neighbor, the attentive reader will immediately notice that neither ψ_1 nor ψ_2 contribute, given Pauli exclusion. By the same token, she will realize that there are 8 virtual processes with 4 inequivalent results obtained:

$$|\uparrow,\downarrow\rangle \to |\uparrow\downarrow,0\rangle \to |\uparrow,\downarrow\rangle \tag{2.13}$$
$$|\uparrow,\downarrow\rangle \to |0,\uparrow\downarrow\rangle \to |\uparrow,\downarrow\rangle \tag{2.14}$$
$$|\uparrow,\downarrow\rangle \to |\uparrow\downarrow,0\rangle \to |\downarrow,\uparrow\rangle \tag{2.15}$$
$$|\uparrow,\downarrow\rangle \to |0,\uparrow\downarrow\rangle \to |\downarrow,\uparrow\rangle, \tag{2.16}$$

and 4 analogous processes with the up and down roles exchanged. Notice that the right counting should mind distinct results only, whereby the effective coupling is in fact $\sim -4t^2/U$, modulo the global sign that is determined in the next step.

[7] Don't forget: we're assuming a half-filled system. Were that not the case, another effective Hamiltonian would emerge

After one tinkers with those relevant virtual processes and exploits single-occupancy space completeness, then either by studying the "emerging" operators due to multiplying the up and down hopping terms, or through the remembrance of fermionic parton/slave-fermion representations for spin-$\frac{1}{2}$ $SU(2)$ operators

$$S_j^a \equiv \frac{1}{2}\sum_{\alpha,\beta} c_{j\alpha}^\dagger \sigma_{\alpha\beta}^a c_{j\beta}, \tag{2.17}$$

where σ^a are the usual Pauli matrices, one arrives at the effective problem

$$H_{\text{eff}} \equiv J\vec{S}_1 \cdot \vec{S}_2 + \text{irrelevant constant}, \tag{2.18}$$

with $J \equiv 4t^2/U$. For an arbitrary lattice in any dimension, given nearest-neighbors hopping only, this is the general form as well, i.e.

$$H_{\text{eff}} \equiv J \sum_{<i,j>} \vec{S}_i \cdot \vec{S}_j + \text{irrelevant constant}. \tag{2.19}$$

This is the celebrated Heisenberg model, which provides a good description of the low-energy sector of the single-orbital Hubbard model at half-filling, provided there is a charge gap of order U - and if that's not so negligible, interesting features, e.g. SDW itinerant magnetism, might arise [32]. The simplification of going from sites with 4 to 2 degrees of freedom is enormous, but this effective problem is a work of art in itself. As usual, it is integrable in none but one dimension. The sign of J determines whether its ground state favors ferro ($J < 0$) or antiferromagnetic ($J > 0$) tendencies. For the problem at hand ($J > 0$), it is clear that antiparallel spins define the low-energy landscape. In one dimension, there is no true long-range order (even at $T = 0$), due to infinitesimal excitations (such as the Nambu-Goldstone bosons) which spoil ordering for this candidate of a symmetry-broken phase, featuring one of Mermin-Wagner's theorem many facets [95–98]. The spin-spin correlations decay algebraically at long separations. Differently from what occurs at large enough dimensions for both antiferro (AF) and ferromagnetic (FM) ground states, where spin waves are propagated by magnons (spin-1 bosons), here fractional excitations dubbed spinons dictate the dominant physics. For other low dimensions, such as 2 and 3, the underlying lattices can heavily modify the kinds of phases that arise. Frustration effects, to be discussed in a later chapter, might appear already with nearest-neighbor interactions only. Extracting meaningful data out of such cases is a great challenge. We also mention for completion that, rather ironically, above this system's *upper critical dimension* $D_c = 4$, the universal properties [42] are exactly captured by mean-field analysis.

2.2.3 Aftermath and how to get things right

We hope that all those failed attempts at finding the ground state properties of the Hamiltonian (2.1), plus the appearence of an effetive problem, highlighted some subtleties in dealing with interactions, while convincingly exemplifying the wealth of phenomena that might occur.

Notwithstanding the 1D peculiarity of having just two points as the "Fermi surface" could be a hint at FLT's demise, this dramatic change in the relevant degrees of freedom persists at higher dimensions, where the Mott transition now happens at finite U.

In 1D, Hubbard's low-energy physics is given by Luttinger Liquid Theory (LLT) [89, 91], and can be analytically found through bosonization, a fairily well-stablished framework for one-dimensional problems. It basically consists of the continuum limit from particle-hole excitations' point of view (+ Wilson RG to get the phase diagrams mostly right). It is then evident how different the excitations/eigenmodes look in LLT contrasted with FLT. Such is more a rule than exception in truly many-body problems. A final quite remarkable fact is that, while the exact solution through Bethe Ansatz gives several information, such as the excitation spectrum and gap conditions, it usually does not tell how to figure the *correlations* out. Bosonization [99] is of particular value in such endeavors.

The already mentioned Wilson RG evidently stands as one of the greatest ideas in physics and science altogether, mainly for how it systematically zooms in on the low-energy degrees of freedom by integrating out high-energy ones iteratively. Its successes are ubiquitous: from unraveling the Kondo effect to quantitatively explaining phase transitions in classical and quantum systems via universal scaling laws as consequences of fixed-point analysis. In that sense, it not only provides a tidy classification of phases near criticality but also instills a powerful picture of how collective behavior emerges as "irrelevant" details get washed out under successive coarse-graining. However, the method can become quite tricky when the physics does not remain local or neatly factorable into a series of scales—particularly when dealing with strong interactions that do not clearly separate high and low energy sectors. Even with these caveats, Wilson's RG remains a monumental insight into how to peel off layers of complexity in a controlled manner.

Dynamical Mean-Field Theory (DMFT) is yet another approach whose impact has been similarly profound, especially in understanding correlated lattice fermions. It effectively captures local quantum fluctuations exactly by replacing the lattice with a single-site (or cluster) impurity problem subject to a self-consistency condition - the true point at which approximations are always made, for the sake of tractability. When it comes to strongly correlated materials, DMFT has proven invaluable for describing Mott transitions at finite temperature and (large-enough) finite dimensions—where perturbation theories so often falter—while retaining a tangible link to realistic electronic structures. Nonetheless, as a purely local scheme, it cannot fully address spatial correlations or collective modes that hinge on nonlocal physics, and extensions to include short-range correlations (like cluster-DMFT) come at the cost of heavier computational demands. Despite these limitations, DMFT stands as a cornerstone for tackling the intricate interplay of bandwidth, interaction strength, and lattice geometry that hallmark modern studies of strongly correlated electron systems.

All those distinct techniques and combinations thereof, beckon at the necessity of developing non-trivial schemes for the treatment of strongly correlated systems. As we have already mentioned, the *collective modes* are customarily not evident from the "primordial" constituents of a microscopic model. Sometimes, if we are lucky enough, deriving an effective Hamiltonian is manageable. But even that problem, as in the Hubbard $\rightarrow$ Heisenberg case, might be an Everest on its own. It seems that having intimacy with phenomena such as quantum phase transitions,

magnetic order and spontaneous symmetry breaking in general is something reserved for those initiated in deep enough ideas that help cracking those mysteries open. Amongst many such great tools that humanity has built, Tensor Network algorithms are probably the most powerful for the task at hand, to this very day.

2.3 Tensor network algorithms

A delightful lineage of ideas flew since the first classical field-theory problems with infinities were highlighted by Max Abraham and Hendrik Lorentz [100, 101]. Too many great researchers were involved in this enterprise to be cited with due justice, so we will keep only a few well-known names. Drawing inspiration from the seminal ideas of Abraham and Lorentz, the founding fathers of Quantum Field Theory tackled UV-divergences under regularization and *parameter-renormalization* schemes, thereby providing the first "proof of concept" for ideas that eventually led to building the most precise scientific theory to date [102–105]. It was Freeman Dyson who first proved foundational theorems on renormalizability, and modern "lagrangian-building" is (happily) constrained by such criteria [106]. We then have Kadanoff's essential *block-renormalization* insights [107], alongside Michael Fisher's inheritance and brilliant expansion of Widom's scaling hypothesis to their fullest powers, pushing the boundaries of what was possible and understood in statistical mechanics [108, 109].

The increasingly visible bridge between *scale-invariance* [110] and assorted tools in phase transitions [42, 98], and general high-energy physics tricks for taming infinites, was perhaps first made concrete through the Renormalization Group "formalization" by Kenneth G. Wilson in the 1970s [111]. One of its crowning achievements was the outstanding solution to the Kondo Problem. As guiding principles, scale[8]-invariance and coarse-graining the right degrees of freedom surely became central to the most precise approximative schemes able to grapple with strongly correlated systems. On the Kondo side of things, the "right way" to proceed is by iteratively coarse-graining the *energy scales* of the problem. However, such protocol won't guide us to the truth in certain systems where, as we have previously alluded, it turns out that *entanglement scales* are the key instead. Steven White published the pioneering example of how to treat a problem with such nature, providing its solution with unprecedent accuracy: the Density Matrix Renormalization Group algorithm was discovered, and numerically rigorous results for the Haldane chain were first given [52, 113]. Inheriting all the maturity, time-tested tools and essential concepts from this large corpus of ideas so elegantly summarized by the initials *RG*, the modern *entanglement-based* renormalization schemes pioneered by DMRG still flourish from its seeds. It is then mandatory that we take a moment to reflect on the essential ideas behind DMRG, before they are generalized to the Tensor Network realm. But this requires a word or two about Wilson's NRG.

2.3.1 The NRG and its limitations, briefly

One could say that the main reason DMRG exists is that NRG fails badly for important problems, even at the 1D tight-binding case exemplified by White and Noack [113]. So, how does

[8] Conformal, to be precise, in 2nd order transitions described by critical systems [42, 98, 112]. But let it be.

NRG work? The idea is starting with a small system that can be numerically diagonalized in an exact manner[9]. One then grows the system, but the maximum Hilbert space size is kept until a target system size is reached. It is visible that this ceremony of increasing the system without letting Hilbert space's vastness get the best of our resources has two stages: (i) one grows both the system and Hilbert space sizes accordingly, as long as the numerically exact result is guaranteed. (ii) a truncation of the Hilbert space is performed, while growing the system, but now true numerical errors are expected. Of course, the central questions now are: 1) how is that growth achieved, precisely? 2) what are the truncation criteria?

Wilson did it as follows. One starts with blocks of small enough systems. In the growth phase, those blocks are linked to form a larger block. The Hamiltonian is then exactly diagonalized and the basis states are its eigenstates. The selection of which states to keep is based on momentum RG ideas of "energy cut-offs". The states are ordered according to their energy, and the lowest ones are kept - those below a certain threshold. The rest are discarded, and those that are kept are then used to build a new block, which is again enlarged and diagonalized. This process is repeated until the target system size is reached.

As we have already mentioned several times through the text, this approach turned out very effective for the Kondo model [111] and, for providing the general RG formalism crowned by the Kondo problem solution, Kenneth Wilson was awarded the Nobel Prize in Physics in 1982. However, albeit well-fit for impurity problems, it fails at other relevant strongly correlated systems, such as the 1D Hubbard model. In fact, quite remarkably, it cannot handle the simplest 1D tight-binding hamiltonians (!). The main reason for this, as was later realized, is that the NRG approach does not take into account the entanglement structure of the system. In a more concrete framing, as was brilliantly discussed by White and Noack in their 1992 paper [113], the usual choice of block eigenstates to be kept "mutilates" the connections of blocks previously detached. As the authors put it:

> *The boundary condition of ignoring the connections T to neighboring blocks corresponds to setting the wave function to 0 at the sites just outside the block(...). Any state made only of low-lying states from the previous iteration must have a "kink" in the middle. In order to accurately represent states in the larger block, one must make use of nearly all the states in the smaller block: Any truncation leads to large errors.*

Their attempts at fixing this problem revealed that the solution was to keep the bipartite entanglement structure of the system as intact as possible, and this is what DMRG does.

2.3.2 A beautiful answer for a beautiful question: DMRG and how to truncate properly

The Density Matrix Renormalization Group (DMRG) addresses the exponential complexity of quantum many-body systems by coarse-graining entanglement [52]. Introduced by White, DMRG vastly outperforms exact diagonalization's reach by targeting the ground state via a

[9] We closely follow [114] in this exposition.

variational ansatz. But that is the modern understanding. Let us dive into the original perspective in which it was introduced, with only a few refinements for the sake of brevity.

Consider a 1D chain with Hamiltonian $H = \sum_i h_{i,i+1}$, under open boundary conditions, whose properties (usually the low-energy ones) we are interested in. Take the ground state as our target. And to be really concrete, consider the following spin-S Heisenberg Hamiltonian:

$$\begin{aligned} H &= \sum_{i=1}^{N-1} \vec{S}_i \cdot \vec{S}_{i+1} \\ &= \sum_{i=1}^{N-1} \left(S_i^x S_{i+1}^x + S_i^y S_{i+1}^y + S_i^z S_{i+1}^z \right). \end{aligned} \tag{2.20}$$

DMRG works in two main acts for optimizing the variational energy of a trial state $|\psi\rangle$

$$E_\psi = \frac{\langle\psi|H|\psi\rangle}{\langle\psi\,|\,\psi\rangle} \tag{2.21}$$

in the Hilbert space of the system, whilst minimizing the error $|||\psi_{\text{exact}}\rangle - |\psi\rangle||^2$. It turns out that entanglement maximization naturally emerges from the last condition[10], and this is the reason why reduced density operators show up with a central role in DMRG. They are:

- The Infinite-System Algorithm (ISA)- the *growth*.
- The Finite-System Algorithm (FSA) - the *sweeping*.

The ISA is the one that builds the system up through a decimation procedure.

The infinite-system algorithm (ISA)

At the ISA stage, DMRG considers a chain of increasing length, usually even. By iteratively keeping a sufficient number of states, in a "special" basis, one finds the best representation in this "reduced state space" which can capture the essential features. As will be properly addressed in a later section, the very existence of such reduced space is at the same time a miraculous finding and deep facet of nature. And DMRG is particularly capable of exploiting those advantages in the case of local 1D Hamiltonians. But let us digress no further.

The ISA DMRG builds the system as follows. We start with left and right *blocks* A and B. Those can consist, for instance, of even just a single site each, in the first step. The left block is then enlarged by adding a new site to its right, and the rightmost analogously. That is, the growth is made by inserting pairs of sites between blocks. If the current block has l sites, then a *superblock* consists of the whole system, i.e. the left block, the new sites and the right block, with a total size[11] of $2l + 2$ sites. This structure is generically represented through the notation $A \bullet\bullet B$, where the bullets evidently represent the new sites. Analogous questions to those asked for the NRG now arise: (i) what is the spectrum of the current superblock? and (ii) how to efficiently obtain it after the system grows? Equivalently, how to truncate the Hilbert space in a physically accurate way?

[10] A straightforward argument can be found in the literature, e.g., [75].

[11] As the discussion progresses, we will be referring to a couple of sizes: Hilbert space's, the block's, the superblock's... Don't forget to be mindful about each one of those!

Following the notation in [74], we start from the fact that any state of the superblock $A\bullet\bullet B$ can be written as

$$|\psi\rangle = \sum_{a_A\sigma_A\sigma_B a_B} \psi_{a_A\sigma_A\sigma_B a_B}|a_A\rangle|\sigma_A\rangle|\sigma_B\rangle|a_B\rangle \equiv \sum_{i_A,j_B} \psi_{i_A j_B}|i_A\rangle|j_B\rangle, \tag{2.22}$$

where the new blocks ($A\bullet$ and $\bullet B$) are represented by the indices i_A and j_B, and the σ indices represent the added sites' degrees of freedom of local dimension $d(=2,$ for our spin Hamiltonian (2.20)). The $\psi_{i_A j_B}$ denote the coefficients of the superblock's wavefunction in the basis of (new) left and right blocks. The next step is to numerically find the minimized variational energy. Given the sparse nature of usual local problems, iterative eigensolvers such as Lanczos or Davidson methods are commonly employed [115, 116] at this stage.

The next step is taking states $\{|i_A\rangle\}$ as the basis for the new (larger) left block. Naturally, the renormalization procedure pressuposes a truncation in Hilbert space dimension. Let D be this maximum dimension, hereafter denoted *bond dimension*. Well, the new left block would now have dimension at most dD. The optimal way to truncate is the following. Consider the reduced density matrix for this new left block $A\bullet$[12]:

$$\rho_{A\bullet} = \mathrm{Tr}_{\bullet B}|\psi\rangle\langle\psi| = \sum_{i_A i'_A j_B} \psi_{i_A j_B}\psi^*_{i'_A j_B}|i_A\rangle\langle i'_A| = \sum_{i_A} \lambda_{i_A}|i_A\rangle\langle i_A|. \tag{2.23}$$

We are now tasked to find the (non negative) eigenvalues λ_{i_A} - or *Schmidt coefficients* - and eigenstates $|i_A\rangle$ of this density matrix[13]. But we must not keep all of them, for the sake of computational efficiency: only the orthonormal eigenstates with D largest λ_{i_A}. We denote them by $|b_A\rangle$. Then, the truncated wavefunction amplitudes for subsystem $A\bullet$ are simply obtained by projecting the previous complete basis states $|a_A\rangle|\sigma_A\rangle$ into the new basis $|b_A\rangle$. All other relevant operators (such as the Hamiltonian, other observables and any simplifying symmetries implemented) must be "rotated" into the new eigenbasis as well. The new left block is then represented by the states $\{|b_A\rangle\}$, and the right block is obtained in an analogous way. The superblock is now $\tilde{A}\tilde{B}$, and the process is repeated until convergence[14]. Also, please observe how this D can vary from step to step, a feature that will make more sense after we discuss the FSA.

The finite-system algorithm (FSA)

The FSA is the second part of the DMRG algorithm. It is a refinement of the ISA, and it is usually performed after the ISA has converged, and a system with L sites was reached. The FSA consists of a series of *sweeps* through the system, where the left and right blocks are updated iteratively. The main idea is to improve the accuracy of the wavefunction by optimizing the left and right blocks separately, while keeping the other block fixed. It is widely reported in the

[12] Evidently, the new right block is obtained in an analogous way. If the system has translational invariance, it is simply a mirror of the left one.

[13] A Singular Value Decomposition (SVD) is assumed.

[14] A very honest convergence measure is the *truncation error* $\varepsilon \equiv 1 - \sum_{a>D} \lambda_a$, with descending order of the λ_a being assumed ($\lambda_1 > \lambda_2 > ...$), and a proper normalization for the lambdas as well. Here, of course, we must diagonalize at least a slightly larger problem in order to estimate ε.

literature, and known by those who have implemented DMRG, that the ISA alone is frequently not enough, wherefore deeming the FSA practically mandatory. Actually, as White pointed in his seminal paper, such lack of accuracy is expected, given that ISA's final state starts with initially small blocks. By yet another conceptual token, UV/IR mixing is not completely taken into account by the infinite algorithm.

The idea here is essentially the same as in the ISA, but, say, block B's growth is now performed at the expense of block A's. So, if B has N sites, A must have $L - N - 2$. This procedure is continued until either A is so small that a chosen D amounts to its Hilbert space being numerically exact, or until A is a single site. Once block B has grown to such maximum size, the process is reversed: A is now the one to grow, and B is accordingly shrinken. This process is repeated until convergence, and it is called a *sweep*.

Some implementation subtleties are worth mentioning. The fact that operator representations in all bases (with varying subsystem sizes) will be needed is not hard to see. But a subtler feature is connected to the fact that, in order to find the ground state $|\psi\rangle$ for a given $A \bullet \bullet B$ configuration, large sparse matrix eigensolvers require an initial guess [116]. Of course, the closer we are to the actual answer[15], the faster the convergence. It is easy to intuit that this is the most time-consuming part of DMRG, and that its acceleration is thus crucial. Therefore, an obvious guess to start the FSA is whichever last converged state was obtained from the ISA. This is a good approximation, but it is not always enough, whereby further "astute" tricks are sometimes required [53, 116]. The reason is that, we insist once more, the ISA does not take into account the entanglement structure of the system as neatly. Hence, should the ISA result be already biased in a negative sense, the final output will perform poorly, as far as the physics of interest is concerned. Supposing that the final ISA wavefunction is "good enough", however, one proceeds with the sweep, whereby the previously computed best state is applied as input to the eigensolver. This is then repeated at each sweep step.

The number of sweeps, for typical 1D systems usually does not exceed 10, and the maximal dimension D ranges from $O(100)$ to $O(1000)$, in order to get energies right up until the nineth decimal place. Although there are other problems (and already found solutions) regarding the simplest DMRG setup of block-site-site-block, this discussion is enough to frame the main ideas behind DMRG. We would like to now contrast its weaknesses and strengths, at the same time as we actually understand those. But in order to do so, we must learn why the *Hilbert space vastness is kind of a hoax*.

2.3.3 The *relevant* Hilbert space is not that large, after all

This is one of the key ingredients to Matrix Product States (MPS) and TNs in general, and we really should savor it later, but the circumstances are such that we must bring it up right now. But to contemplate the gains, we must first gaze at the price before discounts are applied. Take our good old Heisenberg Hamiltonian (2.20). For a spin-1/2 chain with L sites, the comprised Hilbert space is 2^L dimensional. If we want to represent a quantum state of this system just

[15] We should bear in mind: there is always a chance that our guess has no overlap with the true ground state whatsoever. However, since exact diagonalizations are being made up until a maximum size, the ISA+FSA combination usually guarantees we won't be haunted by this ghost. DMRG variations whereby we start directly in the FSA are the most affected by "initial state sensitivity".

by writing all those possible coefficients down, we better have a good friend to deliver us from such madness. To put things in perspective, suppose [49] $L \sim 10^{23}$. Hence, the total number of basis states in Hilbert space is $O(2^{10^{23}})$. We don't even know what to think, when looking at this number, let's be honest. This quantity is *exponentially larger* than the estimated number of atoms in the observable universe ($\sim 10^{80}$). There is just no way we can even think of either writing down all those coefficients, or storing them in a computer[16]. And this is just for a 1D system! The situation gets worse and worse as we increase the number of dimensions.

Whether by nature's laziness or elegance, we are lucky to find that not all those states are relevant for the low-energy physics of local Hamiltonians [117–119]. This very locality has important consequences. The most significant to our ends is that the Entanglement Entropy (EE) of the low-lying eigenstates of such systems obey the so-called *area law*: it scales, for large enough regions, as the size of the *boundary* of said region, rather than its comprised volume. Such feature is remarkably rare: should we throw a multidimensional dice and select an arbitrary state from the Hilbert space, the probability to get an area law state is virtually zero. As people usually put it, the corner of relevant states is a tiny, exponentially small, fraction of the whole Hilbert space [49]. To get a non rigorous feel, consider an arbitrary (randomly picked) state in a lattice with local dimension χ. For a sufficiently large bipartition, it is natural to expect that the reduced density matrix of a typical random state would have entropy close to the logarithm of its Hilbert-space dimension $\sim \chi^{L^D}$, with D the spatial dimension and L a characteristic length scale. This gives $S \sim L^D$, a volume law rather than an area law.

It is quite interesting to ponder about that. Some of the consequences of having the Hilbert space so big are fascinating. In a prism that is particularly relevant for the field of many-body localization, it can be proved that the time-evolved quantum many-body state after a time t that's polynomially big in the system size L only reaches a subspace that is exponentially small [120]. The bottom line reads: it takes an exponentially long time ($\sim \exp(L)$) to access certain regions[17]. This lies at the core of several uncertainties as to whether or not certain states are ergodic, and it is a very active field of research.

Finally, we are now almost equipped to clearly understand why is DMRG so successful. The area law property of the low-lying eigenstates of local Hamiltonians implies that the Entanglement Entropy of a bipartition of the system is small, and that the entanglement structure can be efficiently captured by a MPS representation. This means that the relevant Hilbert space can be approximated by a much smaller space, which is what DMRG does. The MPS ansatz allows for an efficient description of the quantum state, and it can be shown that the DMRG algorithm variationally optimizes within this very class of states [49, 74]. *Almost* because MPS were not properly addressed yet. We will do so afterwards, but first let us keep our promise of discussing the strengths and weaknesses of DMRG.

[16] Actually, such information content, concentrated in a single desk, should be more than enough to develop into a black-hole.

[17] If they are ever to be reached in the first place. But I don't want to open people's scars right now. Let us focus on the main issues.

2.3.4 DMRG's reach

DMRG's strengths include high accuracy in 1D (errors $\sim 10^{-10}$) and adaptability to quasi-1D systems like Heisenberg ladders [121]. Weaknesses include bond dimension scaling ($D \sim 10^3 - 10^4$ for 2D-like systems) and sensitivity to initial state choice in diagonalization routines, mitigated by finite-system sweeps and noise injection [122, 123]. Over the years, DMRG's accuracy has been shown explicitly through its comparison to some exactly solvable systems and the method's expected asymptotic behaviors explored[124–127]. Such analysis reveal that, in one-dimensional gapped local systems, the Schmidt coefficients decay exponentially fast, whereby DMRG becomes enormously facilitated. But in two-dimensional "ribbon-like" geometries where dimensions $L \times W$ with $L \gg W$ are considered, the situation is more complicated [128]. Increasing W makes the Schmidt coefficients decay slower, sometimes even hindering DMRG completely inefficient.

We can see in a somewhat "worst-case scenario" way what causes DMRG to fail in 2D. Suppose our Schmidt coefficients are all $\lambda \sim 1/D$, roughly speaking, with D being the largest Hilbert space dimension required to get "good physics" out of the problem. The Entanglement Entropy is then $S \sim \log D$, and the number of states in the reduced density matrix is then $\sim 2^S$. This means that the number of states in the reduced density matrix grows exponentially with the entropy, which is a clear sign of a problem, given that $S \sim L$, by area law requirements. To be just, 2D systems are generally more difficult to be handled in comparison to 1D ones, essentially by construction. But the fact that DMRG is not able to treat them as well as it does for 1D systems feels like an obstacle that, with a few crucial tweaks, might actually work out.

2.3.5 Early successes of projective methods: the Affleck-Kennedy-Lieb-Tasaki and Majumdar-Ghosh models

The Affleck-Kennedy-Lieb-Tasaki (AKLT) and Majumdar-Ghosh (MG) models [92, 129–131] stand as early examples of reverse-engineered Hamiltonians: models crafted to host specific, analytically tractable ground states with nontrivial, yet controlled entanglement structures. We mention those briefly, for now, as an account of their historical importance. In the AKLT model, designed for spin-1 chains, the ground state is a Valence Bond Solid (VBS) composed of spin-1/2 singlets projected into a symmetric triplet subspace. This construction captures Haldane's conjecture [132, 133] and provides a pedagogical foundation for symmetry-protected topological phases. Similarly, the MG model, a spin-1/2 chain with next-nearest-neighbor interactions, exhibits a (degenerate[18]) dimerized ground state expressible exactly as a product of singlets between neighboring spins. These models are not just pedagogical gems, but also practical stepping stones: their exact solvability, compatibility with valence bond representations, and modest entanglement scaling have informed modern Tensor Network designs. They serve as clear case studies where Matrix Product States can *exactly* capture ground states with minimal bond dimension, exemplifying how simple entanglement structures still encode rich physics, particularly MPS, which can express both ground states in closed form [49, 51]. First, we must have a primer on MPS and their properties. In order to keep this somewhat self-contained, with

[18] A neat example of the celebrated Lieb-Mattis-Schultz theorem on bipartite Heisenberg problems [134]: their ground state is either unique and with a gapless excitation spectrum or degenerate and gapped.

no further pretension to be historically linear any longer, we are now proceeding to introduce the MPS and their properties, referring to the literature whenever possible for the sake of conciseness.

2.3.6 Essentials about Matrix Product States

We follow [49, 50, 74, 135] in our exposition, and mainly focus on 1D or quasi-1D aspects. As can be shown, by working in MPS space, DMRG algorithms and other optimization methods come about quite naturally. Moreover, the graphical notation to be introduced enables a neat compact and correctness-enforcing representation of both states and operators. Although such constructions won't be here addressed, we will lay out some essential notation, definitions and properties.

Tensor networks primer

As far as our purposes are concerned, we can think of a Tensor Network as a multidimensional collection of complex numbers, with the *rank* of the tensor being the number of indices it has. For example, a rank-0 tensor is just a number (a *scalar*), rank-1 tensors can be seen as vectors[19] v_j, whilst rank-2 tensors with indices i and j can be represented as a matrix A_{ij}. An essential operation, *index contraction* is the sum over all possible values of the repeated indices of a set of tensors. Few examples are sufficient to illustrate this. Consider first a vector v_j and construct the rank-2 tensor $A_{ij} \equiv v_i^* v_j$. The only contraction here possible is $\sum_i A_{ii} \equiv \sum_i v_i^* v_i = \sum_i |v_i|^2$, which is the usual euclidean norm of the vector. Now, consider two rank-2 tensors A_{ij} and B_{kl}. The contraction $\sum_j A_{ij} B_{jl}$ gives a new rank-2 tensor C_{il} with components $C_{il} = \sum_j A_{ij} B_{jl}$, as it should, since that's just the usual matrix multiplication. And as the latter, the contracted indices' dimensions must match, unless otherwise explicitly stated - a rule which holds for every contracted pair. This operation is crucial for building more complex TNs, as it allows us to combine different tensors into a single one.

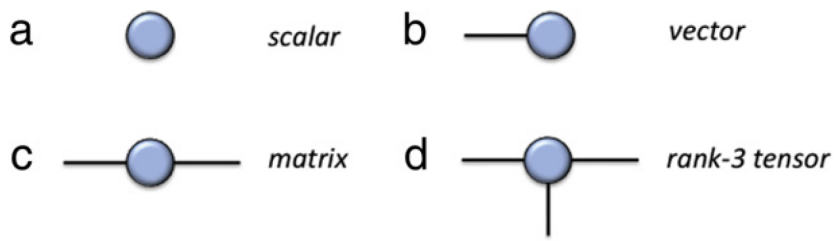

Figure 2.1: Tensor Network diagram taken from [49]. It connects the notion of open/free indices to the existence of those free lines that connect the blue dot to no other dot. **a.** The rank-0 tensor is a scalar, and it has no free indices. **b** The rank-1 tensor is a vector, and it has one free index. **c.** The rank-2 tensor is a matrix, and it visibly has two open indices. Analogously, **d.** the rank-3 tensor has three free indices, and it can be represented as a parallelepiped - or as a stack of matrices.

Please, notice that a blatant difference of indexes' character is presented as soon as contractions are inserted in the rules. The indices i and l are called "free" or *open* indices, meaning that they can take any value - within their respective dimensionality - while the index j is a "dummy" one, given that it is being summed over. This distinction is important because it

[19] Notions such as transformation properties of geometrical entities and the subtletites in defining vectors through them are not necessary in our present level of discussion.

allows us to keep track of which indices are "integrated out" and which ones are free. It is immediate that in the absence of free indices, the tensor is of rank-0, i.e. a scalar. Those notions are diagramatically represented in Fig. 2.1, whilst some contractions are pictured in Fig. 2.2. The reader is invited to find the corresponding diagram for the trace of a transfer matrix like the one that shows up in solving the 1D Ising model under periodic boundary conditions, i.e., $\mathcal{T} = \sum_{\{\sigma_1,\sigma_2,...,\sigma_N\}} V_{\sigma_1\sigma_2} V_{\sigma_2\sigma_3} ... V_{\sigma_N\sigma_1}$, where the V's are the elementary 2x2 transfer matrix elements. This is a very important point to keep in mind, as it will be crucial for understanding the MPS representation of quantum states. As a final note, we would like to point that doing contractions for arbitrarily arranged TNs is a VERY hard task. In fact, it is rigorously known that general Tensor Network contractions are NP-hard [136], and people usually try to optimize by approaching specific cases through certain heuristics. We won't delve into such complications here, but the interested reader would benefit from checking references such as [137, 138].

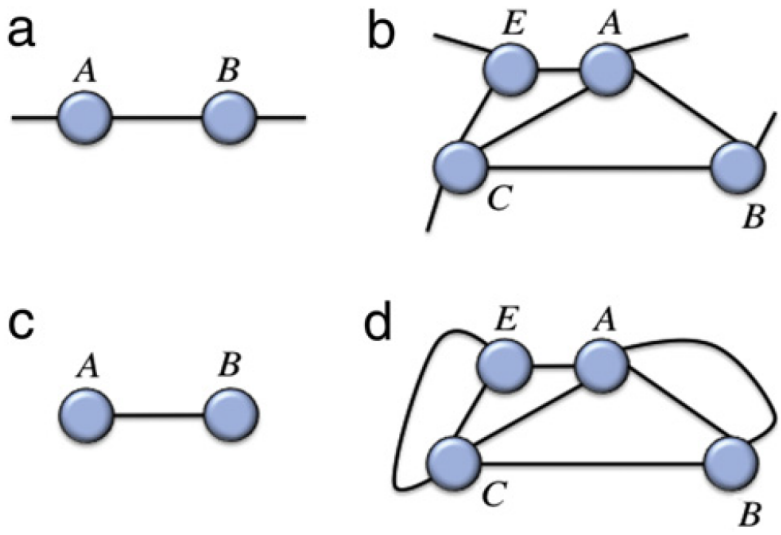

Figure 2.2: Diagrammatic representations in Tensor Network "language" for **a.** a product of matrices (contraction of 2 rank-2 tensors), **b.** the contraction of a complex assembly of 2 rank-3 and 2 rank-4 tensors that yields a rank-4 tensor, **c.** the contraction of two vectors, i.e., the scalar product and **d.** a possible *full contraction* of the rank-4 tensor obtained at **b**. From this depiction, it must be understood that lines connecting tensors (the blue dots) signal contractions. Picture originally found in [49].

MPS overview

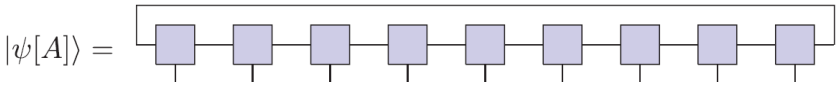

Figure 2.3: MPS representation of a quantum state. The open indices are *physical*, and the closed ones are called *bond* or *ancilliary* indices. Picture from [135].

MPS are essentially one-dimensional Tensor Network states like the one shown in Fig.2.3. Those bonds connecting the tensors (here, the purple boxes) are called *bond* or *ancilliary* indices, and they are the ones that will be contracted in order to obtain the final state. The open indices are called *physical* indices, and they represent the degrees of freedom of the system. Before writing

it down, let us first explain some essential properties of MPS in a somewhat brief manner.

1. **Suitable for 1D translationally invariant systems.** While in principle each of those purple boxes in Fig. 2.3 could host distinct tensors, it is also possible to instill translational invariance by choosing a given unit cell of tensors that is repeated over the lattice - even if an infinite number of times, whereby thermodynamics might be obtained.

2. **The set is dense.** MPS are a complete set of states, meaning that any state can be approximated by an MPS with sufficiently large bond dimension. This is a very important point, as it allows us to use MPS to approximate any state we want, and it is one of the reasons why DMRG works so well. However, to cover "sufficiently distant" states, the bond dimension D must grow exponentially in the system size.

3. **Capture 1D area law by construction.** The Entanglement Entropy of a bipartition of the system is proportional to the number of bonds that cross the cut, which is a direct consequence of the MPS structure. This means that MPS can efficiently represent states with low entanglement, such as the already mentioned ground states of gapped local Hamiltonians. The fact that $O\left(logD\right)$ is proportional to EE's upper bound was highlighted at the end of section 2.3.4 already.

4. **Exponentially decaying correlations.** Pairwise correlation functions of MPS decay exponentially for large distances. This implies that a finite correlation length ξ is always present for any finitely-truncated MPS. Such is the case for DMRG, whereby *finite-size scaling* schemes are implemented whenever gapless hamiltonians are to be studied. This bias must always be kept in mind when interpreting results and doing extrapolations. More about that will be said when the KAF is discussed. A particularly instructive argument for this exponential behavior can be found in [49].

5. **Expectation values are exactly computable.** For instance, the scalar product between two MPS can always be done in at most $O(LdD^3)$ operations, where L is the number of sites, d is the local dimension and D is the bond dimension, as before.

The next step would be showing how might an arbitrary quantum state be decomposed into MPS form. To this, we refer the reader to great expositions such as [49, 74, 135]. The main idea is to use the SVD to express the state in a form that can be represented as an MPS. The SVD allows us to decompose a matrix into a product of three matrices, one of which is diagonal. This decomposition is crucial for understanding the entanglement structure of quantum states and for efficiently manipulating them in TN algorithms - bells that ring in the ears of those who have already read the previous section on DMRG. Lastly, we would like to emphasize that, from a modern viewpoint, DMRG can be understood as a variational method over the space of MPS. Each DMRG sweep optimizes one tensor at a time while keeping others fixed, effectively minimizing the energy with respect to a restricted yet highly expressive variational manifold. Operationally speaking, those sweeping updates across the chain correspond to sequential tensor contractions and Schmidt decompositions that redistribute entanglement efficiently. Even though we believe to have sufficiently stressed already, notice the core idea behind using MPS

ansätze once more: physical ground states of gapped local 1D systems typically obey an area law for entanglement, making them naturally compressible into said form with small bond dimension [53, 117–119].

2.4 Outlook on quantum materials

Quantum materials lie at the confluence of contemporary fundamental physics and technological revolution. Their rich landscape — from topologically protected edge states to entangled magnetic phases — highlight the vast space of possibilities that arise from quantum interactions. However, the full complexity of these systems is often veiled by strong correlations and frustration, requiring novel theoretical and numerical tools. Looking ahead, the road is both steep and promising. Strain engineering, non-equilibrium phases, and multi-orbital quantum simulations are all compelling avenues. TNs, bolstered by entanglement-based reasoning with continued algorithmic refinement, are likely to remain central, and have already found their way into field-theoretical grounds - e.g., cMPS and cMERA, with "c" standing for *continuous*. As experimental capabilities inch closer to theoretical ambitions, the interplay between emergence, effective Hamiltonians, and real materials will demand deeper integration of physical intuition, numerical strategy, and perhaps even machine-learned guidance.

Chapter 3

Many ways to be frustrated

Frustration is a cornerstone concept in condensed matter physics, describing systems where competing interactions prevent the simultaneous minimization of all energy terms, typically leading to highly degenerate ground states and exotic behaviors. This phenomenon, in its subclass dubbed *Geometric Frustration*, is particularly pronounced in lattice structures like the kagome, where corner-sharing triangles inherently defy conventional ordering. Historically, however, it was through the exploration of Spin Glass (SG) physics that frustration was first appreciated. In this chapter, we explore its origins and implications, starting with some words on that particular class of disordered spin systems. We then present the usual example of Ising and XY (planar) spins in a triangle, contrasting their physics with that of Heisenberg spins in the same configuration. By progressing to QSLs, then focusing on the kagome lattice as a key platform, we finally conclude with a concise review of the quantum Kagome Antiferromagnet controversy and some known results for the anisotropic KAF, whence setting the stage for our deformed-lattice investigations in later chapters.

3.1 Origins of frustration: spin glass physics

The study of spin glasses - disordered magnetic systems characterized by random, competing interactions between spins [139] - gave rise to the concept of frustration, embedded in models such as the Edwards-Anderson [140], in the mid 1970s. This model essentially describes classical Ising spins ($S_j = \pm 1$) on a lattice with nearest-neighbor exchanges that are normally-distributed around zero, thereby hosting the competing ferromagnetic (FM) and antiferromagnetic (AF) bonds. Such competitions lead to "rugged" energy landscapes with numerous metastable states [141]. This degeneracy precludes conventional magnetic ordering: it fosters a "frozen" disordered state below a critical temperature, instead. Early theoretical tools, including the "replica-trick" [139] and mean-field approximations[1] enlightened the slow dynamics [142] and memory effects [143] emblematic of SGs. However, while SGs highlight frustration due to disorder, there are alternative paths to explore mutually incompatible arrangements in perfectly ordered lattices, where geometry alone can induce similar effects. This so-called *Geometric Frustration* is of central importance to our work, whereby our attentions will be completely devoted to it, now

[1] As we would intuitively expect, mean-field techniques like Parisi's *cavity-method* [115, 139], are more amenable to long-range models such as the Sherrington-Kirkpatrick [141].

that we made some justice about frustration's historical origin.

3.2 Frustration in simple spin problems: Ising, O(2) and Heisenberg on a triangle.

To grasp frustration intuitively, consider the simplest frustrated system: three spin-1/2 Ising spins on an equilateral triangle with AF nearest-neighbor interactions[2], described by the Hamiltonian:

$$H = J \sum_{\langle i,j \rangle} S_i S_j, \quad J > 0, \quad S_i = \pm 1/2. \tag{3.1}$$

Here, $\langle i, j \rangle$ denotes nearest-neighbor pairs, and J is the coupling strength. For two spins, the ground state is degenerate, but straightforward: one spin up $(+1)$, one down (-1), yielding an energy of $-J/4$. Adding a third spin, and enforcing the loop, introduces a dilemma: if two spins are antialigned (e.g., $S_1 = +1/2$, $S_2 = -1/2$), the third spin (S_3) cannot satisfy both neighbors simultaneously. Aligning $S_3 = +1/2$ satisfies S_2 but conflicts with S_1, and vice versa. The ground state thus has two spins aligned and one opposed (e.g., $+, -, +$), with an energy of $-J/4$, but there are six degenerate configurations due to permutation symmetry (e.g., $\uparrow\downarrow\uparrow$, $\uparrow\uparrow\downarrow$, etc.). This degeneracy arises because the triangular geometry prevents a fully antiferromagnetic arrangement[3], a hallmark of frustration. But that is not an exclusive feature of this Z_2 model.

Let us take the classical model, planar spin with $O(2)$ symmetry: $\vec{S} = \frac{1}{2}(\cos\theta, \sin\theta)$. On the same triangle, exploit the relation

$$H_{planar} = J \sum_{\langle i,j \rangle} \vec{S}_i \cdot \vec{S}_j \tag{3.2}$$

$$= \frac{J}{2}\left(\vec{S}_1 + \vec{S}_2 + \vec{S}_3\right)^2 - \frac{3J}{8}, \tag{3.3}$$

to notice that, minimizing the squared term requires it to vanish, i.e. $\vec{S}_1 + \vec{S}_2 + \vec{S}_3 = 0$. This is a very different situation from the Ising case, where the spins are forced to be aligned or antialigned. Here, the spins can take any direction in the plane, and the only requirement is that they sum to zero - whereby they compromise in a 120^o arrangement - no pair is perfectly happy, but the whole settles into what's possible nevertheless: a *canted* configuration. This leads to a continuous degeneracy of ground states, as any rotation of the spins around the center of mass will yield another ground state. The energy remains constant at $-\frac{3J}{8}$, but the possibilities are much richer[4].

Finally, as our last example on the importance of geometry, underlying symmetries and "quantumness", let us consider the Heisenberg model on the same triangle, in its spin-1/2

[2]Of course, this jargon is perfectly understood by the initiaded, but we insist on a brief clarification: whenever such presentations are made ("AF nearest-neighbor interactions"), specially for finite-sized problems as the case in point, we should understand that it is the low-energy sector that favors *antiparallel* alignment.

[3]Such failure to simultaneously minimize every term can also be achieved by the Villain Lattice [144]: a square with all terms ferromagnetic, but one. Since this is more akin to frustration of "bond-disorder" type, we mention it only for completion.

[4]The reader can easily imagine that this degeneracy would be even greater should we allow for a third dimension, i.e. $\vec{S}_i \in \mathbb{R}^3$, which gives yet another axis of freedom to the spins.

incarnation. The Hamiltonian can be written in analogy to the planar case, but now we have a quantized three-dimensional vector. The Hamiltonian reads:

$$H_{Heisenberg} = J \sum_{\langle i,j \rangle} \vec{S}_i \cdot \vec{S}_j \tag{3.4}$$

$$= \frac{J}{2} \left(\vec{S}_1 + \vec{S}_2 + \vec{S}_3 \right)^2 - \frac{9J}{8}. \tag{3.5}$$

A fundamental difference here arises: the total angular momentum squared cannot vanish, as it would in the planar case. This is because the total angular momentum squared is given by $\vec{S}^2 \equiv \left(\vec{S}_1 + \vec{S}_2 + \vec{S}_3 \right)^2 = S(S+1)$ ($\hbar = 1$), where S is the total spin quantum number. The ground state of this system is now only four-fold degenerate. The frustration here arises from the fact that the system cannot simultaneously minimize all interactions between the spins, as can be seen in the following ($S = 1/2$).

$$E^{GS}_{Heisenberg} = \frac{J}{2} S(S+1) - \frac{9J}{8} \tag{3.6}$$

$$= \frac{J}{2}\frac{3}{4} - \frac{9J}{8} = -\frac{3}{4}J, \tag{3.7}$$

and with the assumption of translational invariance, we can easily evaluate the correlations between each pair of spins. The correlation function is given by:

$$C_{ij} = \langle \vec{S}_i \cdot \vec{S}_j \rangle - \langle \vec{S}_i \rangle \cdot \langle \vec{S}_j \rangle, \tag{3.8}$$

which, by (3.7), gives us the following results for all i, j pairs:

$$C_{ij} = \langle \vec{S}_1 \cdot \vec{S}_2 \rangle - \langle \vec{S}_1 \rangle \cdot \langle \vec{S}_2 \rangle \tag{3.9}$$

$$= \frac{1}{3J} E^{GS}_{Heisenberg} - 0 \tag{3.10}$$

$$= -\frac{1}{4}. \tag{3.11}$$

This result is somewhat intriguing, given that the Heisenberg triangle can, in a sense, achieve what the Ising couldn't (-1/4 "correlation points" per pair). It is noteworthy that such arangement corresponds to an equally weighted combination of singlet and triplet subspaces.

3.2.1 Frustration signalers and quantifiers

Frustration in magnetic systems manifests itself through various indicators, both microscopic and macroscopic. Understanding and quantifying this phenomenon is crucial for exploring exotic magnetic phases. We will now discuss some of the most relevant and known measures of frustration found in the literature, weighting their advantages and disadvantages.

Toulouse's plaquette criterion

Toulouse captured the essence by defining certain "plaquette variables" or "loop-products" like the following [145]:

$$P_W \equiv (-1)^{\#\text{terms}} \prod_{<i,j>\in p} \text{sgn}(J_{ij}). \tag{3.12}$$

The idea is that we should take a given spin hamiltonian, e.g. $H = \sum_{i,j} J_{ij} S_i S_j$, construct elementary loops (the "plaquettes" p) whose connections are given by couplings J_{ij}, compute the latter's signs and evaluate the product. Frustration on a plaquette would then be signaled by $P_W < 0$, and to evaluate the system as a whole, we should gather all plaquette's results. This concept is analogous to the Wilson loop in lattice gauge theories and has been instrumental in understanding spin glasses and related systems. The utmost simplicity makes it instantaneously attractive. Its essential drawback, however, is a certain "low-resolution" nature, for the actual relative strenghts of the couplings are not taken into account.

Ramirez's frustration parameter

Ramirez [146] proposed a macroscopic measure of frustration, the *frustration parameter* f, defined as the following ratio:

$$f = -\frac{\Theta_{CW}}{T_c}, \tag{3.13}$$

with Θ_{CW} being the Curie-Weiss temperature and T_c the ordering temperature. This parameter quantifies the degree of frustration in a system, with $|f| > 1$ indicating strong frustration, as the system fails to order at temperatures where interactions are significant. It is specially useful for comparing different materials and understanding their magnetic properties. The obvious difficulty with this approach is that it requires a well-defined ordering temperature, which is not always present in strongly frustrated systems. Moreover, the Curie-Weiss temperature can be influenced by other factors, such as disorder or anisotropy, complicating the interpretation of f. Finally and most importantly, this parameter requires knowledge from finite temperature physics, which might mask potential critical features, should the measurements (or approximate calculations) have been performed at the inconvenient part of the phase diagram.

Residual entropy and Pauling's spin ice

Linus Pauling's study of water ice-like systems led to the concept of residual entropy, a measure of disorder in a system at absolute zero. In his work on spin ice [147], he found that the ground state is highly degenerate, leading to a non-zero residual entropy even at $T = 0$. This phenomenon arises from the Geometric Frustration present in the system, where competing interactions conspire to prevent it from settling into a unique ground state. The residual entropy can be quantified using the celebrated microscopic definition of entropy by Boltzmann:

$$S_{res} \sim \ln \Omega, \tag{3.14}$$

where Ω is the number of degenerate ground states. This measure is particularly relevant in systems like spin ice, where the residual entropy reflects the underlying frustration and the presence of equivalent low-energy configurations. Nevertheless, it is evident that not every degeneracy is a sign of frustration, as it can also arise from other factors like symmetries. A very sounding complementary result, certainly inspired by Pauling's work, is the one by Wannier [148], who showed that the residual entropy of a triangular lattice with Ising spins subject to no magnetic field is finite. This highlights the role of geometry in determining the ground state properties of a system and serves as a precursor to the concept of Geometric Frustration.

Anderson's block coupling energy

P.W. Anderson[5] introduced a nonlocal definition of frustration for spin glasses [149], focusing on the coupling energy accross boundaries between large blocks of spins. The method involves subdividing a spin system of N sites into m smaller blocks, each containing N/m spins - its volume - and with a surface area $A \propto l^{d-1}$ (where $l = (N/m)^{1/d}$), between neighboring blocks B_1 and B_2. Each block is allowed to independently reach its lowest energy state, with spins set to S_i^0. The coupling energy between said blocks is then given by:

$$E_{AB} = \sum_{i \in B_1, j \in B_2} J_{ij} S_i^0 S_j^0, \tag{3.15}$$

where J_{ij} are the coupling constants between spins in different blocks. A system is then deemed frustrated if the variance of this energy, $\bar{E^2}$, satisfies [149]

$$\lim_{A \to \infty} \frac{\bar{E^2}}{A} = 0 \rightarrow \text{frustrated}, \tag{3.16}$$

whilst for non frustrated local systems $\bar{E^2} \propto A^2$. Anderson interpreted the scaling in Eq. (3.16) as a result of the interactions between blocks having random signs, thus preventing an overall compatible ordered structure. This approach stands out in the study of disordered systems with its general applicability to various spin systems (Ising, Heisenberg, etc) and interaction ranges. It also succeeds in capturing an essential feature of frustration, that is, the globally disrupted long-range order. But its nonlocal nature[6] makes it less intuitive for identifying possible "local sources" of frustration. Moreover, it is more of an all-or-nothing rule, thereby missing out the potential gradients of frustration. Finally, it features the problem of generalizations: they don't seem to come out in an obvious way for, e.g., clean systems where frustration is a result of geometric constraints alone.

Kobe and Klotz's misfit parameter

Kobe and Klotz [150] proposed a quantitative measure of frustration through the so-called *misfit parameter*, which compares the ground-state energy of a frustrated system to that of an idealized

[5] Yes, him again. This gentleman worked until his very last days, and his contributions are so many that it is hard to keep track of them all.

[6] Perhaps an omen to the topological nature of QSL and other-problems-to-come.

reference system. The parameter, for a state i is defined as:

$$\mu_i = \frac{E_i - E_{min}^{id}}{E_{max}^{id} - E_{min}^{id}}, \tag{3.17}$$

where E_i is the energy of the state i, and E_{min}^{id} and E_{max}^{id} are the minimum and maximum energies of the idealized reference system, respectively, assuming all bonds are satisfied or unsatisfied:

$$E_{min}^{id} = -\sum_{<i,j>} |J_{ij}|, \quad E_{max}^{id} = \sum_{<i,j>} |J_{ij}|. \tag{3.18}$$

For the ground state, the misfit is $\mu_0 = \mu(E_0)$, which ranges between 0 (no frustration) and 1 (maximal frustration). For $\pm J$ spin glasses, μ_0 clearly represents the fraction of unsatisfied bonds. This measure somewhat shares Anderson's nonlocal criteria versatility, but it turns out to be even more so. It can be applied to both ordered and disordered systems right out-of-the-box, including spin glasses, Potts models and combinatorial optimization problems like graph partitioning [151–153]. Even more so, in the widening aspect of delving deeper into frustration's shades, it provides a quantification, a scale to measure such quantity. The most serious impediment to its usage seems to be the requirement of a reference system, since that may introduce ambiguity in problems with mixed interactions. Finally, a common feature among every measure that we have already commented in this thesis, with the exception of Toulouse's, is that they do not directly reveal local frustration sources.

3.3 Quantum spin liquids: frustration meets quantum mechanics

Frustration's complexity escalates in quantum systems, where fluctuations and entanglement give new colors to, if not amplify, degeneracy effects. QSLs represent an extreme manifestation, characterized by the absence of conventional magnetic order even at $T = 0$, sustained by massive entanglement and fractionalized excitations. Anderson's RVB theory pioneered this concept, proposing that spins form a superposition of singlet pairs, resonating across the lattice [33]. Unlike classical ordered states, QSL host exotic quasiparticles such as spinons (spin-1/2 excitations) and visons (topological defects), defying Landau's symmetry-breaking paradigm [34].

The theoretical allure of QSL is matched by experimental challenges. Materials like herbertsmithite ($ZnCu_3(OH)_6Cl_2$) and α-$RuCl_3$ are prime candidates, exhibiting no long-range order down to millikelvin temperatures [39, 154]. Herbertsmithite, with its kagome structure, shows a continuum of spin excitations suggestive of fractionalization [155], while α-$RuCl_3$ approximates the Kitaev model, potentially hosting Majorana fermions [156]. These systems underscore frustration's role in stabilizing QSL, but their ground states remain contentious due to experimental limitations (e.g., disorder) and theoretical ambiguities.

3.4 Geometric Frustration in the kagome lattice

The kagome spin lattice, a 2D network of corner-sharing triangles, is an archetypal frustrated system. Its geometry—three sites per unit cell connected by bonds forming a David star-like pattern—ensures that nearest-neighbor antiferromagnetic interactions compete relentlessly. For the classical Ising model on kagome, Ramirez estimated a ground-state degeneracy scaling exponentially with system size ($\sim 2^{0.501N}$, where N is the number of sites), reflecting an extensive entropy [146]. This degeneracy not only persists but is actually enhanced in the Heisenberg case ($H = J\sum_{\langle i,j\rangle} \vec{S}_i \cdot \vec{S}_j$), where continuous spin degrees of freedom amplify frustration effects.

3.5 The quantum kagome antiferromagnet controversy

The quantum Heisenberg model on the kagome lattice ($S = 1/2$) is a battleground for theoretical physics, with its ground state debated for decades. The Hamiltonian,

$$H = J \sum_{\langle i,j \rangle} \vec{S}_i \cdot \vec{S}_j, \quad J > 0, \tag{3.19}$$

looks simple, yet its low-energy physics eludes consensus. Early exact diagonalization studies suggested a disordered ground state with a spin gap [157], hinting at a gapped QSL. However, computational limitations (e.g., ≤ 27 sites) left open questions about finite-size effects.

Analytical approaches, notably the large-N expansions of Read and Sachdev based on Sp(N) symmetry, offered crucial early insights [158]. These expansions identified two distinct regimes: for large N, quantum fluctuations selected an ordered state from classically degenerate manifold configurations, while at smaller N, the system transitioned into a quantum-disordered phase featuring deconfined spinon excitations, thus hinting at potential fractionalization [158, 159]. Further analytical classifications were significantly advanced by Projective Symmetry Group analysis, pioneered by Wen and collaborators, systematically cataloging possible spin-liquid states by considering fractionalized spinon excitations transforming under lattice and local symmetries. This led to identifying numerous candidate states, particularly gapless $U(1)$ Dirac and gapped Z_2 spin liquids [37, 160].

The emergence of powerful Tensor Network methodologies, notably Density Matrix Renormalization Group, revitalized the debate. Yan et al. (2011) performed DMRG calculations on cylinders with circumferences up to 12 lattice spacings and found evidence for a gapped spin liquid with short correlation lengths and indications of Z_2 topological order [68]. Subsequent DMRG investigations by Depenbrock et al. (2012) and Jiang et al. (2012), employing larger bond dimensions and more comprehensive entanglement analyses, strongly argued for a gapped Z_2 QSL characterized by a finite spin gap and distinct topological Entanglement Entropy signatures [161, 162].

Meanwhile, alternative Tensor Network methods such as PEPS, Projected Entangled Simplex States (PESS), and MERA further complicated consensus. PEPS and PESS simulations, designed explicitly for two-dimensional entangled states, favored gapless $U(1)$ spin liquids [163, 164]. Similarly, MERA, optimized for critical systems, also inclined toward gapless phases [165]. The methodological divergences among these numerical approaches, it is worth

mentioning, could be influenced by intrinsic biases: DMRG, despite its precision, struggles with genuine two-dimensional long-range entanglement and is heavily dependent on extrapolations from quasi-one-dimensional geometries. Conversely, PEPS, PESS, and MERA balance accuracy against computational cost, at the expense of potentially introducing biases toward particular types of correlation structures.

Recent breakthroughs have added further complexity. A 2025 study leveraging machine-learning-enhanced variational Monte Carlo suggests an entirely different scenario: the kagome Heisenberg model may host a spinon pair density wave, preserving both time-reversal and lattice symmetries while breaking the conventional expectations of Dirac or Z_2 QSL states [166]. This result challenges prior outcomes rooted in both DMRG and PEPS-based analyses. Concurrently, the possibility of a chiral spin liquid has been theoretically revived, with recent work indicating that the kagome lattice may support time-reversal symmetry-breaking spin-liquid phases under purely Heisenberg interactions [167]. This expands the known landscape beyond Dirac and Z_2 paradigms.

On the experimental side, notably neutron scattering on candidate materials such as herbertsmithite, provide indirect yet compelling support for gapless QSL phases, revealing a broad continuum of excitations without detectable magnetic order [155]. However, the interpretation of such experiments remains challenging due to the complications arising from impurities, interlayer couplings, and lattice distortions, which prevent direct comparisons with ideal theoretical models. Moreover, recent discoveries have broadened the experimental horizon. In 2023, magnetization measurements on YCu3(OH)6.5$Br_{2.5}$ revealed a robust 1/9 magnetization plateau—suggesting the existence of a spin-gapped, potentially fractionalized, phase [168]. Intriguingly, another study demonstrated that moderate bond disorder in $YCu_3(OH)_{6.5}[(Cl_xBr_{1-x})_{3-y}(OH)_y]$ can stabilize a QSL state rather than destroy it, challenging the conventional wisdom that disorder is purely detrimental to topological order [169].

Finally, advanced spectroscopic probes have recently provided compelling evidence for Dirac spinon excitations in kagome antiferromagnets, lending experimental weight to theoretical models of gapless $U(1)$ QSL with Dirac-like dispersions [170].

As of 2025, the quantum Kagome Antiferromagnet controversy remains unresolved, yet increasingly rich. The community broadly agrees on the existence of a quantum spin liquid ground state but remains divided over its precise nature. Whether the kagome lattice hosts a gapped Z_2 liquid, a gapless $U(1)$ Dirac phase, a spinon pair density wave, or even a chiral spin liquid is an open and vibrant question. Achieving resolution will require not only further advances in numerical methods and analytical frameworks but also targeted experimental probes capable of directly interrogating fractionalized excitations, entanglement structures, and subtle symmetry-breaking phenomena.

3.6 Anisotropic kagome lattices

Anisotropy serves as a pivotal parameter in modulating the magnetic properties of kagome antiferromagnets. In the classical Heisenberg model, unequal exchange interactions ($J_1 \neq J_2 \neq J_3$) disrupt the extensive ground-state degeneracy characteristic of the isotropic kagome lattice. This lifting of degeneracy stabilizes various ordered phases, including ferrimagnetism and stripe

order, as demonstrated by Vojta et al. [171]. The authors evidenced how uniaxial strain along a lattice vector (e.g., $\boldsymbol{a}_1$) enhances specific bond strengths, thereby reducing frustration and inducing classical phase transitions.

In the quantum regime, the interplay between frustration, quantum fluctuations, and anisotropy gives rise to a rich and complex phase diagram. Schnyder, Starykh, and Balents [172] investigated the strongly anisotropic limit of the spin-1/2 Kagome Antiferromagnet, showing that spatial anisotropy drives the system away from a QSL towards magnetically ordered phases or valence bond crystals. Their exact diagonalization results indicate that the QSL is destabilized once the ratio between coupling constants crosses a critical threshold.

Further studies of the breathing kagome lattice—a variant where up-pointing and down-pointing triangles have different coupling strengths—demonstrate that the QSL phase is robust under moderate anisotropy but eventually gives way to a lattice-nematic phase as the anisotropy increases [173]. These results suggest that the kagome QSL is not indefinitely robust but exists within a finite window of parameter space.

Additionally, DMRG studies on kagome strip lattices have uncovered the emergence of magnetization plateaus whose stability is highly sensitive to anisotropic perturbations [174]. Certain plateaus remain stable when anisotropy aligns with the external field, while others collapse under transverse anisotropy. This highlights the subtle interplay between field orientation, anisotropy direction, and quantum fluctuations in determining the ground state.

These insights collectively underscore the potential of strain engineering as a powerful tool to systematically explore and manipulate the phase diagram of kagome antiferromagnets. Unlike electric-field-induced anisotropy, which modifies exchange couplings through charge redistribution [175], strain mechanically deforms the lattice, providing a direct geometric handle on frustration and quantum order.

3.7 Summary and outlook

Frustration transforms the already fascinating spin models into playgrounds for yet richer emergent phenomena, from classical degeneracy to quantum entanglement. The kagome lattice epitomizes this, hosting a contentious QSL debate that underscores the interplay of geometry, interactions, and computational methods. Anisotropic variants, particularly under strain, provide a promising avenue to resolve ambiguities and engineer novel states. In the next chapter, we explore straintronics as a tool to manipulate kagome physics, building on this foundation to investigate our strained nanoribbon system.

Chapter 4

Straintronics

Straintronics—the deliberate application of mechanical strain to tune the electronic, magnetic, or optical properties of materials—has emerged as a powerful paradigm in condensed matter physics and materials science. By deforming a lattice, hopping amplitudes can be modified, effective gauge fields might be induced, or phase boundaries may be shifted, offering a versatile control knob for quantum systems. This chapter traces straintronics' foundations in elasticity theory, its evolution through carbon-based nanostructures, and its extension to strongly correlated systems like the kagome lattice. We conclude by framing our Hubbard model study within this context, highlighting strain as a bridge between geometry and quantum many-body physics.

4.1 Elasticity theory and early electron-phonon studies

The roots of straintronics lie in elasticity theory, which describes how materials deform under stress. For a 2D lattice, the strain tensor $\bar{\epsilon}$ quantifies deformations relative to the undeformed state:

$$\bar{\epsilon}_{ij} = \frac{1}{2}\left(\frac{\partial u_i}{\partial x_j} + \frac{\partial u_j}{\partial x_i} + \sum_k \frac{\partial u_k}{\partial x_i}\frac{\partial u_k}{\partial x_j}\right), \tag{4.1}$$

where $\vec{u}(\vec{r})$ is the displacement field, and the nonlinear term accounts for large deformations. In the linear regime, this simplifies to the symmetric part of the displacement gradient. The material's response is governed by elastic constants (e.g., Young's modulus, Poisson ratio ν), linking strain to stress via Hooke's law.

At the microscopic level, electron–phonon coupling provides the bridge between elastic deformations and changes in electronic structure. A central concept here is the *Grüneisen parameter*, which quantifies the sensitivity of phonon frequencies to changes in volume (or, in two dimensions, area). For a phonon mode ν with momentum $\mathbf{q}$, one defines the mode-resolved Grüneisen parameter as

$$\gamma_\nu(\mathbf{q}) = -\frac{\partial \ln \omega_\nu(\mathbf{q})}{\partial \ln V}, \tag{4.2}$$

first introduced in the early 20th century [176, 177]. This quantity can differ strongly between acoustic and optical branches, and between different regions of the Brillouin zone [178].

For thermodynamic properties, such as the thermal expansion coefficient, it is convenient to introduce an *effective* or *macroscopic* Grüneisen parameter, obtained as a heat-capacity-weighted

average over all modes [179, 180]:

$$\gamma(T) = \frac{\sum_{\nu,\mathbf{q}} C_\nu(\mathbf{q},T)\,\gamma_\nu(\mathbf{q})}{\sum_{\nu,\mathbf{q}} C_\nu(\mathbf{q},T)}, \tag{4.3}$$

where $C_\nu(\mathbf{q},T)$ is the mode-specific heat. This effective γ is generally temperature-dependent: at low temperatures only acoustic modes contribute, while at high temperatures many phonon branches are thermally populated.

In the context of electronic structure modeling, a related but distinct parameter often appears: the bond-level Grüneisen parameter, commonly denoted β. This measures how electronic hopping amplitudes change with bond stretching due to the exponential sensitivity of orbital overlap:

$$t_{ij} = t_0 \exp\left[-\beta\left(\frac{|\vec{r}'_{ij}|}{|\vec{r}_{ij}|} - 1\right)\right], \tag{4.4}$$

where t_0 is the unstrained hopping and $\vec{r}'_{ij}$ the strained bond vector. Typical values $\beta \sim 2-4$ have been reported for carbon-based systems, consistent with both density-functional-theory (DFT) calculations and Raman experiments [178, 181, 182].

Experimentally, Grüneisen parameters can be accessed in several ways. Mode-resolved $\gamma_\nu(\mathbf{q})$ is obtained from high-pressure Raman or infrared spectroscopy, by tracking phonon frequency shifts under controlled strain or hydrostatic pressure [183]. The macroscopic $\gamma(T)$ can be extracted from thermal expansion and specific heat measurements [180]. Bond-level β is usually inferred indirectly from the strain dependence of bandgaps (e.g., in carbon nanotubes and graphene) or from fitting tight-binding models to DFT-computed hopping integrals under lattice distortions [184].

4.2 Straintronics in graphene: a pioneering case

Graphene, a 2D honeycomb lattice of carbon atoms, catalyzed straintronics' rise in quantum materials. Its discovery in 2004 [185] revealed exceptional mechanical and electronic properties, making it an ideal testbed. Castro Neto and collaborators pioneered the theoretical framework, showing that strain mimics a pseudo-magnetic field due to lattice distortions [186, 187]. For small, long-wavelength deformations, the displacement field $\vec{u}(\vec{r})$ modifies the Dirac Hamiltonian via an effective vector potential:

$$\vec{A} \propto \beta\,(\epsilon_{xx} - \epsilon_{yy}, -2\epsilon_{xy})\,, \tag{4.5}$$

where ϵ_{ij} are strain tensor components. This gauge field, reaching strengths of 10–300 T in experiments [187], shifts Dirac cones without breaking time-reversal symmetry, unlike real magnetic fields. Experimental observations have confirmed that mechanical deformations in graphene can lead to significant pseudomagnetic fields, resulting in sublattice symmetry breaking and pseudospin polarization. Such effects have been proposed as mechanisms for developing valleytronic devices, including THz valley filters [188]. Strain engineering in graphene nanoribbons has been theoretically shown to induce topological phase transitions between quantum spin Hall and quantum anomalous Hall states without the need for external magnetic fields. This is achieved

through the interplay of strain-induced pseudomagnetic fields and spin-orbit coupling [189]. As a final example on graphene's rich interplay due to its pseudomagnetic field capabilities, we can mention a paper by Faria et al. on strained graphene rings which have brought evidence that circularly symmetric deformations lead to *inhomogeneous* current distributions, thus providing important insights into the differences between "real" and "pseudomagnetic" fields [73].

We also mention in passing that the integration of mechanical strain into graphene systems has significantly advanced the control of transport properties, by offering a versatile approach to modulate electronic states. With strategically applied deformations, it is possible to engineer electronic pathways, induce valley polarization, and create nanoscale waveguides, thereby expanding the functional capabilities of graphene in electronic applications and quantum simulators[190–192].

For larger or uniform strains, the picture shifts to "UV-changes"—direct microscopic renormalization of hopping amplitudes rather than emergent fields. Guinea et al. (2010) modeled uniform strain on graphene, finding that strong uniaxial tension ($\epsilon \sim 20\%$) opens a bandgap by merging Dirac points [72]. This stems from anisotropic hoppings ($t_1 \neq t_2 \neq t_3$) across the honeycomb's three bond directions, disrupting the conical dispersion. Experimentally, straintronics in graphene has enabled pseudomagnetic field mapping via scanning tunneling microscopy (STM) [187] and strain-engineered superconductivity in twisted bilayers [193], thereby highlighting its technological promise once more.

4.3 Strain in non-interacting kagome lattices

The kagome lattice, with its corner-sharing triangles, extends straintronics to frustrated systems. In the non-interacting tight-binding model,

$$H = -\sum_{\langle i,j\rangle,\sigma} t_{ij} c_{i\sigma}^{\dagger} c_{j\sigma}, \tag{4.6}$$

strain modifies hoppings t_{ij} per Eq. (4.4). Liu (2020) theoretically demonstrated that applying specific strain patterns to a kagome crystal can induce uniform pseudomagnetic fields, leading to the formation of pseudo-Landau levels and quantum oscillations in both the density of states and electrical conductivity [194]. This work highlights the potential of strain engineering in manipulating electronic properties of kagome systems, drawing parallels to similar phenomena observed in strained graphene. Mojarro et al. (2023) studied kagome nanoribbons under uniaxial strain, showing that deformation angle θ tunes Dirac cones and flat bands [195]. They found that, at specific angles (e.g., along lattice vectors), strain-induced anisotropy splits the flat band and can trigger the emergence of edge-localized topological states. Notably, when spin-orbit coupling is added to the model, these strained kagome systems can host Chern insulating phases (i.e., inducing topological edge states) or strain-tunable topological transitions.

Topological aspects amplify strain's impact. Kane and Mele's seminal work on spin-orbit coupling in graphene inspired kagome studies, where strain can induce a quantum anomalous Hall effect [196]. Jiang et al. (2019) demonstrated that the Lieb and Kagome lattices can be tuned into one another via strain, leading to topological phase transitions [197]. These non-

interacting results establish strain as a geometric control parameter, but interactions—central to kagome's exotic phases—require further exploration.

4.4 Straintronics in strongly correlated kagome systems

Strong correlations, as in the Hubbard or Heisenberg models, complicate strain's role. Vojta et al. (2022) investigated the classical kagome Heisenberg model under strain, finding that anisotropic couplings ($J_1 \neq J_2 \neq J_3$) lift frustration, stabilizing ferrimagnetic or stripe phases [171]. In the quantum regime, strain's effect on the KAF is less studied. Studies on anisotropic kagome systems, as displayed in Chapter 3, highlight the possibilities of QSL-like and 1D-like states as anisotropy increases. Once more, those corroborate with the idea that strain could interpolate between 2D frustrated and 1D ordered physics, a hypothesis we test in Chapter 5.

Strain contrasts with other anisotropy methods, like electric fields. Sun et al. (2019) applied electric fields to kagome magnets, effectively tuning exchange via charge redistribution [175]. While feasible, this approach lacks strain's direct geometric control, even though the former has the feature of preserving lattice symmetries while reshaping interactions - a quality that is very desirable in certain contexts.

4.5 Framing our problem: strain and the kagome hubbard model

Our work intersects frustration, strong correlations, and straintronics. The kagome lattice's inherent frustration, paricularly in the context of strong Coulomb repulsion (U), hosts a rich phase diagram—metallic, insulating, and very likely QSL-like states [68]. Strain introduces anisotropy, modifying hoppings as:

$$t_{ij}(\theta) = t \exp\left[-\beta\left(|\vec{a}'_\alpha(\theta)| - 1\right)\right], \tag{4.7}$$

where we make a slight change of notation for the nearest-neighbor vectors and write them as $\vec{a}'_\alpha = (\boldsymbol{I}+\bar{\epsilon})\vec{a}_\alpha$. $\bar{\epsilon}$ is the already introduced strain tensor. This framework, inspired by graphene's UV-changes, targets the strong-coupling regime ($U/t \gg 1$), where frustration and magnetism dominate the low-energy physics.

Non-interacting kagome studies provide a baseline: strain tunes band structures and topology. Interacting results suggest that order emerges from anisotropy in certain quantum [173] and classical [171] setups. Quantum correlated cases hint at phase tunability. Our contribution—exploring strained kagome nanoribbons with DMRG—merges these threads, probing how strain reshapes frustration and magnetic correlations. As we have independently realized in our investigations (see Chapter 5), strain can drive transitions between 1D-like and 2D-like phases, potentially allowing the probe of topological characteristics that persist under deformations, thereby offering insights into the KAF controversy and straintronics' broader potential.

4.6 Summary and outlook

Straintronics evolves from elasticity and electron-phonon physics into a transformative tool for quantum materials. Graphene showcased its power, while kagome studies reveal its reach into frustration and topology. In strongly correlated systems, strain promises unprecedented control over quantum phases, bridging classical order and quantum disorder. The next chapter applies this paradigm to our strained kagome nanoribbon, testing strain's ability to sculpt many-body physics.

Chapter 5

Results on the uniaxially strained nanoribbon

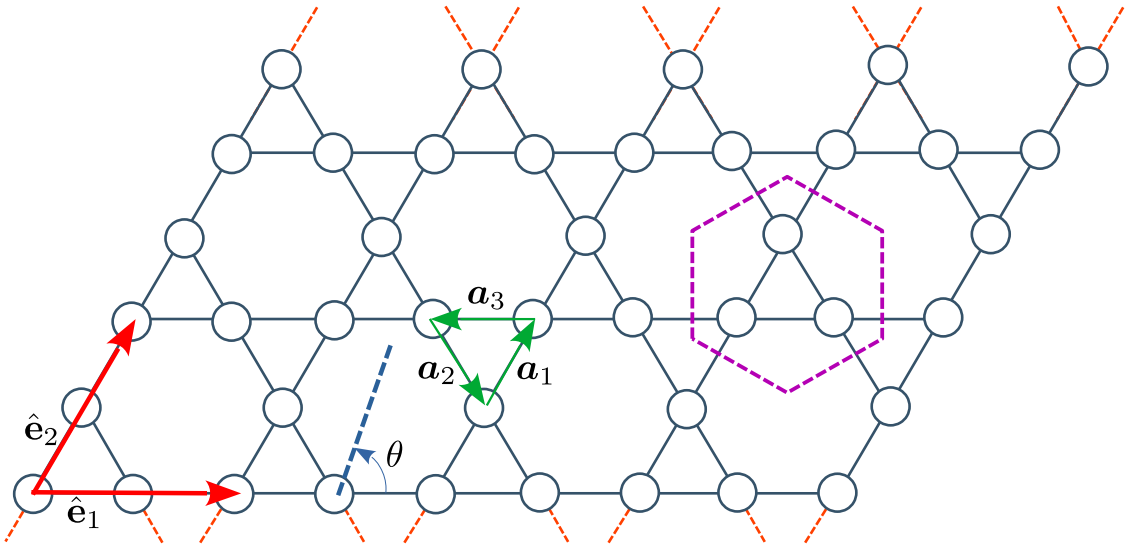

Figure 5.1: Schematic representation of a kagome nanoribbon in the *Flat Ribbon Geometry (FRG)*. The atomic sites with localized orbitals are drawn as circles. Solid lines correspond to nearest-neighbor hopping matrix elements. Dashed orange lines (bottom and top) hint at the possibility of periodic boundaries, in which case the ribbon is arranged into a *Long Cylinder Geometry (LCG)*. The lattice vectors are $\hat{\mathbf{e}}_1$ and $\hat{\mathbf{e}}_2$, whilst $\boldsymbol{a}_j$ $(j = 1, 2, 3)$ connect nearest-neighbors. Dashed blue axis at the lower edge comprises θ: whereby defining the direction of applied strain with respect to $\hat{\mathbf{e}}_1$. This figure corresponds to $L_x = 4$ unit cells along the x direction and $L_y = 3$ unit cells along $\hat{\mathbf{e}}_2$. The dashed hexagon (magenta) contains a convenient unit cell and associated bonds that are shown useful afterwards in the text.

We now wish to explore many-body effects on the kagome lattice subject to uniaxial strain. In Ref. [195] the authors find interesting single-electron features, and a natural inquiry is whether those are persistent, transformed or completely washed away in the presence of interactions. Apart from our findings [1] of *intersticial sites* and their magnetic properties, one of the most interesting contributions we have given is the quantification of frustration through intuitive functions. We show how they agree and display predictive power at the spin-dominant phase.

5.1 Model and methods

Our starting point is the following single-orbital tight-binding Hamiltonian:

$$H = \varepsilon_0 \sum_{j,\sigma} n_{j\sigma} - \sum_{\substack{<i,j> \\ \sigma}} t_{ij} c^{\dagger}_{i\sigma} c_{j\sigma} + \sum_{j} \left(U n_{j\uparrow} n_{j\downarrow} + V_z S^z_j \right), \tag{5.1}$$

where $c^{\dagger}_{j\sigma}$ ($c_{j\sigma}$) are the usual fermion creation (annihilation) operators with on-site energy ε_0 and spin σ at site j, $n_{j\sigma} = c^{\dagger}_{j\sigma} c_{j\sigma}$ is the number operator and $S^z_j = \hbar \left(n_{j\uparrow} - n_{j\downarrow} \right)/2$ is the local spin z-component. U quantifies Coulomb repulsion due to double occupancy, and $V_z = g\mu_B B$ is the Zeeman energy in the presence of a magnetic field B along spin z-direction[1]. The hopping matrix elements between nearest-neighbor sites (denoted by $< i, j >$), are modified by the presence of a spatially homogeneous uniaxial strain in the ribbon as

$$t_{ij} \equiv t_\alpha(\theta) = t \exp\left[-\beta \left(\| \boldsymbol{a}'_\alpha(\theta) \| - 1 \right) \right], \tag{5.2}$$

where β is the material-dependent Grüneisen parameter ($\simeq 3$ for kagome sheets [198]), $\boldsymbol{a}'_\alpha = (\boldsymbol{I} + \bar{\epsilon})\, \boldsymbol{a}_\alpha$ are the strained vectors, $\boldsymbol{a}_1 = \frac{1}{2}\left(1, \sqrt{3}\right)$, $\boldsymbol{a}_2 = \frac{1}{2}\left(1, -\sqrt{3}\right)$ and $\boldsymbol{a}_3 = -(\boldsymbol{a}_1 + \boldsymbol{a}_2) = (-1, 0)$ define the unstrained vectors (see Fig. 5.1), and set the nearest neighbor separation as the unit length. Vector norm is denoted by $\|\boldsymbol{v}\|$, as usual. Finally, the strain tensor is [195]

$$\bar{\epsilon} = \epsilon \begin{bmatrix} \cos^2\theta - \nu \sin^2\theta & (1+\nu)\sin\theta\cos\theta \\ (1+\nu)\sin\theta\cos\theta & \sin^2\theta - \nu\cos^2\theta \end{bmatrix}, \tag{5.3}$$

where, ϵ is the relative deformation, ν the well-known Poisson ratio[2] and θ the direction of applied strain, as indicated in Fig. 5.1.

In order to study its low-energy physics, we subject our system to the Density Matrix Renormalization Group (DMRG) via ITensor library implementation [199, 200] in the Julia language [201][3]. This Matrix Product States[4] platform is by now thoroughly established, and easily allows the calculations of many physical quantities relevant for quantum many-body systems. In the problem at hand, given large enough U, we might achieve quite interesting insights just by looking at local magnetizations $M^z_j = \langle S^z_j \rangle$ and Nearest-Neighbor Spin-Spin Correlations (NNSSC for short, and hereafter dubbed *link correlations*) $C_{ij} = \langle \boldsymbol{S}_i \cdot \boldsymbol{S}_j \rangle - \langle \boldsymbol{S}_i \rangle \cdot \langle \boldsymbol{S}_j \rangle$, where $\mathbf{S}_j$ is the spin operator on a given lattice site j, and $\langle \cdots \rangle$ represents the low-temperature thermal average, done in order to remedy effects of spurious degeneracies.

[1] Chosen to lie along the lattice plane (zero flux), whereby avoiding Peierls phases.

[2] In our implementations, we have used $\nu = 0.165$.

[3] Besides the original papers, we can benefit from very helpful tutorials and code examples found at https://itensor.org/docs.cgi?page=tutorials (C++ centered) or https://docs.itensor.org/ITensors/stable/examples/ITensor.html (Julia language docs). Both hyperlinks were functioning at September 2025.

[4] See discussion on Tensor Networks in Chapter 2.

5.2 Numerical results for the Hubbard model

Hereafter, the energy scale is defined by setting $t = 1$, $\hbar = 1$, and since we want to study half-filling properties, $\varepsilon_0 = -U/2$. The phase-tuning ("metal vs insulator") parameter is thus U, whose representative values of 5, 10 and 20 were used in our numerics. It is important to highlight that, despite being simple to construct and enunciate, the Hubbard nanoribbons in kagome lattices have an intriguing phase diagram whose exploration was only recently started [202]. As one would have thought, the large U behavior seemingly corresponds to Heisenberg physics, whilst an intermediate phase emerges as U decreases. According to [202] $U = 5$ amounts to a metallic system, $U = 10$ gives a so-called "Translational Symmetry Broken Insulator" which nears the QSL/KAF phase and $U = 20$ is deep into that regime. System finiteness, of course, should constantly remind us about the delicacy of applying a "phase" concept. Nevertheless, as we discuss next, qualitative distinctions are appealing enough to enable the resolution between ground state behaviors for distinct U values.

Therefore, following Refs.[68, 202], we construct a ribbon with $L_x = 12$ and $L_y = 3$, thus amounting to a total of $N = L_y(3L_x + 2)$ lattice sites. Under the adopted Long Cylinder Geometry (LCG) this yields the YC6 cylinder, as described in just-referenced papers. If no spatial periodicity is made, we get what will be referred to as a Flat Ribbon Geometry (FRG). Another important set of parameters are given by DMRG tuning choices: we have tolerated truncation errors typically under 10^{-6} and used tensors as building-blocks for Matrix Product States with bond dimensions (χ or m as per the notations used in previous chapters) up to 5000.

5.2.1 Base case: the relaxed system

The unstrained system is an obvious first step to not only gauging the DMRG convergence but also establishing a natural reference to constrast with deformed lattice properties. Even though the Kagome Antiferromagnet is known to be a notoriously difficult problem, with a ground state that supposedly hosts quantum spin liquid order of yet unknown characteristics [65, 67, 68, 155, 157, 161, 202–207], we constrain ourselves to the task of obtaining reliable information about link correlations.

By focusing on spatially representing correlation strengths the idea of *spatial link correlation* obtains:

$$\mathcal{C}_{\text{link}}(x, y) = \sum_{i,j} C_{ij} e^{-d_{ij}(x,y)/b}, \tag{5.4}$$

with $d_{ij}(x, y)$ the distance between some point and the line segment that connect lattice sites i and j. b is but an "aesthetical parameter" to control how sharp the link structure appears and we again have $C_{ij} = \langle \boldsymbol{S}_i \cdot \boldsymbol{S}_j \rangle - \langle \boldsymbol{S}_i \rangle \cdot \langle \boldsymbol{S}_j \rangle$. This quantity enables pictures like the following, thus giving a better grasp of the resulting correlation profile in Fig. 5.2. At (a) we see homogeneous yet mostly fainting link correlations, thereby indicating that no significant magnetic ordering can be inferred from the short-range correlations in that system. This corroborates with a metallic one. As Coulomb repulsion increases, however, besides from the overall antiferromagnetic character becoming clearer, it is easy to notice that bonds' thicknesses are distributed in distinct

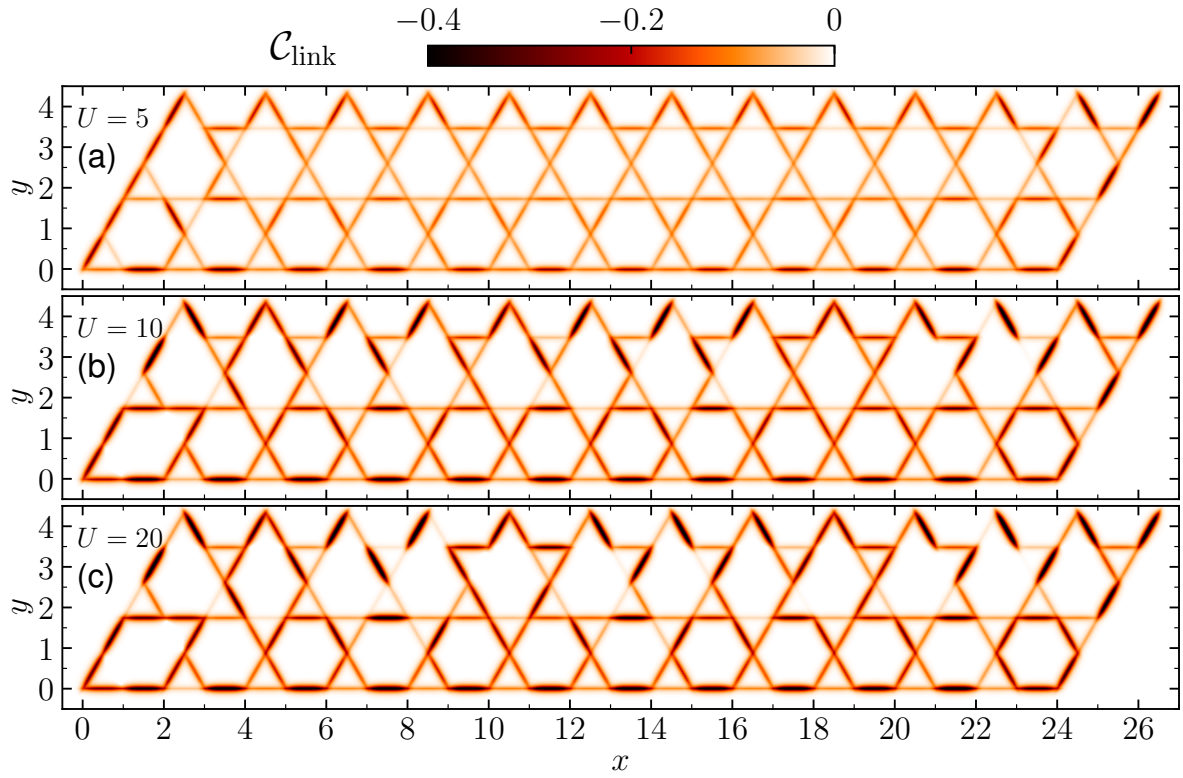

Figure 5.2: Link correlations, $\mathcal{C}_{\text{link}}$, in the absence of strain ($\epsilon = 0$) for (a) $U = 5$, (b) $U = 10$ and (c) $U = 20$. Darker "bonds" represent antiferromagnetically favorable alignments, clearly enhanced for $U = 20$. The uniform link distribution in (a) becomes more inhomogeneous for increasing U. Apart from strong links along the edges of this open ribbon, there appears to be no overall order of the antiferromagnetic bonds in (c).

ways throughout the sample. This is very evident in panels (b) and (c). Those inhomogeneities can be understood if we consider edges that do not belong to triangles. Notice how they always "concentrate" link correlations, whence tending to singlet-like behavior[5]. Such patterns likely emerge as a way out of energetic losses due to Geometric Frustration (GF). Once the otherwise homogeneous structure is perturbed by such correlation rearrangements, the profiles above become reasonable. All $\mathcal{C}_{\text{link}}$ plots are for FRG, unless otherwise stated.

5.2.2 Strained system

The effects of applied unixial strain are now analyzed. Since its consequences depend on the orientation θ, we plot the ground-state energy per site E_0 as a function of θ for several relative deformation values with a fixed repulsion strength of $U = 5$. Going from $\epsilon = 0.10$ up to $\epsilon = 0.30$, we construct the 2x2 plot in Fig. 5.3. Blue circles account for FRG energies, whilst red squares give LCG ones. The black-dashed line is $\zeta(\theta)$, the reciprocated hopping variance, hereby dubbed *coupling isotropicity*. Its interpretation as a *frustration quantifier* will be discussed later on. Some interesting nuances are present in the aforementioned figure. Panel 5.3(a) informs that FRG energies, in the given scale, oscillate little to nothing as a function of θ. On the other hand, LCG behavior is much more sensitive to strain axis orientation: the peak around 0.3π

[5]One might readily conclude so by observing, say, the bottom links: sites that belong to stronger bonds talk little or nothing one to another, even if they have a nearest-neighbor connection.

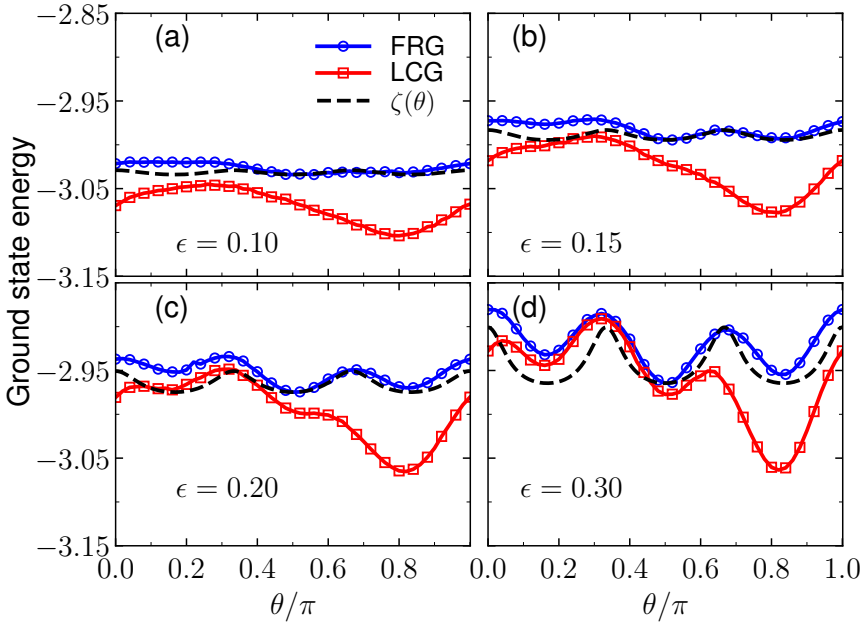

Figure 5.3: (a) Ground state energy per site, E_0/N, as function of strain direction θ for $\epsilon = 0.10$ (a), $\epsilon = 0.15$ (b), $\epsilon = 0.20$ (c) and $\epsilon = 0.30$ (d). Blue and red curves correspond to FRG and LCG respectively. The black dashed line shows $\zeta(\theta)$ defined in Eq. (5.5) and properly scaled. In all panels $U = 5$, i.e., in the metallic regime for the unstrained system.

is shifted about 0.05 units relative to the valley nearing 0.8π. Such order of broadening only shows up for the FRG at panel (d) - a deformation of 30% - but at this point the LCG energies have an amplitude of ~ 0.15 already. Regarding the curve shape, as we could expect from the ribbon geometry, the energies are neither $\frac{\pi}{3}$ periodic nor symmetric around $\frac{\pi}{6}$ - which would be the case for a bulk material. Finally, increasing deformations make the plot develop into well-defined maxima and minima as θ varies. Observe how not only larger strain resolves the energy peaks but it also increases the average values around which oscillations occur. Although the dependence on strain direction for FRG is better defined for $\epsilon = 0.30$ [Fig. 5.3(d)], it is already evident at $\epsilon = 0.10$ [Fig. 5.3(a)], with FRG peaks and valleys very clear when $\epsilon = 0.15$ [Fig. 5.3(b)], whilst the LCG profile becomes somewhat clearer only at $\epsilon = 0.20$ [Fig. 5.3(c)]. Notice that whenever strain is applied *orthogonally* to one of the lattice vectors, a minimum obtains ($\theta \approx \pi/6, \pi/2$ and $5\pi/6$). The maxima, in contrast, correspond to tensioning the lattice *along* some $\boldsymbol{a}_j$.

Let us try to explain some of the aforementioned behaviors. For one, t_j generally approximates zero as ϵ increases, and it does so in an anisotropic way. This suppresses correlations along $\boldsymbol{a}_j$, thus alleviating GF. If, however, the applied strain is large enough, a global elevation of ground state energies will occur. Such energy raising is consistent (as it better be!) with the fact that uniform mechanical stress is, for the case being, a consequence of external work.

Geometric Frustration function

Since the "Geometric Frustration alleviation" issue already showed up, it is time to construct $\zeta(\theta)$ as a frustration sensor. One would expect a tripartite system, in its ground state, to be as frustrated as possible whenever all hoppings were equal. The ansatz is then: smaller dispersions

in t_j's favor frustration at low energies. A simple and natural bonafide dispersion measure for real variables is given by the variance σ^2. We then introduce the following as a Geometric Frustration function:

$$\zeta(\theta) = \frac{1}{\sigma^2} = \frac{N_t(N_t-1)}{\sum_{j=1}^{N_t}\left(t_j - \bar{t}\right)^2} = \frac{6}{\sum_{j=1}^{3}\left(t_j - \bar{t}\right)^2}, \tag{5.5}$$

where $\bar{t} = (t_1 + t_2 + t_3)/3$, and $N_t = 3$ is the number of distinct hoppings in the kagome lattice unit-cell. It is named *coupling isotropicity* and seems to capture the intuition that, should all three couplings be the same, we would have maximal ("infinite") frustration. Notice that Eq. (5.5) depends implicitly on both ϵ and θ through t_j. Its values can be scaled and compared with $E_0(\theta)$[6], and this is exactly what we see displayed as black dashed lines in Fig. 5.3, which follows the FRG energy profiles quite well for $\epsilon = 0.15$ already. Panel (d) shows that DMRG-energies for both FRG and LCG behave quite similarly to $\zeta(\theta)$. In particular, the maxima (minima) of $E_0(\theta)$ occur whenver GF is a local maximum (minimum), even if $U = 5$ (metallic at $\epsilon = 0$). Finally, notice how couplings' maxima (minima) are directly related to ground state energy minima (maxima). A consequence that seems natural in hindsight is the following. Assume stationary ground state energies (in accordance with numerical data) whenever one of the couplings t_j are as well. Then, taking from the unit-cell's energy $\varepsilon(t_1, t_2, t_3) \sim t_1 C_1 + t_2 C_2 + t_3 C_3$[7] and imposing $\frac{d\varepsilon}{d\theta_c} = 0$ with the hypothesis that, say t_1 and S_1 are stationary, and $t_2 = t_3 = t$, we find[8]

$$\frac{d\varepsilon}{d\theta_c} \sim t\left(S_2' + S_3'\right) + t'\left(S_2 - S_3\right) = t\left(S_2' + S_3'\right) = 0, \tag{5.6}$$

whence the opposite derivatives condition is required, since $S_2 = S_3$ by symmetry and $t \neq 0$. This implies a certain dual role between couplings and correlations along a given direction.

LCG sensitivity and link correlation structure changes

The greater LCG sensitivity, relative to FRG, might arise as a consequence of preferential translational symmetry direction alterations: once ϵ is fixed, θ selects the axis along which couplings are weaker. This anisotropy suppresses electron hopping along that direction, effectively driving the spatial density of states toward a minimum near those bonds. Notice that, e.g., at $\theta = \pi/3$ hoppings are favored along $\boldsymbol{a}_2$ and $\boldsymbol{a}_3$, whence a more 2D-like configuration is obtained. At $\theta = 5\pi/6 \approx 0.83\pi$, however, the favored direction is $\boldsymbol{a}_1$, and we might be readily convinced that closed chain-loops are incentivized. Although such arguments do not explain the complete behavior of Fig. 5.3(a), they appeal in an understandable way to account for such striking amplitude between the maximum near $\pi/3$ and the minimum nearing $5\pi/6$. But it is not so difficult to get a clear picture of the asymmetry once we realize that, under LCG, configurations (e) and (f) in Fig. 5.3 loop $\boldsymbol{a}_1$ lines onto themselves (see Fig. 5.1), in great contrast to what happens

[6] The scaling factor is obtained as follows: with $\zeta_{max} \equiv \max\{\zeta(\theta)\}$ and $\zeta_{min} \equiv \min\{\zeta(\theta)\}$; the equivalent minimum (maximum) value of $E_0(\theta)$ for those angles in the FRG curve are E_{min} (E_{max}). Then $\zeta \to \left(\frac{\zeta - \zeta_{min}}{\zeta_{max} - \zeta_{min}}\right)(E_{max} - E_{min}) + E_{min}$ gives the desired scale for $\zeta(\theta)$ shown in Fig. 5.3.

[7] C_j, as we quickly infer, is the connected correlation between a pair bonded by t_j. In the insulating phase, this amounts to just the link correlations. S_j analogously stands for the non-connected correlations.

[8] Eq. A.18 was here used.

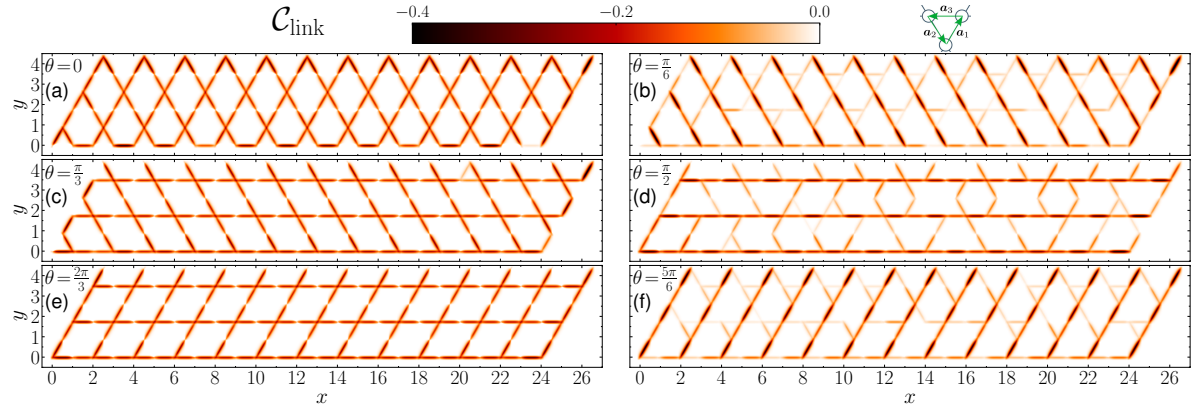

Figure 5.4: Link correlations for $\epsilon = 0.30$ and different strain orientations: $\theta = 0$ (a), $\theta = \pi/6$ (b), $\theta = \pi/3$ (c), $\theta = \pi/2$ (d), $\theta = 2\pi/3$ (e) and $\theta = 5\pi/6$ (f). The left (right) column panels correspond to *maxima (minima) in* $E_0(\theta)$ *of Fig. 5.3.* For *energy maxima (left column)*, links with antiferromagnetic correlations form 2D oblique Lieb-like lattices. For *energy minima (right column)*, links form 1D-like arrays with stronger (darker) antiferromagnetic correlations. $U = 5$ in all panels. At the top-right, an inset with nearest-neighbor vectors to help with identifying the link orientations.

with the remaining ones: for example, $\boldsymbol{a}_2$ lines are alternatingly coupled with one another in (b) and (c).

The kagome ribbon has its link correlations structure affected by strain. Unsurprisingly, the effects depend on θ more dramatically for larger deformations. Fig 5.4 displays a heatmap for $\mathcal{C}_{\text{link}}$ at angles of stationary energies. Notice that it exhibits a structure of connected oblique Lieb-like lattices [197] for directions that give E_0 or ζ maxima (left panels with $\theta = 0, \pi/3, 2\pi/3$). Quite evident at (a) and (c) are dark links at the edges which survive the application of strain. Apart from those, who were previously discussed, links are homogeneous throughout, with correlations between pairs connected along strained directions having nearly vanishing strength.

The $\mathcal{C}_{\text{link}}$ distribution for energy minima (right panels), in contrast, reveal quasi-independent

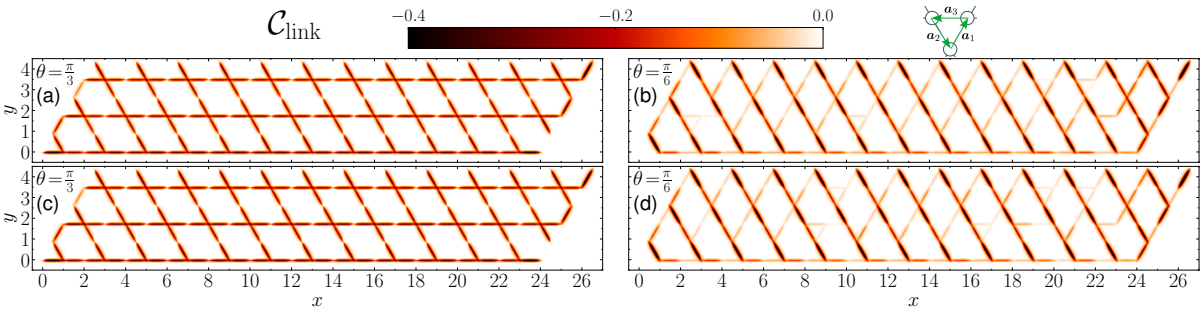

Figure 5.5: Link correlations for $\epsilon = 0.30$ along $\boldsymbol{a_1}$ ($\theta = \pi/3$, left panels, *a maximum in* $E_0(\theta)$) and orthogonally to $\boldsymbol{a_2}$ ($\theta = \pi/6$, left panels, *a minimum in* $E_0(\theta)$). These configurations occur whenever strain is applied along $\boldsymbol{a_1}$ and orthogonally to $\boldsymbol{a_2}$, in this order (see top-right inset). Upper and lower panel rows correspond to $U = 10$ and $U = 20$, respectively. Compared to Fig. 5.4(b) and (c), the correlations here are much more pronounced. Nevertheless, there is little difference between $U = 10$ and 20.

1D chains' configurations of strongly correlated links along directions normal to θ.

Bearing in mind that Fig. 5.4 presents the link correlations for $U = 5$, we would expect that, by increasing the Coulomb repulsion, the antiferromagnetic character becomes enhanced, whereby correlation profiles could then be more pronounced. Fig 5.5 shows that the suppression

of charge fluctuations leads to "nicer" profiles, indeed. Antiferromagnetic links are darker, with the consequence of 1D structures (right panels) being better-defined, i.e., the relative strenghts between strong and weak correlation axis increases, naturally leading to a greater degree of independence between those Neél lines.

While $\zeta(\theta)$ is a good indicator of θ values that most affect the ground state energy E_0, with yet another being discussed in the Appendix A, it does not directly quantify the spin frustration present in the system. In reality, phenomena such as spontaneous symmetry breaking teach us the lesson of constantly being aware that ground states do not always mirror the properties of its Hamiltonian[9]. Thus far, we only "probed" frustration as it might be inferred from the couplings. To obtain real quantum state information, we should calculate some expected values. We have proposed [1] a useful way to quantify the frustration content of the ground state, assuming we're deep in the insulating phase. This is via the following quantity, dubbed the *Local Geometrical Saturation* [1]

$$f_j^G = 1 - \frac{4}{\tilde{J}_j}\left|\sum_{(m,n)\in\mathbb{C}_{\mathbb{B}}^{\mathrm{j}}} J_{mn}\left\langle S_m^z S_n^z\right\rangle\right|, \tag{5.7}$$

which accounts for the longitudinal spin-spin correlations within a given unit cell of the kagome system. In this expression, $J_{mn} = 4t_{mn}^2/U$ represents the exchange coupling between neighbor spins (m,n) in the considered unit cell, $\mathbb{C}_B^j$, and included in the sum. Dashed magenta lines in Fig. 5.1 show the unit cell that is used. Finally, $\tilde{J}_j \equiv \sum_{(m,n)\in\mathbb{C}_{\mathbb{B}}^{\mathrm{j}}} |J_{mn}|$. In this definition, f_j^G accounts for the couplings (including their sign) between each pair of spins in all unit cells. Notice that $f_j^G \to 1$ for uncorrelated cells, while $f_j^G \to 0$ for both fully ferro- and antiferromagnetic correlated links. The intuition behind such expression comes from thinking that (i) the couplings' nature weights Geometric Frustration and (ii) GF reads off the gain-and-lose game as seen by longitudinal correlations. To illustrate, we present an example considering Ising spins. Suppose there are three sites with a spin-1/2 each, say two ups and one down. The answer to *"is this configuration frustrated?"* depends on the sign of each link ($J > 0$ or $J < 0$). To gauge exactly how much the configuration is frustrated, if at all, we must consider the couplings, since they are not only sensitive to signs but also their respective strengths given ϵ and θ. We now show a very useful property of Eq. 5.7. By construction, whenever the effective model is $SU(2)$ invariant, such as for the Heisenberg, we have:

$$\langle S_m^z S_n^z\rangle = \frac{1}{3}\left\langle \vec{S}_m \cdot \vec{S}_n\right\rangle, \tag{5.8}$$

from which we easily obtain

$$f_j^G = 1 - \frac{4}{3}\left|\frac{\varepsilon_j}{\tilde{J}_j}\right|, \tag{5.9}$$

where $\varepsilon_j \equiv \sum_{(m,n)\in\mathbb{C}_{\mathbb{B}}^{\mathrm{j}}} J_{mn}\left\langle \vec{S}_m \cdot \vec{S}_n\right\rangle$ defines the local energy associated to cluster/unit-cell $\mathbb{C}_{\mathbb{B}}^{\mathrm{j}}$.

[9] A complementary example is that of a disordered ferromagnetic Heisenberg chain: although the Hamiltonian lacks translational symmetry, the $|\uparrow\uparrow ...\rangle$ state still has it, and remains within the ground state manifold! Of course, the excitations are not expected to resemble magnons any longer.

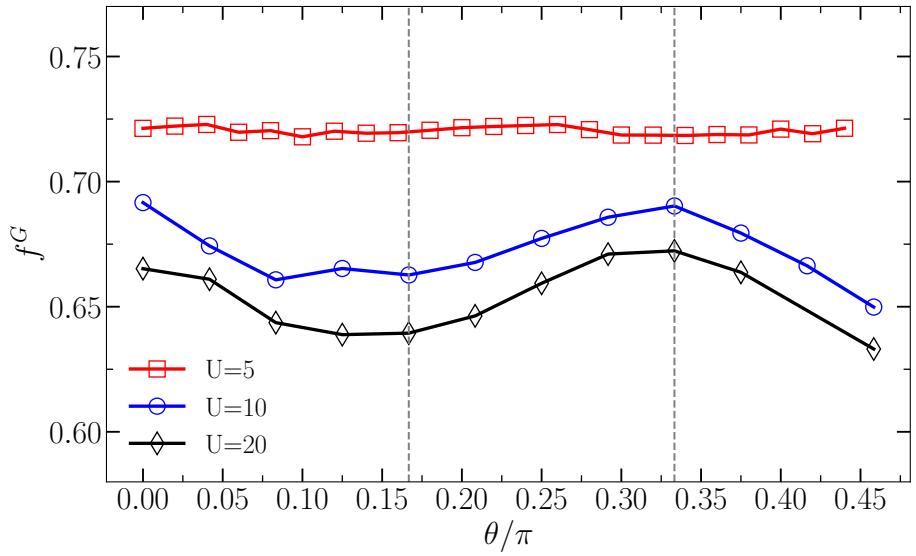

Figure 5.6: $f^G(\theta)$ vs θ for $\epsilon = 0.30$, $U = 5$ (red squares), $U = 10$ (blue circles) and $U = 20$ (black diamonds). Note that for larger values of U, the maxima and minima become more pronounced, as expected. Dashed lines indicate $\theta = \pi/6$, $\pi/3$, for the minimum and maximum in E_0. See also Fig. A.1.

Therefore, in absolute value, energy minima correspond to index maxima and vice-versa. This satisfies the "lose-or-gain" intuition that motivated our construction in the first place. Our definition is conveniently local and able to explicitly capture $SU(2)$ breaking. This is for Eq. (5.9) would not hold, whence the Local Geometrical Saturation would possibly not be related to the energy in a nice way as the one if $SU(2)$ is intact. Should there be confidence that the system is in a spin-dominant phase - whereby avoiding trivialities such as expectedly null correlations - the possibility of magnetic ordering must be seriously considered. A couple of sidenotes on Eq. (5.7) are in order: first, since it is defined locally, it can be used to spatially resolve frustration patterns throughout the lattice. Second, it is not restricted to kagome lattices. We also have no reason to expect that this quantity is exclusively useful for the Heisenberg model. The insights should be transferable, provided this "lose-and-gain" reasoning is properly set up for whatever system one studies.

Enough of definitions for now. The next plot shows an averaged value of this indicator over the entire system, $f^G(\theta)$, for three distinct U values, with $\theta \in (0, \pi/2)$. Notice that for large U, in Fig. 5.6, f^G settles onto lower values (contrast with $U = 5$) with increasingly better defined stationary points that closely resemble the behavior of E_0 in Fig. 5.3. Points in red squares show very small fluctuations somewhere around 0.72; this almost flat shape might be understood considering charge fluctuations in the system, which are not favorable to the localization of magnetic moments at lattice sites. On the one hand, this indicator seems to be not as effective in providing quantitative value whenever the system is weakly interacting - even though Fig. 5.4 clearly displays the impacts of strain over link correlations. However, the distinct profiles there shown may hint at the possibility of using f^G as a marker for the insulating phase: it could be the case that f^G starts to mold into proper energy shapes at the onset of <phase>→insulator transitions.

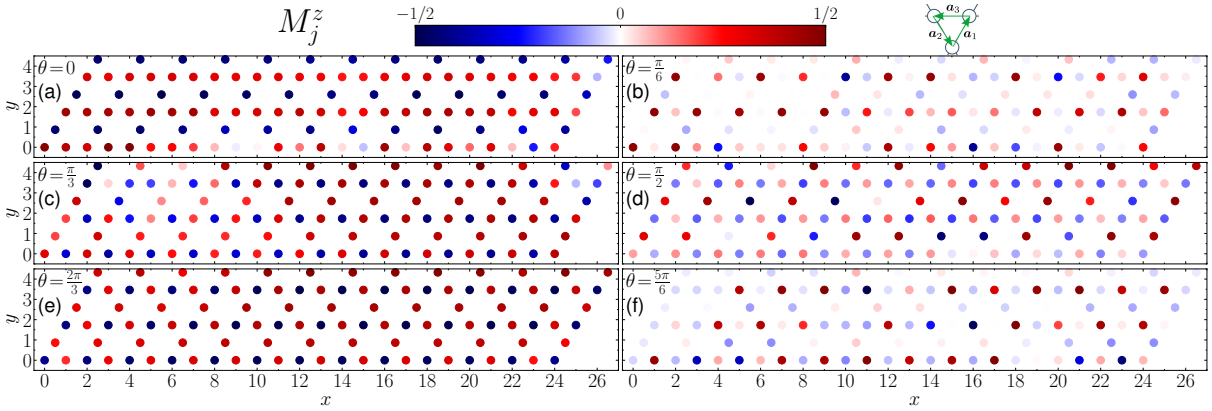

Figure 5.7: Magnetization M_j^z for the coplanar applied field of strength $V_z = 0.05$ and $\theta = 0$ (a), $\theta = \pi/6$ (b), $\theta = \pi/3$ (c), $\theta = \pi/2$ (d), $\theta = 2\pi/3$ (e) and $\theta = 5\pi/6$ (f). For all panels, we set $U = 5$ and $\epsilon = 0.30$. Faint dots on the right panels *(where E_0 has minima in Fig. 5.3)* feature sites belonging to Néel-like lines, while dark red dots correspond to loose sites readily polarized by the field. The top-right inset helps with identifying, e.g., the red lines in (c) as a product of V_z when strain is applied along $\boldsymbol{a_1}$.

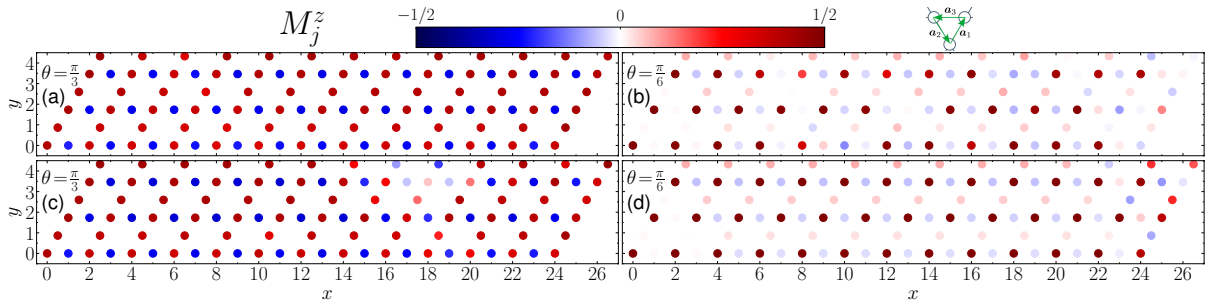

Figure 5.8: Local magnetization M_j^z for coplanar field with strength $V_z = 0.05$ and strain applied along $\theta = \pi/3$ (left) and $\theta = \pi/6$ (right). Upper and lower panels show results for $U = 10$ and $U = 20$, respectively. As in Fig. 5.7, faint color dots on the right panels represent sites belonging to Néel AF lines, while dark red dots correspond to loose sites more easily polarized by the field. Notice how the most energetically favorable top-left to bottom-right red-then-blue pattern results along a_2-connected spins. For all pannels, $\epsilon = 0.30$.

Interstitial sites and Neél lines

If some attention is given to the right panels at Fig. 5.5, the existence of loosely coupled sites is realized. They arise as a result of 1D weakly-correlated lines leaving sites between them nearly free (given large enough strain). It is very tempting to conclude the possibility of paramagnetic sites coexisting with Neél lines. Perhaps the simplest way to verify this reasoning is by applying a magnetic field that is weak enough to preserve the low-energy levels of 1D chains, while strong enough to excite those *interstitial sites*. When the field is applied uniformly along the sheet in a conventional z-direction, spatially-resolved polarization patterns can be analyzed over the lattice.

Fig. 5.7 shows the local magnetization $M_j^z = \left\langle S_j^z \right\rangle$ calculated with low-temperature thermal averages as always. The field strength is $V_z = 0.05$ and the stationary energy configurations are those very same from Fig. 5.7. As the color scale suggests, red (blue) dots at each lattice site indicate whether the localized moment is polarized in favor of (against) $\vec{B}$ or remains unpolarized - white color.

The $\theta = 0$ profile [Fig. 5.7(a)], for example, showcases a pattern consisting of alternatingly positive-negative polarizations on the lines that are not the one along which the system is strained, namely $\boldsymbol{a}_3$. This is understandable, since greater deformations shrink the couplings. In its ground state, given the energy to be gained by alligning with the field, which most likely enhances Neél lines as well, the system chooses to pay the price of ferromagnetic correlations nevertheless. Completely analogous conclusions are reached for the remaining maxima, with the difference that their weak links turn out to lay along $\boldsymbol{a}_1$ and $\boldsymbol{a}_2$. It is very important, thus we emphatize once again, that AF lines are either not affected or actually benefit from polarized sites. This will be shown in greater detail, afterwards, with $\mathcal{C}_{\text{link}}$ panels.

Next, the right panels, for which energy are minima. One sees not so clearly defined polarization profiles as in the left panels, which could stem from the fact that enhanced lines ($\boldsymbol{a_2}$ if $\theta = \pi/6$, for instance) are locally brought deeper into the metallic phase and the relative link strength (J_{strong}/J_{weak}) is not great enough to let loose sites be freely oriented with $V_z = 0.05$. If our physics is good, increasing U will make those almost-free spins very susceptible. Moving forward, Fig. 5.8 shows M_j^z with $U = 10$ ($U = 20$) at the upper (lower) row, where we are still applying the same field strength $V_z = 0.05$. The relative deformation is, as always, $\epsilon = 0.30$ (see Fig. 5.5). Left and right panels inform that $\theta = \pi/3$ and $\theta = \pi/6$ configurations, respectively, become very well-rounded in terms of either Neél lines or loose sites polarization. The right panels show that the energy is minimized when the system organizes its local magnetization on alternating diagonal lines which weakly polarize in the field, but at the same time there coexists strongly polarized moments: could para and antiferromagnetism be good neighbors?

In a first glance, we might think that the spin pattern (right-blue from top to bottom) would have a red $\leftrightarrow$ blue symmetry along Néel lines, but the presence of polarized interstitial sites guarantee non-degeneracy as follows. Should the blue and red sites be flipped, it is easy to see that the decisive energy balances are due to whatever results along weak links, since it is not the true many-body ("connected") correlations that define energies in the Heisenberg model. Hence, the a_3-connected links would all be ferromagnetically aligned, whilst a_1 ones would be antiferro, thus reversing what is displayed in Fig. 5.8 (b) and (d). The state is then a higher

energy one since there are more a_3 than a_1-connected links. At last, a conjecture posits itself: could in the bulk material ($L_x, L_y >> 1$) the ground state display a degeneracy with regards to those configurations, or will it solve the issue with "quantumness"?

Chapter 6

Conclusions and outlook

The world of quantum many-body systems presents a vast and intricate landscape where interactions, geometry, and external fields intertwine to produce a remarkable diversity of phenomena. Quantum materials exhibit exotic states such as topological insulators, Quantum Spin Liquids, and unconventional superconductors, yet many fundamental questions—from high-temperature superconductivity to quantum entanglement—remain open. Strongly correlated systems, characterized by intense particle interactions, defy conventional frameworks, as illustrated by phenomena in models like the 1D Hubbard model. The ongoing development of sophisticated theoretical frameworks, including quantum field theory and RG techniques, continues to deepen our understanding and fuel practical advances in materials science, quantum computing, and information processing.

Progress in the study of strongly correlated systems is propelled by innovative theoretical, experimental, and computational methodologies. Experimental advances such as angle-resolved photoemission spectroscopy (ARPES), scanning tunneling microscopy (STM), and ultracold atom setups have provided extraordinary insights into electronic structures, magnetic behaviors, and dynamics. On the computational front, numerical techniques like DMRG —again, part of the broader Tensor Network family—have revolutionized our capacity to simulate complex quantum states. TNs excel due to their efficient representation of modestly entangled states, exploiting area law scaling of the Entanglement Entropy. These methods have become pivotal tools in probing quantum phase transitions, topological order, and quantum information theory.

Within this rich methodological context, the kagome lattice emerges as an ideal platform to investigate frustration and interactions. Its unique geometry, composed of corner-sharing triangles, leads to Geometric Frustration, degeneracies, and complex low-energy configurations. The Kagome Antiferromagnet, in particular, is recognized as a potential host for QSL, characterized by highly entangled ground states, fractional excitations, and absence of conventional magnetic order. Understanding the subtle interplay of frustration, interactions, and lattice anisotropies within kagome systems promises both fundamental insights and avenues for tailoring novel quantum materials.

In this thesis, we have embarked on a journey through the physics of kagome nanoribbons, by exploring its behavior under the influence of strain and external fields. We have employed a combination of theoretical and numerical techniques, including the DMRG method, to investigate the ground state properties of a half-filled single band Hubbard model - plus a tunable

constant external magnetic field - with a focus on the strongly repulsive (Heisenberg) regime. Altough the topological aspects of QSL are compelling, we delve not much further into the perfectly isotropic problem beyond what's minimally required to establish a "reference line" to which strained cases are to be compared. Rather, we explore correlations and local spin polarizations, in the face of strain effects on the lattice. Given the uniformity of in-plane axial deformations, the problem can be described by anisotropic coupling terms, whether those are the original hoppings or the effective Heisenberg exchanges. That is to be contrasted with the cases which give rise to pseudomagnetic fields, for example, where deformations large in comparison to the lattice size - i.e., are more of a long-wavelenght nature - typically involve non-uniform strain fields. Just as naturally, the question of whether these anisotropies can be linked to the amount of frustration present in the system arises. By deforming our ribbon along different directions, we have observed significant changes in the ground state energy, local magnetization profiles, and spin-spin correlations. But what about the frustration content of the system? How may we quantify it?

To better orient ourselves through the tuning of "frustrationness", we have introduced two functions that seem to capture the Geometric Frustration of the system: the coupling isotropicity $\zeta(\theta)$ and the Local Geometrical Saturation (LGS) f_j^G, whose bulk-average is then used. The former should hint at low-energies behavior only, whereby the comparable strength of competing couplings is already expected to be a good indicator of how frustrated the system is. The latter, on the other hand, is a local measure of the Nearest-Neighbor Spin-Spin Correlations (NNSSC) explicitly linked to frustration. It is able to capture the effects of strain on the local geometry of the system, by directly targeting a given state or superposition of those, should we be considering the ever-present degeneracies in frustrated systems. As we believe to have evidenced, the aforementioned functions, the ground state energy, NNSSC patterns and local magnetization profiles are all closely related to one another. Indeed, despite the infinite distance that separate our numerics and the thermodynamic limit, we believe they are possibly able to classify different (quantum) phases of the system. In fact, it is quite evident from its definition that f_j^G should be sensitive to, e.g., the presence of local magnetic order. Another expectation, hinted at by Fig. 5.6, is that f_j^G should be able to distinguish between the insulating and metallic phases of the system - more nuanced and sensitive to angle changes in the former, whilst practically flat in the latter. As a final remark on the geometrical saturation, we would like to highlight that it is the first local, correlation-only, measure of Geometric Frustration found in the literature, to the best of our knowledge. Apart from the magnetic order sensitivity that we have already alluded to, it is able to capture the system's local geometry, and is sensitive to anisotropy effects. We firmly believe that applications of f_j^G are not limited to the model at hand, and that its generalizations/particular instances can be readily inferred by looking for local operators relevant to the underlying symmetries and energy content of a chosen system, analogously to what we did with the longitudinal correlations $S_i^z S_j^z$.

In a display of its versatility, the strained kagome makes it possible to interpolate between 1D-like and 2D-like configurations, as a function of the strain angle θ. The angles for which frustration is maximized and ground state energy is minimized are those displaying ferrimagnetic Lieb-like lattices, while frustration minima correspond to energy minima and behave as

collections of weakly coupled 1D chains. We believe this result is meaningful, not just because *interstitial* sites appear in the latter case, but also given the possible interpretation of ferrimagnetism as a "suppressed form" of either ferro or antiferromagnetism. Our findings indicate that ferrimagnetic order can arise not despite frustration, but precisely as a resolution to it under certain lattice anisotropies. Strain serves as a control knob that either relieves or redistributes Geometric Frustration, giving rise to emergent ferrimagnetism when the system transitions toward oblique Lieb structures. Frustration if often associated with magnetic order suppression, as in Quantum Spin Liquids. However, under directional strain, certain anisotropic paths stabilize ordered moments that align ferromagnetically within sublattices and antiferromagnetically between them, yielding ferrimagnetism. This points to a reconfiguration rather than suppression of frustration. This interplay between strain, frustration, and emergent order suggests new directions in materials engineering — where mechanical control could enable the tuning of magnetic textures for quantum applications. Ferrimagnetism here, we think, is not merely an artifact of geometry, but a signature of frustration's adaptive role in strained quantum materials.

The energy minima configurations have their own interesting features. Local magnetization profiles reveal that the system organizes itself into alternating diagonal lines of polarized spins, with interstitial sites remaining unpolarized. Added to the NNSSC profiles seen, for instance, at 5.5, this suggests a coexistence of "1D-antiferromagnetic" ordering tendencies and paramagnetic behavior, raising intriguing questions about the nature of magnetism in the presence of strain. The presence of interstitial sites, which are weakly coupled to their neighbors, hints at the possibility of a more complex magnetic landscape, where different types of order can coexist. Such indirect, emerging, interactions are particularly relevant in the context of Quantum Spin Liquids. In fact, the resulting spin textures for such anisotropic kagome couplings with [208] and without [172, 209, 210] an applied field were explored in the literature. Despite us not aiming to understand the spin structures in that level of detail, specially within a context of no external fields, the striking appearence of easily polarized interstitial sites is a valuable product in itself. It is a clear indication of the presence of a non-trivial magnetic landscape, where different types of order can coexist and interact in unexpected ways.

As in every problem worth considering, the answers we harvest come with the pleasing debt of new questions. It is thus in order to mention at least a couple of the ones we were either capable to envision or kindly gifted by others. We have tried to keep the good taste of not offending our reader's intelligence with too trivial observations, and hopefully did succeed. First, we highlight that the LGS should be sensible to VBS defects, specially localized ones, since null correlations induced therein are signaled through f_j^G spikes. Of course, this is not the only mechanism by which those peaks might occur, and additional probes are likely needed. Next, as we have already suggested, it is quite possible that the LGS may serve as a guide to the onset of insulating phases, thereby providing a useful tool for identifying "magnetically active" phase transitions and understanding the underlying mechanisms at play. In this very spirit, we envision the possibility of finding a "metallic counterpart" from which a generalized notion of Geometric Frustration could be defined, and used in a dual sense to that of LGS. For perfectly $SU(2)$ invariant states, a straightforward connection might be made through (5.9), since the operators $\left\langle \vec{S}_m \vec{S}_n \right\rangle$ are directly proportional to the "spin permutation operators": by properly defining the

"charge permutation operators" as its complementary set, perhaps something worth exploring is to be found. In our third speculation, we note a suggestive metaphor: one could think of spin frustration as "Anderson localization without disorder", where destructive interferences - here enforced by lattice geometry and competing exchanges - localizes short-wavelength modes. If that holds any water, this metallic analog of ours should be probed through local charge current patterns or localized electronic states in (nearly?) flat bands.

A fourth route is the consideration of yet another generalized notion of frustration: the idea of "quantum frustration", with many definitions and not all equivalent, scattered in the literature. We have tinkered with a seemingly original expression that purely considers the spin exchange/permutation operator (mentioned above). By essentially measuring how much "singlet-like" or "triplet-like" is the average pairing of one given spin or of a given unit cell, the results appear quite promising and intuitive, for the ground state energy profiles could be predicted rather confidently, and a metallic counterpart is more amenable to both definitions and interpretations. The final outlook, in order to be somewhat economic, has its roots in the quite well-informed observation of an anonymous referee: the possibility of distortions spontaneously happening, through Jahn-Teller-like mechanisms, whence the configurations otherwise achieved through external deformations could emerge. Our recent efforts are completely devoted to this end, and we hope to be able to report on it in the near future. The preliminary results, albeit stepping through early stages with more restricted conditions, are quite promising, and we already have a humble proof of concept for electron-phonon coupling in a Holstein-Hubbard ribbon driving anisotropies in the Heisenberg limit.

Appendix A

Strained couplings

The deformed nearest-neighbour vectors are given by

$$\boldsymbol{a}_j' = (\boldsymbol{I} + \bar{\epsilon})\, \boldsymbol{a}_j. \tag{A.1}$$

With

$$\boldsymbol{a_1} = \frac{a_0}{2}\left(1, \sqrt{3}\right),$$
$$\boldsymbol{a_2} = \frac{a_0}{2}\left(1, -\sqrt{3}\right),$$
$$\boldsymbol{a_3} = a_0\,(-1, 0)\,.$$

and the strain tensor $\bar{\epsilon}$ as follows

$$\bar{\epsilon} = \epsilon \begin{bmatrix} \cos^2(\theta) - \nu \sin^2(\theta) & (1+\nu)\sin(\theta)\cos(\theta) \\ (1+\nu)\sin(\theta)\cos(\theta) & \sin^2(\theta) - \nu\cos^2(\theta) \end{bmatrix}. \tag{A.2}$$

ϵ gives the strain intensity/modulus, θ the azimuth angle in position space, and ν is the Poisson ratio (a material-dependent value).

In order to both simplify our calculations and expound some properties of $\bar{\epsilon}$, we use the trigonometric identities $\cos^2(\theta) = \frac{1+\cos(2\theta)}{2}$, $\sin^2(\theta) = \frac{1-\cos(2\theta)}{2}$ and $\sin(\theta)\cos(\theta) = \frac{1}{2}\sin(2\theta)$ to rewrite Eq.(*A.2*) as

$$\bar{\epsilon} = \frac{\epsilon}{2}\left\{(1-\nu)\,\boldsymbol{I} + (1+\nu)\,\widetilde{\mathrm{R}}(\theta)\right\}, \tag{A.3}$$

where

$$\widetilde{\mathrm{R}}(\theta) = \begin{bmatrix} \cos(2\theta) & \sin(2\theta) \\ \sin(2\theta) & -\cos(2\theta) \end{bmatrix} = \widetilde{\mathrm{R}}^{\mathrm{T}}(\theta), \tag{A.4}$$

which[1] is then an orthogonal symmetric tensor:

$$\widetilde{\mathrm{R}}(\theta)\,\widetilde{\mathrm{R}}^{\mathrm{T}}(\theta) = \widetilde{\mathrm{R}}^{\mathrm{T}}(\theta)\,\widetilde{\mathrm{R}}(\theta) = \left[\widetilde{\mathrm{R}}(\theta)\right]^2 = \boldsymbol{I}. \tag{A.5}$$

Therefore, by defining

$$\alpha_{\pm} \equiv \frac{(1 \pm \nu)}{2}\epsilon \tag{A.6}$$

[1] We also note in passing that it can be decomposed as a clockwise rotation of 2θ about the z-axis, followed by a reflection about the zOx plane, that is, mapping $y \to -y$ while keeping the other coordinates intact.

we might cast Eq.(A.1) as follows

$$\boldsymbol{a}'_{\boldsymbol{j}} = \boldsymbol{a}'_{\boldsymbol{j}}(\theta) = \left[(1+\alpha_-)\boldsymbol{I} + \alpha_+ \widetilde{\mathrm{R}}(\theta)\right]\boldsymbol{a}_{\boldsymbol{j}}. \tag{A.7}$$

The strained hopping terms to be calculated are given by

$$t_j(\theta) = t_j \exp\left\{-\beta\left[\left(\frac{\left\|\boldsymbol{a}'_{\boldsymbol{j}}(\theta)\right\|}{a_0}\right) - 1\right]\right\}, \tag{A.8}$$

with β the Grüneisen parameter

and t_j is the hopping along $\boldsymbol{a}_{\boldsymbol{j}}$'s direction. Even though the expression above is generic, we restrict ourselves to $t_j = t_0\ \forall\, j$ in the main text.

With that in mind, we must calculate the strained vectors moduli $\left\|\boldsymbol{a}'_{\boldsymbol{j}}(\theta)\right\| = \sqrt{\boldsymbol{a}'_{\boldsymbol{j}}(\theta)\cdot\boldsymbol{a}'_{\boldsymbol{j}}(\theta)}$. Now, since $\widetilde{\mathrm{R}}$ is both symmetric and orthogonal, we get

$$\boldsymbol{a}'_{\boldsymbol{j}}(\theta)\cdot\boldsymbol{a}'_{\boldsymbol{j}}(\theta) = \left[\alpha_+^2 + (1+\alpha_-)^2\right]\boldsymbol{a}_{\boldsymbol{j}}\cdot\boldsymbol{a}_{\boldsymbol{j}} + 2\alpha_+(1+\alpha_-)\,\boldsymbol{a}_{\boldsymbol{j}}\cdot\widetilde{\boldsymbol{a}}_{\boldsymbol{j}}(\boldsymbol{\theta}), \tag{A.9}$$

where $\widetilde{\boldsymbol{a}}_{\boldsymbol{j}}(\boldsymbol{\theta}) \equiv \widetilde{\mathrm{R}}(\theta)\,\boldsymbol{a}_{\boldsymbol{j}}$.

But $\boldsymbol{a}_{\boldsymbol{j}}\cdot\boldsymbol{a}_{\boldsymbol{j}} = a_0^2\ \forall j$, and for a (real) vector of the form $\boldsymbol{a}_{\boldsymbol{j}} = \frac{a_0}{\sqrt{\mathrm{x}_j^2+\mathrm{y}_j^2}}\left(\mathrm{x}_j + \mathrm{y}_j\right)$ we have

$$\boldsymbol{a}_{\boldsymbol{j}}\cdot\widetilde{\boldsymbol{a}}_{\boldsymbol{j}}(\boldsymbol{\theta}) = \frac{a_0^2}{\mathrm{x}_j^2+\mathrm{y}_j^2}\left[\left(\mathrm{x}_j^2 - \mathrm{y}_j^2\right)\cos(2\theta) + 2\mathrm{x}_j\mathrm{y}_j\sin(2\theta)\right], \tag{A.10}$$

thus, finally

$$t_j(\theta) = t_j \exp\left\{-\beta\left[\left(\left[\alpha_+^2 + (1+\alpha_-)^2\right] + 2\alpha_+(1+\alpha_-)\frac{1}{\mathrm{x}_j^2+\mathrm{y}_j^2}\left[\left(\mathrm{x}_j^2-\mathrm{y}_j^2\right)\cos(2\theta) + 2\mathrm{x}_j\mathrm{y}_j\sin(2\theta)\right]\right)^{1/2} - 1\right]\right\}. \tag{A.11}$$

Now, we see that the effective strained Heisenberg couplings are

$$J_n(\theta) = J_n \exp\left\{-2\beta\left[\left(\left[\alpha_+^2 + (1+\alpha_-)^2\right] + 2\alpha_+(1+\alpha_-)\frac{1}{\mathrm{x}_n^2+\mathrm{y}_n^2}\left[\left(\mathrm{x}_n^2-\mathrm{y}_n^2\right)\cos(2\theta) + 2\mathrm{x}_n\mathrm{y}_n\sin(2\theta)\right]\right)^{1/2} - 1\right]\right\}, \tag{A.12}$$

with the obvious definition $J_n \equiv \frac{4t_n}{U}t_n$.

Zero-sum property

Notice that

$$\sum_{n=1}^{3}\left(\mathrm{x}_n^2 - \mathrm{y}_n^2\right)\cos(2\theta) + 2\mathrm{x}_n\mathrm{y}_n\sin(2\theta) = 0. \tag{A.13}$$

This motivates working with Eq.(A.12)[2] as follows. First, define

$$c_1 \equiv \alpha_+^2 + \left(1+\alpha_-^2\right), \tag{A.14}$$

[2] An analogous result obviously holds for Eq. (A.11).

$$c_2 \equiv \frac{2\alpha_+ \left(1+\alpha_-\right)}{a_0^2}, \tag{A.15}$$

and

$$s_n\left(\theta\right) \equiv \left(\mathrm{x}_n^2 - \mathrm{y}_n^2\right)\cos\left(2\theta\right) + 2\mathrm{x}_n\mathrm{y}_n \sin\left(2\theta\right), \tag{A.16}$$

such that $J_n\left(\theta\right) = J_n \exp\left\{-2\beta\left[\left(c_1 + c_2 s_n\left(\theta\right)\right)^{1/2} - 1\right]\right\}$. Hence

$$\left[1 - \frac{\ln\left(\frac{J_n(\theta)}{J_n}\right)}{2\beta}\right]^2 = c_1 + c_2 s_n\left(\theta\right),$$

which by (A.11) implies

$$\sum_{n=1}^{3}\left[1 - \frac{\ln\left(\frac{J_n(\theta)}{J_n}\right)}{2\beta}\right]^2 = 3c_1,$$

thus showing the zero-sum property

$$\sum_{n=1}^{3}\left[1 - \frac{\ln\left(\frac{J_n(\theta)}{J_n}\right)}{2\beta}\right]\frac{J_n}{J_n\left(\theta\right)}\frac{\mathrm{d}}{\mathrm{d}\theta}J_n\left(\theta\right) = 0. \tag{A.17}$$

Suppose $\theta = \theta_c$ for some stationary point θ_c; thus, one coupling is stationary whilst the remaining have the same value, as the reader might both readily infer from the problem's geometry or calculate with Eq. (A.12) for each n. At the end of the day, yet another geometrically anticipated result is stabilished: if $J_m'\left(\theta_c\right) = 0$, then for $n, n' \neq m$ we have an "opposed derivatives" relation

$$\frac{\mathrm{d}}{\mathrm{d}\theta_c}\left(J_n + J_{n'}\right) = 0. \tag{A.18}$$

It's also easy to see, by symmetry arguments, that

$$J_n''\left(\theta_c\right) = J_{n'}''\left(\theta_c\right),$$

whose equivalent statement is "the natural continuity" of Eq.(A.18), i.e.

$$J_{n_1}'\left(\theta_c + \epsilon\right) + J_{n_2}'\left(\theta_c + \epsilon\right) = 0. \tag{A.19}$$

Coupling ratios

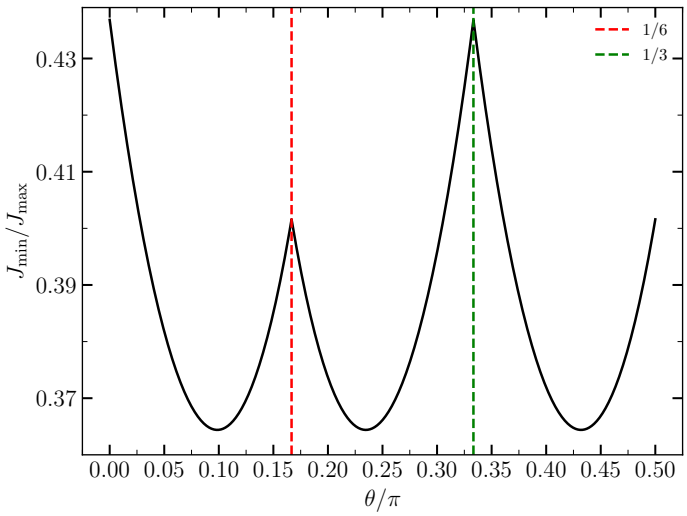

Figure A.1: $r(\theta)$ vs θ for $\epsilon = 0.30$. Note that this quantity is U-independent. Dashed lines indicate $\theta = \pi/6, \pi/3$, for a minimum and maximum in E_0.

For each angle θ, we display the ratio $r(\theta) \equiv J_{\min}(\theta)/J_{\max}(\theta)$ between the smallest and largest couplings $J_n(\theta)$ per each theta, in Fig. A.1. This is an obviously non analytical function, but its maxima are clearly located at the very stationary points in Fig. 5.3. Consistent with Eqs. (5.5) and (5.7) the plot reflects that $r(\theta)$ values closer to one indicate greater homogeneity for the couplings, thus implying higher frustration - whence the peak at, e.g., $\pi/3$ being taller than the one at $\pi/6$. Curiously, however, we have no direct link between our frustration measures and the minima in Fig. A.1, thus rendering a satisfactory interpretation, if any, still lacking. Nevertheless, we realize that $r(\theta)$ is a much coarser way to infer frustration, since there are not two but up to three distinct couplings whose spread is better captured by Eq (5.5).

Bibliography

[1] R. F. P. Costa, E. Vernek, and S. E. Ulloa. Magnetic response and antiferromagnetic correlations in strained kagome ribbons. *Phys. Rev. B*, 110:115101, Sep 2024. URL https://link.aps.org/doi/10.1103/PhysRevB.110.115101.

[2] Chunguang Bai, P. Dallasega, G. Orzes, Joseph Sarkis, and J. Sarkis. Industry 4.0 technologies assessment: A sustainability perspective. *International Journal of Production Economics*, 229:107776, 2020. URL https://doi.org/10.1016/j.ijpe.2020.107776.

[3] S. I. Vallarta-Serrano, E. Santoyo-Castelazo, E. Santoyo, Esther O. García-Mandujano, and Holkan Vázquez-Sánchez. Integrated sustainability assessment framework of industry 4.0 from an energy systems thinking perspective: Bibliometric analysis and systematic literature review. *Energies*, 2023. URL https://doi.org/10.3390/en16145440.

[4] A. Zhavoronkov, Y. Ivanenkov, A. Aliper, M. Veselov, V. Aladinskiy, Anastasiya V Aladinskaya, V. Terentiev, Daniil Polykovskiy, Maksim Kuznetsov, Arip Asadulaev, Yury Volkov, Artem Zholus, Shayakhmetov Rim, Alexander Zhebrak, L. Minaeva, B. Zagribelnyy, Lennart H Lee, R. Soll, D. Madge, Li Xing, Tao Guo, and Alán Aspuru-Guzik. Deep learning enables rapid identification of potent ddr1 kinase inhibitors. *Nature Biotechnology*, 37:1038 – 1040, 2019. URL https://doi.org/10.1038/s41587-019-0224-x.

[5] John et al. Jumper. Highly accurate protein structure prediction with alphafold. *Nature*, 596(7873):583–589, 2021. URL https://doi.org/10.1038/s41586-021-03819-2.

[6] Seonwoo Min, Byunghan Lee, and Sungroh Yoon. Deep learning in bioinformatics. *Briefings in Bioinformatics*, 18:851–869, 2016. URL https://doi.org/10.1093/bib/bbw068.

[7] Daniel Yamins and J. DiCarlo. Using goal-driven deep learning models to understand sensory cortex. *Nature Neuroscience*, 19:356–365, 2016. URL https://doi.org/10.1038/nn.4244.

[8] J. Carrasquilla and R. Melko. Machine learning phases of matter. *Nature Physics*, 13:431 – 434, 2016. URL https://doi.org/10.1038/nphys4035.

[9] Jens Kober, J. Bagnell, and Jan Peters. Reinforcement learning in robotics: A survey. *The International Journal of Robotics Research*, 32:1238 – 1274, 2013. URL https://doi.org/10.1177/0278364913495721.

[10] K. Butler, D. Davies, H. Cartwright, O. Isayev, and A. Walsh. Machine learning for molecular and materials science. *Nature*, 559:547 – 555, 2018. URL https://doi.org/10.1038/s41586-018-0337-2.

[11] Ashish Vaswani, Noam Shazeer, Niki Parmar, Jakob Uszkoreit, Llion Jones, Aidan N. Gomez, Łukasz Kaiser, and Illia Polosukhin. Attention is all you need. 2017. URL https://doi.org/10.48550/arXiv.1706.03762.

[12] A. Krizhevsky, I. Sutskever, and Geoffrey E. Hinton. Imagenet classification with deep convolutional neural networks. *Communications of the ACM*, 60:84 – 90, 2012. URL https://doi.org/10.1145/3065386.

[13] Yann LeCun, Yoshua Bengio, and Geoffrey Hinton. Deep learning. *Nature*, 521:436–444, 2015. URL https://doi.org/10.1038/nature14539.

[14] Sukhpal Singh Gill, Oktay Cetinkaya, Stefano Marrone, Daniel Claudino, David Haunschild, Leon Schlote, Huaming Wu, et al. Quantum Computing: Vision and Challenges. *arXiv preprint*, 2024. URL https://doi.org/10.48550/arXiv.2403.02240. arXiv:2403.02240.

[15] Rajat Kumar Goyal, Shivam Maharaj, Pawan Kumar, and M. Chandrasekhar. Exploring quantum materials and applications: a review. *Journal of Materials Science: Materials in Engineering*, 20(1):4, 2025. URL https://doi.org/10.1186/s40712-024-00202-7.

[16] Chuang Hou, G. Tai, Zenghui Wu, and J. Hao. Borophene: Current status, challenges and opportunities. *ChemPlusChem*, 85 9:2186–2196, 2020. URL https://doi.org/10.1002/cplu.202000550.

[17] M.Zahid Hasan and C.L. Kane. Colloquium: Topological Insulators. *Reviews of Modern Physics*, 82(4):3045–3067, 2010. URL https://doi.org/10.1103/RevModPhys.82.3045.

[18] Wenhui Duan et al. Topological quantum materials for spintronics. *Materials for Metallurgy and Energy*, 2024. URL https://doi.org/10.1002/metm.24.

[19] Sangjin Lee, Kyung-Hwan Jin, Byungmin Kang, B. J. Kim, and Gil Young Cho. Metrology of Band Topology via Resonant Inelastic X-ray Scattering. *Physical Review B*, 107:045129, 2023. URL https://doi.org/10.1103/PhysRevB.107.045129.

[20] Hilbert v. Löhneysen, Achim Rosch, Matthias Vojta, and Peter Wölfle. Fermi-liquid instabilities at magnetic quantum phase transitions. *Reviews of Modern Physics*, 79(3): 1015–1075, 2007. URL https://doi.org/10.1103/RevModPhys.79.1015.

[21] Thomas Schaefer. Fermi liquid theory: A brief survey in memory of Gerald E. Brown. *arXiv preprint*, 2014. URL https://doi.org/10.48550/arXiv.1403.7166. arXiv:1403.7166.

[22] R. O. Jones. Density functional theory: Its origins, rise to prominence, and current status. *Reviews of Modern Physics*, 87(3):897–923, 2015. URL https://doi.org/10.1103/RevModPhys.87.897.

[23] N. Taleb. Antifragile: Things that gain from disorder. Random House, Inc., 2012. ISBN 978-0812985924.

[24] B. Keimer, S. A. Kivelson, M. R. Norman, S. Uchida, and J. Zaanen. From quantum matter to high-temperature superconductivity in copper oxides. *Nature*, 518:179–186, 2015. URL https://doi.org/10.1038/nature14165.

[25] Mukul S. Laad and Luis Craco. Mott transitions: A brief review. *Advanced Quantum Technologies*, 7(12):2200186, 2024. URL https://doi.org/10.1002/qute.202200186.

[26] Alessandra Milloch, Michele Fabrizio, and Claudio Giannetti. Mott materials: unsuccessful metals with a bright future. *npj Spintronics*, 2:49, 2024. URL https://doi.org/10.1038/s44306-024-00047-y.

[27] J.K. Jain. Theory of the fractional quantum hall effect. *Physical Review B*, 41(11):7653–7665, 1990. URL https://doi.org/10.1103/PhysRevB.41.7653.

[28] HorstL. Stormer, DanielC. Tsui, and ArthurC. Gossard. The fractional quantum hall effect. *Reviews of Modern Physics*, 71(2):S298–S305, 1999. URL https://doi.org/10.1103/RevModPhys.71.S298.

[29] Ipsita Mandal and Sung-Sik Lee. Ultraviolet/infrared mixing in non-fermi liquids. *Phys. Rev. B*, 92:035141, Jul 2015. URL https://doi.org/10.1103/PhysRevB.92.035141.

[30] Weicheng Ye, Sung-Sik Lee, and Liujun Zou. Ultraviolet-infrared mixing in marginal fermi liquids. *Physical review letters*, 128 10:106402, 2021. URL https://doi.org/10.1103/PhysRevLett.128.106402.

[31] N. F. Mott. The basis of the electron theory of metals, with special reference to the transition metals. *Proceedings of the Physical Society. Section A*, 62(7):416–422, 1949. URL https://doi.org/10.1088/0370-1298/62/7/303.

[32] N. F. Mott. Metal–insulator transition. *Reviews of Modern Physics*, 40(4):677–683, 1968. URL https://doi.org/10.1103/RevModPhys.40.677.

[33] P. Anderson. Resonating valence bonds: A new kind of insulator? *Materials Research Bulletin*, 8:153–160, 1973. URL https://doi.org/10.1016/0025-5408(73)90167-0.

[34] L. Balents. Spin liquids in frustrated magnets. *Nature*, 464:199–208, 2010. URL https://doi.org/10.1038/nature08917.

[35] C. Broholm, R. J. Cava, S. A. Kivelson, D. G. Nocera, M. R. Norman, and T. Senthil. Quantum spin liquids. *Science*, 367(6475):eaay0668, Jan 2020. ISSN 1095-9203. URL https://doi.org/10.1126/science.aay0668.

[36] Steven Kivelson and Shivaji Sondhi. 50 years of quantum spin liquids. *Nature Reviews Physics*, 5(7):368–369, May 2023. ISSN 2522-5820. URL https://doi.org/10.1038/s42254-023-00596-x.

[37] Xiao-Gang Wen. Quantum orders and symmetric spin liquids. *Physical Review B*, 65(16): 165113, 2002. URL https://doi.org/10.1103/PhysRevB.65.165113.

[38] Yi Zhou, Kazushi Kanoda, and Tai-Kai Ng. Quantum spin liquid states. *Rev. Mod. Phys.*, 89:025003, Apr 2017. URL https://doi.org/10.1103/RevModPhys.89.025003.

[39] M. R. Norman. Colloquium: Herbertsmithite and the search for the quantum spin liquid. *Rev. Mod. Phys.*, 88:041002, Dec 2016. URL https://doi.org/10.1103/RevModPhys.88.041002.

[40] H. Takagi, T. Takayama, G. Jackeli, G. Khaliullin, and S. Nagler. Concept and realization of kitaev quantum spin liquids. *Nature Reviews Physics*, 1:264–280, 2019. URL https://doi.org/10.1038/s42254-019-0038-2.

[41] Yuji Matsuda, Takasada Shibauchi, and Hae-Young Kee. Kitaev quantum spin liquids, 2025. URL https://doi.org/10.48550/arXiv.2501.05608.

[42] Subir Sachdev. *Quantum Phase Transitions*. Cambridge University Press, 2nd edition, 2011. ISBN 9780521514682.

[43] Elbio Dagotto. Complexity in strongly correlated electronic systems. *Science*, 309(5732): 257–262, 2005. URL https://doi.org/10.1126/science.1107559.

[44] Qimiao Si and Frank Steglich. Heavy fermions and quantum phase transitions. *Science*, 329(5996):1161–1166, 2010. URL https://doi.org/10.1126/science.1191195.

[45] T. Senthil, Ashvin Vishwanath, Leon Balents, Subir Sachdev, and Matthew P. A. Fisher. Deconfined quantum critical points. *Science*, 303(5663):1490–1494, 2004. URL https://doi.org/10.1126/science.1091806.

[46] Johnpierre Paglione and Richard L. Greene. High-temperature superconductivity in iron-based materials. *Nature Physics*, 6(9):645–658, 2010. URL https://doi.org/10.1038/NPHYS1759.

[47] Antoine Georges, Gabriel Kotliar, Werner Krauth, and Marcelo J. Rozenberg. Dynamical mean-field theory of strongly correlated fermion systems and the limit of infinite dimensions. *Rev. Mod. Phys.*, 68:13–125, Jan 1996. URL https://link.aps.org/doi/10.1103/RevModPhys.68.13.

[48] *Dynamical Mean-Field Theory of Strongly Correlated Electron Systems*. URL https://doi.org/10.7566/JPSCP.30.011001.

[49] R. Orús. A practical introduction to tensor networks: Matrix product states and projected entangled pair states. *Annals of Physics*, 349:117–158, 2013. URL https://doi.org/10.1016/j.aop.2014.06.013.

[50] Román Orús. Tensor networks for complex quantum systems. *Nature Reviews Physics*, 1 (9):538–550, 2019. URL https://doi.org/10.1038/s42254-019-0086-7.

[51] I. Cirac, D. Pérez-García, N. Schuch, and F. Verstraete. Matrix product states and projected entangled pair states: Concepts, symmetries, theorems. *Reviews of Modern Physics*, 2020. URL https://doi.org/10.1103/RevModPhys.93.045003.

[52] Steven R. White. Density matrix formulation for quantum renormalization groups. *Phys. Rev. Lett.*, 69:2863–2866, Nov 1992. URL https://doi.org/10.1103/PhysRevLett.69.2863.

[53] Ulrich Schollwöck. The density-matrix renormalization group. *Reviews of Modern Physics*, 77(1):259–315, 2005. URL https://doi.org/10.1103/RevModPhys.77.259.

[54] F. Verstraete and J. Cirac. Renormalization algorithms for quantum-many body systems in two and higher dimensions. *arXiv: Strongly Correlated Electrons*, 2004. URL https://doi.org/10.48550/arXiv.cond-mat/0407066.

[55] G. Vidal. Entanglement renormalization. *Phys. Rev. Lett.*, 99:220405, Nov 2007. URL https://doi.org/10.1103/PhysRevLett.99.220405.

[56] G. Vidal. Class of quantum many-body states that can be efficiently simulated. *Phys. Rev. Lett.*, 101:110501, Sep 2008. URL https://doi.org/10.1103/PhysRevLett.101.110501.

[57] W. Meissner and B. Voigt. Messungen mit hilfe von flüssigem helium xi widerstand der reinen metalle in tiefen temperaturen. *Annalen der Physik*, 399(7):761–797, 1930. URL https://doi.org/10.1002/andp.19303990702.

[58] W.J. de Haas, J. de Boer, and G.J. van dën Berg. The electrical resistance of gold, copper and lead at low temperatures. *Physica*, 1(7):1115–1124, 1934. ISSN 0031-8914. URL https://doi.org/10.1016/S0031-8914(34)80310-2.

[59] P. W. Anderson. Localized magnetic states in metals. *Phys. Rev.*, 124:41–53, Oct 1961. URL https://doi.org/10.1103/PhysRev.124.41.

[60] Jun Kondo. Resistance minimum in dilute magnetic alloys. *Progress of Theoretical Physics*, 32(1):37–49, 07 1964. ISSN 0033-068X. URL https://doi.org/10.1143/PTP.32.37.

[61] J. Kondo. Theory of dilute magnetic alloys. volume 23 of *Solid State Physics*, pages 183–281. Academic Press, 1970. URL https://doi.org/10.1016/S0081-1947(08)60616-5.

[62] N. Andrei, K. Furuya, and J. H. Lowenstein. Solution of the kondo problem. *Rev. Mod. Phys.*, 55:331–402, Apr 1983. URL https://doi.org/10.1103/RevModPhys.55.331.

[63] Daniel P. Arovas, Erez Berg, Steven A. Kivelson, and Srinivas Raghu. The hubbard model. *Annual Review of Condensed Matter Physics*, 13(Volume 13, 2022):239–274, 2022. ISSN 1947-5462. URL https://doi.org/10.1146/annurev-conmatphys-031620-102024.

[64] Mingpu Qin, Thomas Schäfer, Sabine Andergassen, Philippe Corboz, and Emanuel Gull. The hubbard model: A computational perspective. *Annual Review of Condensed Matter Physics*, 13(Volume 13, 2022):275–302, 2022. ISSN 1947-5462. URL https://doi.org/10.1146/annurev-conmatphys-090921-033948.

[65] Cheng Peng, Yi-Fan Jiang, Dong-Ning Sheng, and Hong-Chen Jiang. Doping quantum spin liquids on the kagome lattice. *Advanced Quantum Technologies*, 4(3):2000126, Jan 2021. ISSN 2511-9044. URL https://doi.org/10.1002/qute.202000126.

[66] Oleg Starykh. Viewing a quantum spin liquid through QED. *Physics*, 17:17, Apr 2024. ISSN 1943-2879. URL https://doi.org/10.1103/Physics.17.63.

[67] Siegfried Guertler. Kagome lattice Hubbard model at half filling. *Phys. Rev. B*, 90:081105, Aug 2014. URL https://doi.org/10.1103/PhysRevB.90.081105.

[68] Simeng Yan, David A. Huse, and Steven R. White. Spin-liquid ground state of the s= 1/2 kagome Heisenberg antiferromagnet. *Science*, 332(6034):1173–1176, June 2011. ISSN 1095-9203. URL https://doi.org/10.1126/science.1201080.

[69] Eun-Ah Kim and Antonio H. Castro Neto. Graphene as an electronic membrane. *EPL (Europhysics Letters)*, 84:57007, 2007. URL https://doi.org/10.1209/0295-5075/84/57007.

[70] A. Neto, F. Guinea, N. Peres, K. Novoselov, and A.K. Geim. The electronic properties of graphene. *Reviews of Modern Physics*, 81:109–162, 2007. URL https://doi.org/10.1103/RevModPhys.81.109.

[71] M. Fogler, F. Guinea, and M. Katsnelson. Pseudomagnetic fields and ballistic transport in a suspended graphene sheet. *Physical review letters*, 101 22:226804, 2008. URL https://doi.org/10.1103/PhysRevLett.101.226804.

[72] F. Guinea, A. K. Geim, M. I. Katsnelson, and K. S. Novoselov. Energy gaps, topological insulator state and zero-field quantum hall effect in graphene by strain engineering. *Nature Physics*, 6(1):30–33, 2010. URL https://doi.org/10.1038/nphys1420.

[73] D. Faria, A. Latgé, S. E. Ulloa, and N. Sandler. Currents and pseudomagnetic fields in strained graphene rings. *Physical Review B*, 87(24):241403, 2013. URL https://doi.org/10.1103/PhysRevB.87.241403.

[74] Ulrich Schollwöck. The density-matrix renormalization group in the age of matrix product states. *Annals of Physics*, 326(1):96–192, 2011. ISSN 0003-4916. URL https://doi.org/10.1016/j.aop.2010.09.012. January 2011 Special Issue.

[75] Gonçalo Catarina and Bruno Murta. Density-matrix renormalization group: a pedagogical introduction. *The European Physical Journal B*, 96(8):575, 2023. URL https://doi.org/10.1140/epjb/s10051-023-00575-2.

[76] Kin Fai Mak, Changgu Lee, James Hone, Jie Shan, and Tony F. Heinz. Atomically thin mos_2: A new direct-gap semiconductor. *Physical Review Letters*, 105(13):136805, 2010. URL https://doi.org/10.1103/PhysRevLett.105.136805.

[77] O. Samy and et al. A review on mos_2 properties, synthesis, sensing applications and challenges. *Crystals*, 11(4):355, 2021. URL https://doi.org/10.3390/cryst11040355.

[78] Alexander Anferov, Kan-Heng Lee, Fang Zhao, Jonathan Simon, and DavidI. Schuster. Improved coherence in optically defined niobium trilayer-junction qubits. *Physical Review Applied*, 21(2):024047, 2024. URL https://doi.org/10.1103/PhysRevApplied.21.024047.

[79] Mustafa Bal, AkshayA. Murthy, Shaojiang Zhu, Francesco Crisa, Xinyuan You, Ziwen Huang, Tanay Roy, David van Zanten, Roman Pilipenko, et al. Systematic improvements in transmon qubit coherence enabled by niobium surface encapsulation. *npj Quantum Information*, 10:43, 2024. URL https://doi.org/10.1038/s41534-024-00840-x.

[80] B.Q. Lv, H.M. Weng, B.B. Fu, X. Wang, H. Miao, J. Ma, P. Richard, X.C. Huang, L.X. Zhao, G.F. Chen, et al. Experimental discovery of weyl semimetal taas. *Physical Review X*, 5:031013, 2015. URL https://doi.org/10.1103/PhysRevX.5.031013.

[81] S.Y. Xu, I. Belopolski, N. Alidoust, M. Neupane, G. Bian, C. Zhang, R. Sankar, G. Chang, Z. Yuan, C.C. Lee, et al. Discovery of a weyl fermion semimetal and topological fermi arcs. *Science*, 349(6248):613–617, 2015. URL https://doi.org/10.1126/science.aaa9297.

[82] Andrei N. Vasiliev. Milestones of low-dimensional quantum magnetism. *npj Quantum Materials*, 2018. URL https://doi.org/10.1038/s41535-018-0090-7.

[83] Wei Ruan and Yuanbo Zhang. Strong correlations in two-dimensional transition metal dichalcogenides. *Science China Physics, Mechanics & Astronomy*, 66(11):117506, 2023. URL https://doi.org/10.1007/s11433-023-2141-9.

[84] L Rondin, J-P Tetienne, T Hingant, J-F Roch, P Maletinsky, and V Jacques. Magnetometry with nitrogen-vacancy defects in diamond. *Reports on Progress in Physics*, 77(5): 056503, may 2014. URL https://doi.org/10.1088/0034-4885/77/5/056503.

[85] C. L. Degen, F. Reinhard, and P. Cappellaro. Quantum sensing. *Rev. Mod. Phys.*, 89: 035002, Jul 2017. URL https://doi.org/10.1103/RevModPhys.89.035002.

[86] P. Simon and Y. Gogotsi. Materials for electrochemical capacitors. *Nature materials*, 7 11:845–54, 2008. URL https://doi.org/10.1038/nmat2297.

[87] K. Novoselov, V. Fal'ko, L. Colombo, P. Gellert, M. Schwab, and K. Kim. A roadmap for graphene. *Nature*, 490:192–200, 2012. URL https://doi.org/10.1038/nature11458.

[88] Elliott H Lieb and F Y Wu. Absence of mott transition in an exact solution of the short-range, one-band model in one dimension. *Physical Review Letters*, 20(25):1445–1448, 1968. URL https://doi.org/10.1103/PhysRevLett.20.1445.

[89] Thierry Giamarchi. *Quantum Physics in One Dimension*. Oxford University Press, 2003. ISBN 978-0-19-852500-4.

[90] Sin-itiro Tomonaga. Remarks on bloch's method of sound waves applied to many-fermion problems. *Progress of Theoretical Physics*, 5:544–569, 1950. URL https://doi.org/10.1143/PTP.5.544.

[91] F. D. M. Haldane. "luttinger-liquid theory" of one-dimensional quantum fluids. i. properties of the luttinger model and their extension to the general 1d interacting spinless fermi gas. *Journal of Physics C: Solid State Physics*, 14:2585–2609, 1981. URL https://doi.org/10.1088/0022-3719/14/19/010.

[92] Assa Auerbach. *Interacting Electrons and Quantum Magnetism*. Springer, 1994. ISBN 9780387942862.

[93] Alexander Altland and Ben D Simons. *Condensed Matter Field Theory*. Cambridge University Press, 2nd edition, 2010. ISBN 9780521769754.

[94] Eduardo Fradkin. *Field Theories of Condensed Matter Physics*. Cambridge University Press, 2nd edition, 2013. ISBN 9780521764445.

[95] N. David Mermin and Herbert Wagner. Absence of ferromagnetism or antiferromagnetism in one- or two-dimensional isotropic heisenberg models. *Physical Review Letters*, 17(22): 1133–1136, 1966. URL https://doi.org/10.1103/PhysRevLett.17.1133.

[96] Nigel Goldenfeld. *Lectures on Phase Transitions and the Renormalization Group*. Frontiers in Physics. Perseus Books, Reading, Massachusetts, 1992. ISBN 978-0-201-51512-5.

[97] P.M. Chaikin and T.C. Lubensky. *Principles of Condensed Matter Physics*. Cambridge University Press, Cambridge, 1995. ISBN 978-0-521-79450-5.

[98] John Cardy. *Scaling and Renormalization in Statistical Physics*, volume 5 of *Cambridge Lecture Notes in Physics*. Cambridge University Press, Cambridge, 1996. ISBN 978-0-521-48158-0.

[99] E. Miranda. Introduction to bosonization. *Brazilian Journal of Physics*, 33(1):3–35, March 2003. URL https://doi.org/10.1590/S0103-97332003000100002.

[100] Max Abraham. *Theorie der Elektrizität*, volume II. Teubner, Leipzig, 1905.

[101] Hendrik Antoon Lorentz. *The Theory of Electrons and its Applications to the Phenomena of Light and Radiant Heat*. Teubner, Leipzig, 2nd edition, 1915.

[102] Sin-Itiro Tomonaga. On a relativistically invariant formulation of the quantum theory of wave fields. *Progress of Theoretical Physics*, 1(2):27–42, 1946. URL https://doi.org/10.1143/PTP.1.27.

[103] Julian Schwinger. On quantum-electrodynamics and the magnetic moment of the electron. *Physical Review*, 73:416–417, 1948. URL https://doi.org/10.1103/PhysRev.73.416.

[104] Richard P. Feynman. Space-time approach to quantum electrodynamics. *Physical Review*, 76(6):769–789, 1949. URL https://doi.org/10.1103/PhysRev.76.769.

[105] Freeman J. Dyson. The radiation theories of tomonaga, schwinger, and feynman. *Physical Review*, 75:486–502, 1949. URL https://doi.org/10.1103/PhysRev.75.486.

[106] Freeman J. Dyson. The s matrix in quantum electrodynamics. *Physical Review*, 75:1736–1755, 1950. URL https://doi.org/10.1103/PhysRev.75.1736.

[107] Leo P. Kadanoff. Scaling laws for ising models near T_c. *Physics*, 2(6):263–272, 1966. URL https://doi.org/10.1103/PhysicsPhysiqueFizika.2.263.

[108] Benjamin Widom. Equation of state in the neighborhood of the critical point. *The Journal of Chemical Physics*, 43(11):3898–3905, 1965. URL https://doi.org/10.1063/1.1696618.

[109] Michael E. Fisher. The nature of critical points. In W. E. Brittin, editor, *Lectures in Theoretical Physics*, volume VII C, pages 1–159. University of Colorado Press, Boulder, 1965.

[110] Kenneth G. Wilson. Renormalization group and critical phenomena. i. renormalization group and the kadanoff scaling picture. *Physical Review B*, 4(9):3174–3183, 1971. URL https://doi.org/10.1103/PhysRevB.4.3174.

[111] Kenneth G. Wilson. The renormalization group: Critical phenomena and the kondo problem. *Rev. Mod. Phys.*, 47:773–840, Oct 1975. URL https://doi.org/10.1103/RevModPhys.47.773.

[112] A. A. Belavin, A. M. Polyakov, and A. B. Zamolodchikov. Infinite conformal symmetry in two-dimensional quantum field theory. *Nuclear Physics B*, 241(2):333–380, 1984. URL https://doi.org/10.1016/0550-3213(84)90052-X.

[113] Steven R. White and Reinhard M. Noack. Real-space quantum renormalization groups. *Physical review letters*, 68 24:3487–3490, 1992. URL https://doi.org/10.1103/PhysRevLett.68.3487.

[114] A. L. Malvezzi. An introduction to numerical methods in low-dimensional quantum systems. *arXiv preprint cond-mat/0304375*, 2003. URL https://doi.org/10.48550/arXiv.cond-mat/0304375.

[115] Ada Altieri and Marco Baity-Jesi. An introduction to the theory of spin glasses. pages 361–370, 2024. URL https://doi.org/10.1016/B978-0-323-90800-9.00249-3.

[116] Yousef Saad. *Iterative Methods for Sparse Linear Systems*. SIAM, 2nd edition, 2003. ISBN 9780898715347.

[117] Matthew B Hastings. An area law for one-dimensional quantum systems. *Journal of Statistical Mechanics: Theory and Experiment*, 2007(08):P08024, 2007. URL https://doi.org/10.1088/1742-5468/2007/08/P08024.

[118] Jens Eisert, Marcus Cramer, and Martin B Plenio. Colloquium: Area laws for the entanglement entropy. *Reviews of Modern Physics*, 82(1):277, 2010. URL https://doi.org/10.1103/RevModPhys.82.277.

[119] Fernando GSL Brandão and Michał Horodecki. Exponential decay of correlations implies area law. *Communications in Mathematical Physics*, 333(2):761–798, 2015. URL https://doi.org/10.1007/s00220-014-2213-8.

[120] Dmitry A. Abanin, Ehud Altman, Immanuel Bloch, and Maksym Serbyn. Colloquium: Many-body localization, thermalization, and entanglement. *Reviews of Modern Physics*, 91(2):021001, 2019. URL https://doi.org/10.1103/RevModPhys.91.021001.

[121] F. B. Ramos and J. C. Xavier. N-leg spin-s heisenberg ladders: A density-matrix renormalization group study. *Physical Review B*, 89(9):094424, 2014. URL https://doi.org/10.1103/PhysRevB.89.094424.

[122] Steven R. White and Adrian E. Feiguin. Real-time evolution using the density matrix renormalization group. *Physical Review Letters*, 93(7):076401, 2004. URL https://doi.org/10.1103/PhysRevLett.93.076401.

[123] Steven R. White. Density matrix renormalization group algorithms with a single center site. *Physical Review B*, 72(18):180403, 2005. URL https://doi.org/10.1103/PhysRevB.72.180403.

[124] Ingo Peschel, Matthias Kaulke, and Örs Legeza. Density-matrix spectra for integrable models. *Annalen der Physik*, 511(2):153–164, 1999. URL https://doi.org/10.1002/andp.19995110203.

[125] Kouichi Okunishi, Yasuhiro Hieida, and Yasuhiro Akutsu. Universal asymptotic eigenvalue distribution of density matrices and the corner transfer matrices in the thermodynamic limit. *Physical Review E*, 59(1):R622–R625, 1999. URL https://doi.org/10.1103/PhysRevE.59.R6227.

[126] Ming-Chiang Chung and Ingo Peschel. Density-matrix spectra of solvable fermionic systems. *Physical Review B*, 64(6):064412, 2001. URL https://doi.org/10.1103/PhysRevB.64.064412.

[127] Garnet Kin-Lic Chan, Paul W. Ayers, and Ernest S. Croot. On the distribution of eigenvalues of grand canonical density matrices. *Journal of Statistical Physics*, 107(5–6):1077–1095, 2002. URL https://doi.org/10.1023/A:1019999930923.

[128] Frank Verstraete and J. Ignacio Cirac. Matrix product states represent ground states faithfully. *Physical Review B*, 73(9):094423, 2006. URL https://doi.org/10.1103/PhysRevB.73.094423.

[129] Chanchal K. Majumdar and Dipan K. Ghosh. On next-nearest-neighbor interaction in linear chain. i. *Journal of Mathematical Physics*, 10(8):1388–1398, 08 1969. ISSN 0022-2488. URL https://doi.org/10.1063/1.1664978.

[130] C K Majumdar. Antiferromagnetic model with known ground state. *Journal of Physics C: Solid State Physics*, 3(4):911, apr 1970. URL https://doi.org/10.1088/0022-3719/3/4/019.

[131] Ian Affleck, Tom Kennedy, Elliott H. Lieb, and Hal Tasaki. Rigorous results on valence-bond ground states in antiferromagnets. *Physical Review Letters*, 59(7):799–802, 1987. URL https://doi.org/10.1103/PhysRevLett.59.799.

[132] F. Duncan M. Haldane. Nonlinear field theory of large-spin heisenberg antiferromagnets: Semiclassically quantized solitons of the one-dimensional easy-axis néel state. *Physics Letters A*, 93(9):464–468, 1983. URL https://doi.org/10.1103/PhysRevLett.50.1153.

[133] F. Duncan M. Haldane. Continuum dynamics of the 1-d heisenberg antiferromagnet: Identification with the o(3) nonlinear sigma model. *Physical Review Letters*, 50(15):1153–1156, 1983. URL https://doi.org/10.1016/0375-9601(83)90631-X.

[134] Elliott Lieb, Theodore Schultz, and Daniel Mattis. Two soluble models of an antiferromagnetic chain. *Annals of Physics*, 16(3):407–466, 1961. URL https://doi.org/10.1016/0003-4916(61)90115-4.

[135] Jacob C Bridgeman and Christopher T Chubb. Hand-waving and interpretive dance: An introductory course on tensor networks. *Journal of Physics A: Mathematical and Theoretical*, 50(22):223001, 2017. URL https://doi.org/10.1088/1751-8121/aa6dc3.

[136] Norbert Schuch, Michael M. Wolf, Frank Verstraete, and J. Ignacio Cirac. Computational complexity of projected entangled pair states. *Physical Review Letters*, 98(14):140506, 2007. URL https://doi.org/10.1103/PhysRevLett.98.140506.

[137] Adam S. Jermyn. Automatic contraction of unstructured tensor networks. *SciPost Physics*, 8(1):005, 2020. URL https://doi.org/10.21468/SciPostPhys.8.1.005.

[138] Mihail Stoian, Richard M. Milbradt, and Christian B. Mendl. On the optimal linear contraction order of tree tensor networks, and beyond. *SIAM Journal on Scientific Computing*, 46(5):B647–B668, 2024. URL https://doi.org/10.1137/23M161286X.

[139] M. Mezard, G. Parisi, and M. A. Virasoro. *Spin Glass Theory and Beyond: An Introduction to the Replica Method and Its Applications*. World Scientific, 1987.

[140] S. F. Edwards and P. W. Anderson. Theory of spin glasses. *Journal of Physics F: Metal Physics*, 5(5):965–974, 1975. URL https://doi.org/10.1088/0305-4608/5/5/017.

[141] D. Sherrington and S. Kirkpatrick. Solvable model of a spin-glass. *Physical Review Letters*, 35(26):1792–1796, 1975. URL https://doi.org/10.1103/PhysRevLett.35.1792.

[142] H. Sompolinsky and A. Zippelius. Relaxational dynamics of the edwards-anderson model and the mean-field theory of spin-glasses. *Physical Review B*, 25(10):6860–6875, 1981. URL https://doi.org/10.1103/PhysRevB.25.6860.

[143] L. F. Cugliandolo and J. Kurchan. Analytical solution of the off-equilibrium dynamics of a long-range spin-glass model. *Phys. Rev. Lett.*, 71:173–176, Jul 1993. URL https://doi.org/10.1103/PhysRevLett.71.173.

[144] Jacques Villain. Theory of one- and two-dimensional magnets with an easy magnetization plane. ii. the planar, classical, two-dimensional magnet. *Journal de Physique*, 36(6):581–590, 1975. URL https://doi.org/10.1051/jphys:01975003606058100.

[145] J Vannimenus and G Toulouse. Theory of the frustration effect. ii. ising spins on a square lattice. *Journal of Physics C: Solid State Physics*, 10(18):L537, sep 1977. URL https://doi.org/10.1088/0022-3719/10/18/008.

[146] A. P. Ramirez. Strongly geometrically frustrated magnets. *Annual Review of Materials Science*, 24(1):453–480, 1994. URL https://doi.org/10.1146/annurev.ms.24.080194.002321.

[147] Linus Pauling. The structure and entropy of ice and of other crystals with some randomness of atomic arrangement. *Journal of the American Chemical Society*, 57(12):2680–2684, 1935. URL https://doi.org/10.1021/ja01315a102.

[148] G. H. Wannier. Antiferromagnetism. The triangular ising net. *Physical Review*, 79(2): 357–364, 1950. URL https://doi.org/10.1103/PhysRev.79.357.

[149] P. W. Anderson. The concept of frustration in spin glasses. *Journal of the Less-Common Metals*, 62:291–294, 1978. URL https://doi.org/10.1016/0022-5088(78)90040-1.

[150] S. Kobe and T. Klotz. Frustration: How it can be measured. *Phys. Rev. E*, 52:5660–5663, Nov 1995. URL https://doi.org/10.1103/PhysRevE.52.5660.

[151] J R Banavar, D Sherrington, and N Sourlas. Graph bipartitioning and statistical mechanics. *Journal of Physics A: Mathematical and General*, 20(1):L1, jan 1987. URL https://doi.org/10.1088/0305-4470/20/1/001.

[152] M. J. Oliveira. Graph optimization problems on a bethe lattice. *Journal of Statistical Physics*, 54:477–493, 1989. URL https://doi.org/10.1007/BF01023490.

[153] P. Sibani, J. C. Schön, P. Salamon, and J.-O. Andersson. Emergent hierarchical structures in complex-system dynamics. *Europhysics Letters*, 22(7):479, jun 1993. URL https://doi.org/10.1209/0295-5075/22/7/001.

[154] A. Banerjee, C. A. Bridges, J.-Q. Yan, A. A. Aczel, L. Li, M. B. Stone, G. E. Granroth, M. D. Lumsden, Y. Yiu, J. Knolle, S. Bhattacharjee, D. L. Kovrizhin, R. Moessner, D. A. Tennant, D. G. Mandrus, and S. E. Nagler. Proximate kitaev quantum spin liquid behaviour in a honeycomb magnet. *Nature Materials*, 15:733–740, 2016. URL https://doi.org/10.1038/nmat4604.

[155] Tian-Heng Han, Joel S Helton, Shaoyan Chu, Daniel G Nocera, Jose A Rodriguez-Rivera, Collin Broholm, and Young S Lee. Fractionalized excitations in the spin-liquid state of a kagome-lattice antiferromagnet. *Nature*, 492(7429):406–410, 2012. URL https://doi.org/10.1038/nature11659.

[156] Alexei Kitaev. Anyons in an exactly solved model and beyond. *Annals of Physics*, 321(1): 2–111, 2006. URL https://doi.org/10.1016/j.aop.2005.10.005.

[157] P. Lecheminant, B. Bernu, C. Lhuillier, L. Pierre, and P. Sindzingre. Order versus disorder in the quantum heisenberg antiferromagnet on the kagomé lattice using exact spectra analysis. *Physical Review B*, 56(5):2521, 1997. URL https://doi.org/10.1103/PhysRevB.56.2521.

[158] N Read and S Sachdev. Large-n expansion for frustrated quantum antiferromagnets. *Physical Review Letters*, 66(13):1773, 1991. URL https://doi.org/10.1103/PhysRevLett.66.1773.

[159] Subir Sachdev. Kagomé- and triangular-lattice heisenberg antiferromagnets: Ordering from quantum fluctuations and quantum-disordered ground states with unconfined bosonic spinons. *Physical Review B*, 45(21):12377, 1992. URL https://doi.org/10.1103/PhysRevB.45.12377.

[160] Yuan-Ming Lu, Ying Ran, and Patrick A Lee. Z2 spin liquids in the s=1/2 heisenberg model on the kagome lattice: A projective symmetry-group study of schwinger fermion mean-field states. *Physical Review B*, 83(22):224413, 2011. URL https://doi.org/10.1103/PhysRevB.83.224413.

[161] Stefan Depenbrock, Ian P. McCulloch, and Ulrich Schollwöck. Nature of the spin-liquid ground state of the $s = \frac{1}{2}$ heisenberg model on the kagome lattice. *Physical Review Letters*, 109(6):067201, 2012. URL https://doi.org/10.1103/PhysRevLett.109.067201.

[162] Hong-Chen Jiang, Zhenghan Wang, and Leon Balents. Identifying topological order by entanglement entropy. *Nature Physics*, 8(12):902–905, 2012. URL https://doi.org/10.1038/nphys2465.

[163] Norbert Schuch, Ignacio Cirac, and David Pérez-García. Topological order in the projected entangled-pair states formalism: Transfer operator and boundary hamiltonians. *Annals of Physics*, 325(10):2153–2192, 2010. URL https://doi.org/10.1103/PhysRevLett.111.090501.

[164] Z. Y. Xie, J. Chen, J. F. Yu, X. Kong, B. Normand, and T. Xiang. Tensor renormalization of quantum many-body systems using projected entangled simplex states. *Phys. Rev. X*, 4:011025, Feb 2014. URL https://doi.org/10.1103/PhysRevX.4.011025.

[165] Glen Evenbly and Guifre Vidal. Frustrated antiferromagnets with entanglement renormalization: Ground state of the spin-1/2 heisenberg model on a kagome lattice. *Physical Review Letters*, 104(18):187203, 2010. URL https://doi.org/10.1103/PhysRevLett.104.187203.

[166] Hanyu Liao, Zhao Liu, Yu He, and Zi Yang Meng. Spin-1/2 kagome heisenberg antiferromagnet: Machine learning evidence for spinon pair density wave. *Physical Review X*, 15 (1):011047, 2025. URL https://link.aps.org/doi/10.1103/PhysRevX.15.011047.

[167] Rong-You Sun, Xiao-Yu Zhang, Fan Yang, and Zi Yang Meng. Possible chiral spin liquid state in the s=1/2 kagome heisenberg model. *npj Quantum Materials*, 9:16, 2024. URL https://doi.org/10.1038/s41535-024-00627-5.

[168] S. Suetsugu, T. Asaba, Y. Kasahara, Y. Kohsaka, K. Totsuka, B. Li, Y. Zhao, Y. Li, M. Tokunaga, and Y. Matsuda. Emergent spin-gapped magnetization plateaus in a spin-1/2 perfect kagome antiferromagnet. *Phys. Rev. Lett.*, 132:226701, May 2024. URL https://doi.org/10.1103/PhysRevLett.132.226701.

[169] Aini Xu, Qinxin Shen, Bo Liu, Zhenyuan Zeng, Lankun Han, Liqin Yan, Jun Luo, Jie Yang, Rui Zhou, and Shiliang Li. Magnetic ground states in the kagome system $ycu_3(OH)_6[(Cl_xBr_{1-x})_{3-y}(OH)_y]$. *Phys. Rev. B*, 110:085146, Aug 2024. URL https://doi.org/10.1103/PhysRevB.110.085146.

[170] Zhen Zeng and Yi Zhou. Spectral evidence for dirac spinons in a kagome lattice antiferromagnet. *Nature Physics*, 2024. URL https://doi.org/10.1038/s41567-024-02495-z.

[171] Mary Madelynn Nayga and Matthias Vojta. Strain tuning of highly frustrated magnets: Order and disorder in the distorted kagome heisenberg antiferromagnet. *Phys. Rev. B*, 105:094426, Mar 2022. URL https://doi.org/10.1103/PhysRevB.105.094426.

[172] Andreas P. Schnyder, Oleg A. Starykh, and Leon Balents. Spatially anisotropic Heisenberg kagome antiferromagnet. *Phys. Rev. B*, 78:174420, Nov 2008. URL https://doi.org/10.1103/PhysRevB.78.174420.

[173] Cécile Repellin, Yin-Chen He, and Frank Pollmann. Stability of the spin-$\frac{1}{2}$ kagome ground state with breathing anisotropy. *Phys. Rev. B*, 96:205124, Nov 2017. URL https://doi.org/10.1103/PhysRevB.96.205124.

[174] Yixuan Huang Chiara Bruzzi, Jian-Xin Zhu. Magnetic anisotropy effect on stabilizing magnetization plateaus of kagome strip chain heisenberg antiferromagnets. *arXiv preprint arXiv:2405.19512*, 2025. URL https://doi.org/10.48550/arXiv.2409.19512.

[175] Kazuaki Takasan and Masahiro Sato. Control of magnetic and topological orders with a dc electric field. *Phys. Rev. B*, 100:060408, Aug 2019. URL https://doi.org/10.1103/PhysRevB.100.060408.

[176] E. Grüneisen. Theorie des festen zustandes einatomiger elemente. *Annalen der Physik*, 344(12):257–306, 1912. URL https://doi.org/10.1002/andp.19123441202.

[177] J. M. Ziman. *Electrons and Phonons: The Theory of Transport Phenomena in Solids*. Oxford University Press, Oxford, 1960.

[178] S. Piscanec, M. Lazzeri, F. Mauri, A. C. Ferrari, and J. Robertson. Kohn anomalies and electron-phonon interactions in graphite. *Physical Review Letters*, 93(18):185503, 2004. URL https://doi.org/10.1103/PhysRevLett.93.185503.

[179] M. Born and K. Huang. *Dynamical Theory of Crystal Lattices*. Oxford University Press, Oxford, 1954.

[180] B. Fultz. Vibrational thermodynamics of materials. *Progress in Materials Science*, 55(4): 247–352, 2010. URL https://doi.org/10.1016/j.pmatsci.2009.05.002.

[181] J.-C. Charlier, X. Gonze, and J.-P. Michenaud. First-principles study of the electronic properties of graphite. *Physical Review B*, 43(6):4579–4589, 1991. URL https://doi.org/10.1103/PhysRevB.43.4579.

[182] T. Ando. Theory of electronic states and transport in carbon nanotubes. *Journal of the Physical Society of Japan*, 74(3):777–817, 2005. URL https://doi.org/10.1143/JPSJ.74.777.

[183] M. Balkanski, R. F. Wallis, and E. Haro. Anharmonic effects in light scattering due to optical phonons in silicon. *Physical Review B*, 28(4):1928–1934, 1983. URL https://doi.org/10.1103/PhysRevB.28.1928.

[184] L. Yang and J. Han. Electronic structure of deformed carbon nanotubes. *Physical Review Letters*, 85(1):154–157, 2000. URL https://doi.org/10.1103/PhysRevLett.85.154.

[185] K. S. Novoselov, A. K. Geim, S. V. Morozov, D. Jiang, Y. Zhang, S. V. Dubonos, I. V. Grigorieva, and A. A. Firsov. Electric field effect in atomically thin carbon films. *Science*, 306(5696):666–669, 2004. URL https://doi.org/10.1126/science.1102896.

[186] María A. H. Vozmediano, M. I. Katsnelson, and F. Guinea. Gauge fields in graphene. *Physics Reports*, 496(4):109–148, 2010. URL https://doi.org/10.1016/j.physrep.2010.07.003.

[187] Niv Levy, Sarah A. Burke, K. L. Meaker, Michelle Panlasigui, A. Zettl, F. Guinea, A. H. Castro Neto, and Michael F. Crommie. Strain-induced pseudo–magnetic fields greater than 300 tesla in graphene nanobubbles. *Science*, 329(5991):544–547, 2010. URL https://doi.org/10.1126/science.1191700.

[188] Alexander Georgi, Peter Nemes-Incze, Ramon Carrillo-Bastos, Daiara Faria, Silvia Viola Kusminskiy, Dawei Zhai, Martin Schneider, Dinesh Subramaniam, Torge Mashoff, Nils M. Freitag, Marcus Liebmann, Marco Pratzer, Ludger Wirtz, Colin R. Woods, Roman V. Gorbachev, Yang Cao, Kostya S. Novoselov, Nancy Sandler, and Markus Morgenstern. Tuning the pseudospin polarization of graphene by a pseudomagnetic field. *Nano Letters*, 17(4):2240–2245, 2017. URL https://doi.org/10.1021/acs.nanolett.6b04870.

[189] Marcos R. Guassi, Ginetom S. Diniz, Nancy Sandler, and Fanyao Qu. Zero-field and time-reserval-symmetry-broken topological phase transitions in graphene. *Phys. Rev. B*, 92:075426, Aug 2015. URL https://doi.org/10.1103/PhysRevB.92.075426.

[190] R. Carrillo-Bastos, D. Faria, A. Latgé, F. Mireles, and N. Sandler. Gaussian deformations in graphene ribbons: Flowers and confinement. *Phys. Rev. B*, 90(4):041411, 2014. URL https://doi.org/10.1103/PhysRevB.90.041411.

[191] R. Carrillo-Bastos, C. León, D. Faria, A. Latgé, E. Y. Andrei, and N. Sandler. Strained fold-assisted transport in graphene systems. *Phys. Rev. B*, 94(12):125422, 2016. URL https://doi.org/10.1103/PhysRevB.94.125422.

[192] V. Torres, D. Faria, and A. Latgé. Tuning transport properties of graphene three-terminal structures by mechanical deformation. *Physical Review B*, 97(16):165429, 2018. URL https://doi.org/10.1103/PhysRevB.97.165429.

[193] Yuan Cao, Valla Fatemi, Shiang Fang, Kenji Watanabe, Takashi Taniguchi, Efthimios Kaxiras, and Pablo Jarillo-Herrero. Unconventional superconductivity in magic-angle graphene superlattices. *Nature*, 556(7699):43–50, 2018. URL https://doi.org/10.1038/nature26160.

[194] Tianyu Liu. Strain-induced pseudomagnetic field and quantum oscillations in kagome crystals. *Physical Review B*, 102(4):045151, 2020. URL https://doi.org/10.1103/PhysRevB.102.045151.

[195] M A Mojarro and Sergio E Ulloa. Strain-induced topological transitions and tilted dirac cones in kagome lattices. *2D Materials*, 11(1):011001, October 2023. ISSN 2053-1583. URL https://doi.org/10.1088/2053-1583/acfe88.

[196] C. L. Kane and E. J. Mele. Z_2 topological order and the quantum spin hall effect. *Phys. Rev. Lett.*, 95:146802, Sep 2005. URL https://doi.org/10.1103/PhysRevLett.95.146802.

[197] Wei Jiang, Meng Kang, Huaqing Huang, Hongxing Xu, Tony Low, and Feng Liu. Topological band evolution between lieb and kagome lattices. *Phys. Rev. B*, 99:125131, Mar 2019. URL https://doi.org/10.1103/PhysRevB.99.125131.

[198] Ge He, Leander Peis, Emma Frances Cuddy, Zhen Zhao, Dong Li, Yuhang Zhang, Romona Stumberger, Brian Moritz, Haitao Yang, Hongjun Gao, Thomas Peter Devereaux, and Rudi Hackl. Anharmonic strong-coupling effects at the origin of the charge density wave in CsV_3Sb_5. *Nature Communications*, 15(1):1895, 2024. URL https://doi.org/10.1038/s41467-024-45865-0.

[199] Matthew Fishman, Steven R. White, and E. Miles Stoudenmire. Codebase release 0.3 for ITensor. *SciPost Phys. Codebases*, pages 4–r0.3, 2022. URL https://doi.org/10.21468/SciPostPhysCodeb.4-r0.3.

[200] Matthew Fishman, Steven R. White, and E. Miles Stoudenmire. The ITensor Software Library for Tensor Network Calculations. *SciPost Phys. Codebases*, page 4, 2022. URL https://doi.org/10.21468/SciPostPhysCodeb.4.

[201] Jeff Bezanson, Alan Edelman, Stefan Karpinski, and Viral B Shah. Julia: A fresh approach to numerical computing. *SIAM Review*, 59(1):65–98, 2017. URL https://doi.org/10.1137/141000671.

[202] Rong-Yang Sun and Zheng Zhu. Metal-insulator transition and intermediate phases in the kagome lattice Hubbard model. *Phys. Rev. B*, 104:L121118, Sep 2021. URL https://doi.org/10.1103/PhysRevB.104.L121118.

[203] Yaojia Wang, Heng Wu, Gregory T. McCandless, Julia Y. Chan, and Mazhar N. Ali. Quantum states and intertwining phases in kagome materials. *Nature Reviews Physics*, 5(11):635–658, September 2023. ISSN 2522-5820. URL https://doi.org/10.1038/s42254-023-00635-7.

[204] Yasir Iqbal, Federico Becca, and Didier Poilblanc. Valence-bond crystals in the kagomé spin-1/2 heisenberg antiferromagnet: a symmetry classification and projected wave function study. *New Journal of Physics*, 14(11):115031, November 2012. ISSN 1367-2630. URL https://doi.org/10.1088/1367-2630/14/11/115031.

[205] F. Mila. Low-energy sector of the $S = 1/2$ kagome antiferromagnet. *Phys. Rev. Lett.*, 81: 2356–2359, Sep 1998. URL https://doi.org/10.1103/PhysRevLett.81.2356.

[206] Shou-Shu Gong, Wei Zhu, Leon Balents, and D. N. Sheng. Global phase diagram of competing ordered and quantum spin-liquid phases on the kagome lattice. *Physical Review B*, 91:075112, Feb 2015. URL https://doi.org/10.1103/PhysRevB.91.075112.

[207] H. C. Jiang, Z. Y. Weng, and D. N. Sheng. Density matrix renormalization group numerical study of the kagome antiferromagnet. *Phys. Rev. Lett.*, 101:117203, Sep 2008. URL https://doi.org/10.1103/PhysRevLett.101.117203.

[208] E. Stoudenmire and L. Balents. Ordered phases of the anisotropic kagome-lattice antiferromagnet in a magnetic field. *Physical Review B*, 77:174414, 2007. URL https://doi.org/10.1103/PhysRevB.77.174414.

[209] Fa Wang, Ashvin Vishwanath, and Yong Baek Kim. Quantum and classical spins on the spatially distorted kagomé lattice: Applications to volborthite $Cu_3V_2O_7(OH)_2{\cdot}2H_2O$. *Phys. Rev. B*, 76:094421, Sep 2007. URL https://doi.org/10.1103/PhysRevB.76.094421.

[210] T. Yavors'kii, W. Apel, and H. Everts. Heisenberg antiferromagnet with anisotropic exchange on the kagome lattice: Description of the magnetic properties of volborthite. *Physical Review B*, 76:064430, 2007. URL https://doi.org/10.1103/PhysRevB.76.064430.